Global Power System Transformation (G-PST)

Stage 2: Topic 6 - Services

Frequency Support and Generation-Demand Active Power Balance Services for Enabling Global Power System Transformation in Australia

2022-23 CSIRO G-PST Stage 2 Research

Commonwealth Scientific and Industrial Research Organisation

28 April 2023

Chief Investigators:

Dr. Hassan Haes Alhelou, Monash University, Australia

Dr. Behrooz Bahrani, Monash University, Australia

A/Prof. Jin Ma, The University of Sydney, Australia

Prof. David J. Hill, Monash University, Australia

Funding Acknowledgement: The research presented in this report was funded by CSIRO, Australia's national science agency, and carried out as part of CSIRO's contribution to the initiatives of the Global Power System Transformation (GPST) Consortium. This research supports Australia's transition to a stable, secure and affordable power system and contributes to critical research identified by the Consortium required to accelerate the decarbonisation of our electricity grid. More details can be found at https://www.csiro.au/en/research/technology-space/energy/G-PST-Research-Roadmap

Funding Acknowledgement:

The research presented in this report was funded by CSIRO, Australia's national science agency, and carried out as part of CSIRO's contribution to the initiatives of the Global Power System Transformation (GPST) Consortium. This research supports Australia's transition to a stable, secure and affordable power system and contributes to critical research identified by the Consortium required to accelerate the decarbonisation of our electricity grid. More details can be found at https://www.csiro.au/en/research/technology-space/energy/G-PST-Research-Roadmap

Acknowledgements:

The research team of the project (**Hassan Haes Alhelou**, **Behrooz Bahrani**, **Jin Ma**, and **David J. Hill**) acknowledges the support received from **CSIRO**, **AEMO**, **GHD**, and **AEMC** during the project's lifetime. We appreciate the detailed discussions during the bi-weekly meetings in the last 12 months that enriched the research and the useful and helpful feedback provided for this research project.

We thank CSIRO's scientists, AEMO's expert leaders and engineers, and GHD's team for their efforts, time, and detailed feedback and comments. We should mention the following CSIRO scientists who have contributed to this project throught their discussions and comments (**John Ward, Nariman Mahdavi Mazdeh, Thomas Brinsmead, Brian Liu, Chris Knight, and Julio Braslavsky**). We are especially thankful to the following AEMO experts and leaders who contributed significantly and enriched the discussion on the research topic through regular meetings (**Luke Robinson, Jane Yu, Chris Mock, Andrew Groom, and Germane Athanasius**). We highly appreciate the help and detailed discussions by the GHD team's leader and the team (**Christian Schaefer, Berk Bakici, and Alexander Marcoux**). Finally, we are gratitude to **Ben Hiron** and the AEMC team who provided useful information and feedback at the beginning of the project.

Table Contents

Title	Page #
Table of Contents	i
Table of Figures	iv
Table of Tables	viii
Glossary of Terms	ix
List of Appendices	v
Executive Summary	1
Chapter 1: An Overview of the NEM and its Frequency Control	6
1.1. Introduction to the NEM	6
1.2. The Market Bodies and National Energy Governance for the NEM	7
1.3. The NEM's Frequency Operating Standard	8
1.4. Frequency Support Services in the NEM	9
1.5. Conclusion	10
Chapter 2: Advanced Low-order System Frequency Response Model to Facilize Frequency Support Studies for Power System Transformation	11
2.1. An overview of the proposed SFR and its applications	11
2.2. The proposed methodology to achieve the advanced SFR	12
2.3. Full-order frequency response model of synchronous generating units-based power plants	13
2.4. Order-reduction of synchronous generating units in a specific power region	18
2.5. Forming A Power Region Swing Equation	18
2.6. Forming A Power Region SFR Model	19
2.7. Integrating different power regions to form interconnected SFR model	20
2.8. Systems of systems and state Space Representative of the system frequency response	21
2.9. Modelling of Generated/Consumed Active Power Variation in Renewable Energy Sources/Demand	23
2.10. Modelling of modern frequency support providers: DR, EV, and Virtual Inertia	23
2.11. A New methodology to identify the parameters of the proposed SFR model	25

2.12. Validation of the proposed methodology for Obtaining SFR Data 34

2.13. Validation of the proposed SFR Methodology: Time-Domain Analysis 37

2.14. Application to NEM system 39

2.15. Insights and Outstanding Outcomes 44

Chapter 3: An advanced frequency control and FCAS activation technique for power systems 47

3.1. An overview 47

3.2. A statement of the problem, a review of related literature, and a highlight of research gaps 47

3.3. Discussion on the problem and the needs to address it 49

3.4. The Developed Novel Methodology 50

3.5. Generic Multi-Area & Interconnectors Frequency Response Models 54

3.6. Numerical Results and Discussions 57

3.7. Remarks, Conclusions, main insights and outcomes 61

Chapter 4: Demand-side Based Frequency Support Services 64

4.1. An overview 64

4.2. Estimating the available frequency control reserve from EVs at system level 64

4.3. A new system frequency response model and aggregation method of EV to support frequency 70

4.4. Estimation of Available Active Power Reserve from Ambient Temperature-Dependent Loads 76

4.5. A Novel Dynamic Model to Assess Frequency Response from Thermostatically-Controlled Loads 81

Chapter 5: The requirements of Inertia and FFR for Modern Power Systems 87

5.1. An Overview 87

5.2. Current and Future Inertia for the NEM 87

5.3. Simultaneous Estimation of Inertia Constant and Damping Coefficient 89

5.4. Inertia Requirements in Power systems 90

5.5. Minimum Synchronous Inertia Requirements in a Bulk Power System 90

5.6. Minimum Synchronous Inertia Requirements in a Multi-Area Power System Under Regionalisation Concept 92

5.7. Inertia Sources for Modern Interconnected Power Systems: Synchronous and Synthesis Inertia 93

5.8. Discussion on Synthesis Inertia and Synchronous Inertia 94

Chapter 6: Research Gaps and Future Research Directions 100

6.1. Inertia Response Services 100

6.2. Primary Frequency Control Services 100

6.3. Secondary Frequency Control Services 101

6.4. Current FCAS Market Issue 101

6.5. Current Technical Issues in NEM’s FCAS 101

6.6. Emerging Issues 102

Table of Figures

Caption	Page #
Figure 1.1. Physical interconnection between power regions in the system of the NEM	6
Figure 1.2. General topology under investigation and its sub topologies	7
Figure 1.3. Graphical illustration of FOS in NEM with the activation time of each FCAS market	8
Figure 2.1. The generic structure of power systems	14
Figure 2.2. The generic SFR model of a power region where frequency supported by thermal power plants and EVs	19
Figure 2.3. The topology of the studied interconnected power system	21
Figure 2.4. Model of Wind turbines' fluctuating active power	23
Figure 2.5. Active power fluctuation model for solar energy systems	23
Figure 2.6. The EV battery-charge frequency response model	24
Figure 2.7. Illustration of the oblique projection	27
Figure 2.8. Combined deterministic-stochastic system	28
Figure 2.9. Orthogonal projection of input/output data	31
Figure 2.10. Oblique projection of input/output data	32
Figure 2.11. The estimation error of inertia in a generic power system model	34
Figure 2.12. The frequency response due to a 0.1 p.u. disturbance.	37
Figure 2.13. The RoCoF due to a 0.1 p.u. disturbance	37
Figure 2.14. The measurements of the input and output of the original governor-turbine system	38
Figure 2.15. Validating the estimated governor-turbine model against the original model	38
Figure 2.16. Validating the estimated low-order governor-turbine model for SFR model usage	39
Figure 2.17. Validating the estimated excessively low-order governor-turbine model for SFR model usage	39
Figure 2.18. The National Electricity Market System	40
Figure 2.19. The topology of the main SFR model built for the system	41
Figure 2.19. Sample of power region model	42
Figure 2.20. Sample of the active power fluctuation from wind power	42

Figure 2.21. Sample of the active power fluctuation from solar power 42

Figure 2.21. Frequency deviations in different power regions during normal operation 43

Figure 2.22. RoCoF in different power regions during normal operation 43

Figure 2.23. Tie-line power deviations in different power regions during normal operation 43

Figure 2.24. Frequency deviations in different power regions during abnormal operation 44

Figure 2.25. RoCoF in different power regions during abnormal operation 44

Figure 2.26. Tie-line power deviations in different power regions during abnormal operation 44

Figure 3.1. General topology under investigation and its sub topologies 49

Figure 3.2. The block diagram of the proposed observer in (7-8) 51

Figure 3.3. The suggested procedure for designing the observer 54

Figure 3.4. The system topology under investigation 57

Figure 3.5. Estimation error of different dynamic states due to RES disturbances in SA and 0.015 pu step disturbance in NSW: a) SA and b) QLD power region. 58

Figure 3.6. Dynamic responses due to RES disturbances in SA and 0.015 pu step disturbance in NSW: a) the frequency deviation and b) the power deviation through interconnector 58

Figure 3.7. Dynamic responses due to 0.03 pu in SA and 0.015 p.u step in NSW: a) the frequency deviation and b) the interconnector power deviation 59

Figure 3.8. Dynamic responses due to 0.03 pu in SA and 0.015 pu step in NSW, -0.02 pu QLD and 0.01 pu TAS with NEM practice-based controller: a) F and b) power deviation in tie-lines 60

Figure 3.9. Compassion of dynamic responses due to 0.03 pu in SA and 0.015 pu step in NSW, -0.02 pu QLD and 0.01 pu TAS with ENTSO-E, NEM and proposed controllers: a) F and b) Power deviation through tie-lines 61

Figure 4.1. the charging pattern for different types of vehicles' batteries 67

Figure 4.2. The EV demand estimation for 2030 and 2050 in Victorian Power region in case of the worst-case scenario 69

Figure 4.3. The EV demand estimation for 2030 and 2050 cross NEM system for worst-case scenario 70

Figure 4.4. Electric model of individual EV's battery and charger 71

Figure 4.5. Dynamic model of EVs for primary frequency control 72

Figure 4.6. The typical demand of NEM used in the simulation 73

Figure 4.7. The frequency nadir in NEM system for a typical day under different scenarios of EV for 2030 based on ISP scenarios 73

Figure 4.8. The frequency nadir in NEM system for a typical day under different scenarios of EV for 2030 based on ISP scenarios 74

Figure 4.9. the aggregation of the estimated demand of thermostatically controlled loads at the DNSP and power region levels in VIC power region 78

Figure 4.10. The estimated demand of thermostatically controlled loads at the power regions and system levels of NEM 78

Figure 4.11. The estimated demand of thermostatically controlled loads at the power regions and system levels of NEM 79

Figure 4.12. The estimated demand of thermostatically controlled loads at the power regions and system levels of NEM for one month-July 2014. 79

Figure 4.13. The estimated demand of thermostatically controlled loads at the power regions and system levels of NEM for one day-20 July 2013 79

Figure 4.14. Thermal and electrical model of the thermostatically controlled loads 81

Figure 4.15. The frequency response after a large disturbance; w/o without AC participation, AC Tc=0.02 s means the time constant of AC is set to 0.02 seconds 83

Figure 4.16. The frequency nadir if a disturbance occurred at different times in the first week of September 2022 under different scenarios of AC participation 84

Figure 4.17. The active power response from power plants if a disturbance occurred under different scenarios of AC participation 84

Figure 4.18. The required maximum active power from power plants if a disturbance occurred at different times in the first week of September 2022 under different scenarios of AC participation 84

Figure 4.19. The active power response from ACs if a disturbance occurred under different scenarios of AC participation 85

Figure 4.20. The maximum active power response from ACs if a disturbance occurred in different times during the first week of Sep 2022 under different scenarios of AC participation 85

Figure 4.21. The maximum RoCoF if a disturbance occurred in different times during the first week of Sep 2022 under different scenarios of AC participation 86

Figure 4.22. The maximum time of operating under frequency declining if a disturbance occurred in different times during the first week of Sep 2022 under different scenarios of AC participation 86

Figure 5.1. 2022 inertia review outcomes for the NEM, for the five-year period to December 2027 87

Figure 5.2. The calculation of the minimum synchronous inertia for each operational time interval during a one day. 91

Figure 5.3. A general topology of N power regions (N=4) interconnected through different types of interconnectors and the topology of the NEM where red interconnectors represents HVDC links. 92

Figure 5.4. The frequency deviation due to 0.1 p.u. disturbance at t=1 Sec: a) under system operation with synchronous inertia of 3.62 Sec; b) under different scenarios of compensating synchronous inertia shortfall by virtual inertia and FFR. 95

Figure 5.5. The deviation of the generated active power as a response to 0.1 p.u. disturbance at t=1 Sec: a) under system operation with synchronous inertia of 3.62 Sec; b) under different scenarios of compensating synchronous inertia shortfall. 95

Figure 5.6. The RoCoF as a response to 0.1 p.u. disturbance at t=1 Sec: a) under system operation with synchronous inertia of 3.62 Sec; b) under different scenarios of compensating synchronous inertia shortfall; c) zoom in around t=1 Sec 96

Figure 5.7. The frequency and RoCoF in different power regions due to a 0.1 p.u. disturbance in SA: a-b) no virtual inertia, c-d) an additional Hv=5 sec as virtual inertia in SA 97

Figure 5.8. The frequency deviation in different power regions due to different step active power disturbances occur in SA as shown in the topology (f) considering different virtual inertia levels. 98

Table of Tables

Caption	Page #
Table 1.1. Frequency Bands defined in Australian FOS	8
Table 1.2. FCAS markets and their required outcomes in NEM	10
Table 2.1. The estimation results of IEEE 39-bus system in case of a 0.1 p.u. disturbance in demand-side	35
Table 2.2. The estimation results of IEEE 39-bus system in case of injecting PRBS in G1	35
Table 4.1. The number of substations considered for estimation by NEAR project under each DNSP in VIC power region; i.e. the $Nsubstation$ used for (1) when it is solved for VIC power region	77
Table 5.1. Current inertia requirements in MWs in the NEM	88

,

Glossary of Terms

AEMC	Australian Energy Market Commission
AEMO	Australian Energy Market Operator
AGC	Automatic Generation Control
ARENA	Australian Renewable Energy Agency
ATEL	Accumulated Time Error Limit
BESS	Battery Energy Storage System
DR	Demand Response
DSM	Demand Side Management
ENTSO-E	European Network of Transmission System Operators for Electricity
ESS	Energy Storage System
EV	Electric Vehicles
FCAS	Frequency Control Ancillary Service
FOS	Frequency Operating Standard
IBR	Inverter-based Resource
ISP	Integrated System Plan
LFC	Load Frequency Control
NEM	National Electricity Market
NOFB	Normal Operating Frequency Band
RES	Renewable Energy Source
SFR	System Frequency Response
TCPS	Thyristor Controlled Phase Shifters
VPP	Virtual Power Plant

Executive Summary

Essential and ancillary services are necessary to enable power system transformation and energy transition for ensuring stable and secure operation of energy systems during and beyond energy transition. Global Power Systems Transformation. Topic 6 of CSIRO's Australian G-PST research Roadmap is carefully designed to answer urgent research questions, providing better understanding of the services needed to enable the energy transition. This report concisely summarises the research outcomes from Topic 6 – Services, undertaken as part of the Global Power Systems Transformation project.

The currently underway research of Topic 6 focuses on services needed to ensure active power supply-demand balance, and stable and secure operation of the frequency in power systems, with more focus on the NEM, with high penetration of inverter-based resources (IBRs). To achieve the research goals topic 6 covers six different research phases:

1. In phase I, the project proposes a new system frequency response (SFR) model that considers different potential providers of services to support frequency in power systems. The proposed SFR model considers the services from energy storage systems (ESSs), renewable energy sources (RESs) and IBRs, and conventional power plants. It is useful for studying the dynamic interaction between different services and hence has some merits for minimising the required services for stabilizing the system from frequency stability view of point.
2. Phase II of the project develops new dynamic and static metrics for providing a better understanding of the active power balance and frequency stability of the NEM power system. The designed metrics are intended to provide the required knowledge to the system operators in light of the required services and what actions are required to maintain the power system frequency stability.
3. Phase III takes advantage of the previously designed research phases on this project to evaluate and assess the dynamic response from a frequency stability view of point. In this regard, different scenarios are considered including future scenarios of power system transformation based on the integrated system plan (ISP), especially scenarios for 2030 and 2050. The outcomes of the assessment are intended to give the power systems operators and planners the required knowledge to consider risks and to optimally plan for power system transformation.
4. Phase IV investigates the capability of some future features of the grid for providing affordable services. The work has carefully and in-depth analysed the ability of eMobility, especially electric vehicles (EVs), and thermostatically controlled loads to provide an affordable reserve for controlling the frequency after severe contingencies and credible events. To this end, a new tool has been proposed to estimate the available contingency frequency control ancillary services (FCAS) from EVs and demand-side thermostatically controlled loads. The tool has estimated the EV demand on the system level in Australia for 2030 and 2050 based on the ISP's scenarios.
5. Phase V the looks at optimally setting the frequency controllers' and FCAS providers' parameters in order to achieve the best dynamic performance in power systems with high power share from IBRs, which enable power system transformation and energy transition.

The project focuses on services from regional perspectives, meaning that the project considers modelling the power systems as multi-machine interconnected power systems with focus on the multi-area modelling of the system and considering the boundaries between different power regions. This might be important to achieve regionalised services, e.g. the need for regionalised FCAS, which is still under investigation by the Australian Electricity Market Operator (AEMO).

The project is designed to answer some of the research questions presented in the GPST research roadmap. This project also looks at technical challenges presented to AEMO in operating the NEM. Our research team has done research to address some issues related to regionalisation of FCAS and inertia services, that would be provided as additional deliverable of the project. The completion of these additional deliverables is subjected to a next step of the research as future work.

Furthermore, the project has proposed a new sophisticated automatic generation control (AGC) system capable of enhancing the frequency response in modern power systems with a high-power share from renewable energy sources (RES) and inverter-based resources (IBRs), like National Electricity Market (NEM) system. The proposed AGC system is developed based on a revolutionary idea by modelling the interconnectors as unknown inputs, resulted in converting the centralised and quasi-decentralised AGC systems to fully decentralised systems. The main steps are introduced in Chapter 3 of this report and can be summarised as follows:

1- The load disturbances and RES variation are modelled as unknown disturbances to the frequency control model.
2- The interconnectors between different power regions are modelled as unknown inputs to the system.
3- A dynamic state estimator is developed for each power region based on a sophisticated unknown input observer.
4- The tracked internal states can be used to detect any issues with the system such as faulty measurements, cyberattacks, disturbances, etc.
5- The observer is developed to estimate the amount of active power imbalance (the total disturbances) in real-time manner which bring several advantages to control room of future that might be applied to future power systems.
6- An advanced optimal controller based on optimal control theory is then developed to control the frequency in each power region based on the developed AGC system.

Moreover, the project has reviewed the current situation of modern power systems, especially the NEM, and identified some issues and challenges that need to be carefully considered in order to enable the energy transition and power system transformation. The required actions to enable the energy transition from frequency stability and associated services viewpoints have been identified for NEM system which can be generalized for international power systems as well.

Based on the underway research and the achieved outcomes, the required future research and research questions are also identified. The project outcomes provide a clear vision on how to offer and handle the required frequency services during power system transformation and present sophisticated tools and controllers for operating the power systems under transition in stable, reliable and secure mode, especially from active power balance and power system frequency view of points.

The Project Assumptions on data, validation, and results

This proposed investigates the needed upgrades on frequency control ancillary services for enable energy transition towards almost 100% renewable energy sources integration with future power systems. The project highlights issues and challenges in current power systems from frequency view of point with focus on the NEM. However, due to the scale of the work needed to finalise this project and to get a comprehensive lessons and meaningful results in a short-term research, almost one year, several assumptions have been applied to the project. The assumptions were necessary due to the following reasons:

1- Data availability: the project is proposed under the assumption of the availability of real-world power system data required for simulation and analysis. Real-world data related to governor and control settings, models of governor-turbine systems used for analysing frequency in the NEM, detailed model of the NEM either in PSS/e and/or PSCAD, etc are also considered available at the design of this project. However, due to confidentiality, some of these data was not available. The team has overcome this obstacle by using typical data where possible to avoid any delay or uncompletion of the project in a timely manner.
2- Measurements availability: the project team tried to get some important synchronised measurements especially for the frequency in each power region and the active power flow through different interconnectors, where such measurements were not available due to confidentiality and because of such measurements were not available or not recorded in the past.
3- Model availability: the project was also designed in the view that the models that would be needed to driven a simplified low-order frequency response (SFR) model would be available. However, due to data confidentiality was not easy to get the model in a timely manner to complete the validation of the developed SFR model of the NEM by comparing to developed model to the detailed one and the RTDS model based

on part of the detailed NEM model. Likewise, the data from real-world events in NEM with synchronised measurements that needed for some validation studies were not available.

However, the above obstacles have been overcome through using common practice scientific techniques to either replace the required data with typical data and performing the validation using alternative methods that are acceptable in scientific community. Therefore, rational assumptions that are scientifically proven in literature are used in this project. These assumptions can be summarised as follows:

1. The typical data are used for modelling turbine-governor systems, controllers, swing-equations in power regions, etc. It is assumed that typical values would provide reasonable and correct conclusions and lessons just like real-world power systems. It is a rational assumption in academia proven by several literature which can also avoid the disclosure of confidential data that might harm the system security.
2. Simulation results obtained from other simulated detailed models are considered as measurements where real-world measurements can not be obtained. It is also a common practice to use such assumption when the real-world power systems measurements are not available.
3. Due to the unavailability of the NEM model (PSS/e and/or PSCAD) that affect some of the planned validation such as the validation of the developed SFR model using RTDS and the comparison between PSS/e and SFR model, other academically acceptable techniques are used to validate the developed methodologies. Such as the development of a system identification tool based on N4SID to estimate the data that should be used in SFR model including inertia, parameters of turbine-governor systems etc. The guidance of how to use such tool is provided in the next chapter with validation results.

The Project Report Organisation and The Link between Chapters to the Project Research Phases

As mentioned-above in the executive summary, the project is designed to investigate the frequency ancillary services required to enable power system transformation with a focus on the NEM. To this end, five different phases, i.e. Phases I-V, have been recommended in the proposal of this project. It is to acknowledge that it is not rational to look at these phases in a separate way because the frequency services are usually treated as a comprehensive framework to maintain the system stability and security from frequency framework. To the best of the authors, the report has been designed to highlight some of the phases in separate chapters where applicable, while some of other research phase combined together due to the fact that such research agenda in the different phases are designed to achieve high-level goals in securing and stabling power system frequency during energy transition. In what follows, the link between the chapters and phases I-V are provide:

1. **Chapter 1:** this chapter provides an overview of the frequency control framework in the NEM. It is necessary to provide the readers with the required knowledge of the NEM and its frequency control. However, a complete and an in-depth analysis of the current frequency control framework in the NEM as a result of the G-PST Stage 2 is available in [1]. The work in [1] by this G-PST project chief investigators provides a unique and critical analysis of the current FCAS and other frequency arrangements in the NEM with critical thinking results of the technical challenges that would impact power system transformation and the potential solutions. In fact, [] provides an alternative way to look at frequency control services especially during energy transition and could be considered as a research roadmap not only for systems like the NEM but also for international power systems from frequency services needed for energy transition. The authors work in [1], available online for the readers, with Chapter 1 covers a link between the different phases, i.e. Phases I-V.
2. **Chapter 2:** this chapter mainly covers research agenda of phase I with some parts related partially to phases II-III, such as the dynamic performance of interconnected power systems model through SFR modelling technique. In phase I, the low-order SFR model is driven theoretically. Then, the model mapped to the NEM to develop an SFR model with the same topology of the NEM. Due to unavailability of data/measurements/PSSe model of the NEM due to confidentiality, the validation has been done through developing a novel system identification technique based on N4SID tool to estimate the needed model parameters. Although the PSS/e model of the NEM was not available for this research to validate against it and against an RTDS model driven from the detailed model, the validation has been done based other generic models and the methodology of achieving low-order SFR model has been also validated using different methods including RTDS over 9-bus system. The Chapter 2 presents the developed methodology and some required results for the understanding of the report readers.

3. **Chapter 3:** this chapter provides a novel technique for designing and coordinating frequency controller in interconnected power systems, like the NEM system. It starts with an in-depth analysis of the current approach used for AGC system in the NEM and develops a novel method to improve the dynamic performance. It also introduces an observer to track internal dynamic states and develops a method to online estimate the total active power imbalance and disturbance in power systems. It develops two optimization techniques, one for optimal design of the observer in each power region that can result in a better coordination of frequency control in power systems and the other one is for optimal design of frequency controller to achieve the best combination of frequency services activation in different power regions in a response to a disturbance. The last one can be expanded to achieve the optimal activation of reserve needed for frequency control based on combination from different ancillary services resources, which can be considered as future work subjected to the availability of the data of the NEM. Therefore, this chapter focuses mainly in Phase V and provides good results align with phases II-III.
4. **Chapter 4:** this chapter is designed to address the phase IV research questions. The chapter mainly focuses on the consideration of demand-side in providing services from demand-side sources such as EVs and thermostatically controlled loads. The chapter includes a tool to estimate the EV demand in Australia in 2030 and 2050 based on the ISP scenarios. Additionally, it develops models of EV and thermostatically controlled loads. Furthermore, an aggregator based on SCIRO NEAR project data is developed to estimate the flexible demand that could be used to provide services for frequency control. Therefore, this chapter is dedicated for Phase IV with dynamic analysis and other results related to Phase II-III.
5. **Chapter 5:** this chapter provides further based on the knowledge gained from the project to provide critical thinking on inertia and FFR requirements to enable power system transformation in interconnected power systems, like the NEM.
6. **Other research outcomes in project publications:** this project has resulted in a number of publications either as direct results from the project or as a collaboration with other team through the project activities. So far, the project has resulted in 4 publication and there is an intention to write down 4 more publication based on this project outcomes. Ref. [2] provides an advanced optimisation technique for frequency controller setting to achieve optimal frequency dynamic performance and optimal allocation of services in different power regions. The same publication also uses Opal-RT to validate the results and properly acknowledge the support from G-PST Stage 2. Likewise, the work in [3] provide an advanced technique for frequency control which is partially supported by this G-PST project. Our work in [1] provides an overview of the current challenges and draws a research roadmap in frequency control services based on the authors' opinions. The other work by this project team in [4] suggests advanced AGC system for the NEM and compares with European interconnected power system frequency control practices. It also introduces a sophisticated observer for tracking dynamic states and optimisation for the frequency controller based on optimal control theory to achieve better dynamic performance. The aforementioned publications can be considered as further chapters/ appendix to this report considering the fact they are available online as open access publications.

Progress on Addressing The 2021 Research Roadmap Open Question

The research undertaken through the G-PST stage 2 project address important open questions identified in the 2021 G-PST Research Roadmap with focus given on the frequency services that needed for power systems to enable power system transformation. Although the focus of this project is given to the frequency services and related technical and metrics issues in the NEM, the results can be mapped for other interconnected power systems. The high-level progress is as follows: Open Question 1 is **30% completed**; Open Question 2 is **60% completed**; Open Question 4 is **40% completed**. These percentages are achieved based on the team experiences and evaluation of the work done through this project and the work that needs to be done in order to achieve the gaols of the G-PST stage 1 roadmap. However, the team recommends a regular update of the research roadmap. For the frequency control research roadmap, we suggest updating it based on our research published in [1].

The detailed research progresses addressing the open research questions in the research roadmap is given in the following Table:

Table 1.1. Research Progress on addressing open questions of the research roadmap

Open questions identified in the 2021 Research Roadmap	2022/23 Completed	2023/24 Expected
Open Question 1: What services are needed to achieve **the technical requirements** of Australia's future power grid to maintain?	**30%**	**70%**
The necessity for and the requirements of expanding frequency and voltage support services to the distribution grid in Australia need further studies.	50%	90%
There is an appetite to unlock flexibility, either by way of matching customer needs with Variable Renewable Energy (VRE), or providing a new level of system preparedness through applications such as virtual power plants (VPPs).	40%	70%
Flexibility, an attribute on top of all services, needs standalone research in the Australian grid.	-	50%
Open Question 2: Are **frequency support services** suitably configured to achieve the long-term interests of electricity stakeholders?	**60%**	**100%**
What type of resources and configurations are more efficient for Fast Frequency Response (FFR) provision?	70%	100%
Virtual inertia in existing (or future) wind farms	50%	100%
Open Question 3: Are voltage support services suitably configured to achieve the long-term interests of electricity stakeholders?	**-**	**40%**
Open Question 4: What **metrics** should be used to define services in IBR dominated grids?	**40%**	**80%**
Open Question 5: What [Essential System] services are needed to maximise the benefits of stakeholders and to achieve an at least cost transition?	-	50%

References:

[1] H.H. Alhelou, B. Bahrani, J. Ma, D. Hill, "Australia's Power System Frequency: Current Situation, Industrial Challenges, Efforts, and Future Research Directions", In IEEE TechRxiv, 2023.

[2] AX Irudayaraj, V. Veerasamy, M. Premkumar, M. Radzi, NB. Sulaiman, and H. Haes Alhelou, "Decentralized frequency control of restructured energy system using hybrid intelligent algorithm and non-linear fractional order proportional integral derivative controller", IET Renewable Power Generation, Jun 2023.

[3] H. H. Alhelou, N. Nagpal, N. Kassarwani and P. Siano, "Decentralized Optimized Integral Sliding Mode-Based Load Frequency Control for Interconnected Multi-Area Power Systems," in IEEE Access, vol. 11, pp. 32296-32307, Jun 2023, doi: 10.1109/ACCESS.2023.3262790.

[4] Haes Alhelou, Hassan; Bahrani, Behrooz; Ma, Jin, "An Affordable Sophisticated Frequency Control for Australian National Electricity Market System Considering Industry and Infrastructure Challenges", TechRxiv. Preprint 2023. https://doi.org/10.36227/techrxiv.22709575.v1

1. Chapter 1: An Overview of the NEM and its Frequency Control

Note: *Part of the work in this chapter has been developed based on the following preprint: H.H. Alhelou, B. Bahrani, J. Ma, D. Hill, "Australia's Power System Frequency: Current Situation, Industrial Challenges, Efforts, and Future Research Directions", In IEEE TechRxiv, 2023.*

This Chapter of the final report briefly introduces an overview of the National Electricity Market (NEM) system and its frequency control approaches and the associated services to stabilise the frequency across the system. For more details, readers are referred to our scientific paper [1] that comprehensively reviews the current situation of the NEM's frequency and the efforts by AEMO to maintain the system operated within desirable situations based on the frequency operating standard (FOS). Reference [1] provides an in-depth analysis of the frequency control ancillary services and highlights challenges and research gaps associated with frequency control during energy transition and beyond. It also presents recommendations to make modern power systems ready from their frequency control perspective for energy transition to achieve almost 100% penetration of renewable energy resources and inverter-based resources.

1.1. Introduction to the NEM

There are two main power systems in Australia, NEM in the eastern and south-eastern states and the Wholesale Electricity Market (WEM) in Western Australia. Additionally, there are several isolated systems in various territories. In terms of demand, installed generation capacity, and number of consumers, NEM could be considered to constitute a large power system. Both NEM and WEM are operated by AEMO, which acts as an independent system operator. NEM is an interconnected grid comprising several interconnected state-wise networks and approximately 45,900 MW of installed generation. The NEM spot pool market is operated by AEMO across the eastern states of the mainland and Tasmania, including the power regions of Queensland (QLD), New South Wales (NSW), Victoria (VIC), South Australia (SA), and Tasmania (TAS).

Figures 1.1 and 1.2 depict the different power regions in NEM and the topology of the connections. The QLD power region is connected to NSW through DirectLink and QNI interconnectors, while the NSW power region is connected to VIC through SNO. Currently, the SA power system is connected to the VIC transmission network using high-voltage direct current (HVDC) MurrayLink and AC VIC-SA, so-called the Heywood Interconnector, transmission links. TAS is connected to the power regions of the mainland through BassLink, which is an underwater HVDC link. Generally, these interconnectors (tie-lines) between different power regions in NEM forms a unique challenging system from frequency control, stability and security viewpoints. The power regions are connected radially, forming a stringy network topology, instead of forming a strong mesh connection due to the location and distribution of human and industrial activities in Australia. The Australian power system encounters technical challenges related to its stability and security due to its unique structure, and the Australian leadership of the world's deployment of RESs and rooftop photovoltaic systems, resulted in frequency and active power challenges witnessed in NEM before these types of issues had (will) been seen in other international systems.

Figure 1.1. Physical interconnection between power regions in the system of the NEM

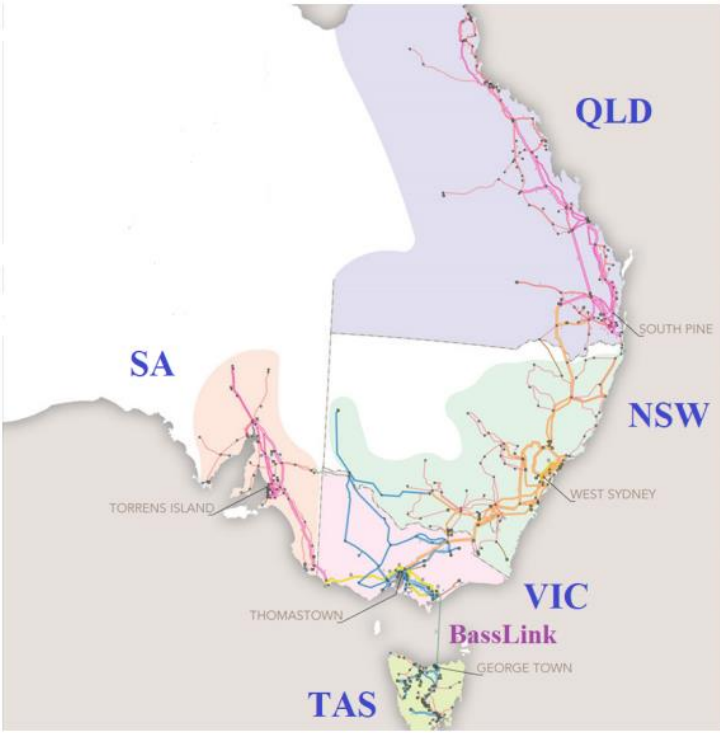

Figure 1.2. General topology under investigation and its sub topologies

1.2. The Market Bodies and National Energy Governance for the NEM

Australian national electricity market activities were initiated in all states in 1998 by the Energy National Cabinet Reform Committee (ENCRC). To enhance the management and operations of the energy market in Australia, ENCRC introduced three main bodies, namely the Australia Electricity Market Commission (AEMC) in 2005, the Australian Energy Regulator (AER) in 2005, and the aforementioned AEMO in 2009, to replace NEMMCO, which was responsible for operating the grid between 1998 and 2009. These active bodies are independent decision-makers with specified powers, boundaries, and liabilities that are designed to achieve the efficient operation of the electricity market in Australia.

AEMC makes the rules for electricity and gas services. It makes and amends the National Electricity Rules (NER), the National Gas Rules, and the National Energy Retail Rules and also provides market development advice to governments. AER is the regulator of the wholesale electricity and gas markets in Australia. AER can set prices and revenues for networks and is responsible for enforcing national regulations. AEMO is responsible for the real-time and day-to-day management of wholesale and retail energy market operations. AEMO serves as the ISO for the Australian energy systems and has statutory functions under the National Energy Laws. It is worth mentioning that AEMO is also the Victorian jurisdictional planning authority. In addition to the above technical and legislative bodies, the Reliability Panel and Energy Security Board (ESB) was created in 2017 to implement the recommendations of the Independent Review on the Future Security of the National Electricity Market, that is, the Finkel Review [1-3]. The ESB is made up of senior AEMC, AER, and AEMO leaders and plays a vital role in reviewing and updating grid operation requirements from reliability and security perspectives.

The aforementioned market bodies, panel, and board create integrity in the legislation, implementation, and enforcement of frequency control and active-power balance services in Australia's power system in terms of keeping it operating safely, stably, and securely. AEMC regularly reviews frequency stability and security in NEM based on technical reports it receives from AEMO, service providers, and stakeholders, especially TNSPs. It also receives rule change requests and reviews them based on technical advice from AEMO and experts. Its evaluation results are reported to ESB and higher legislative and governance bodies so that they can put forward and implement new rules or amendments to existing rules to keep the system operating in a best acceptable situation. On the other hand, AEMO, which is the technical operator of the grid, enforces the secure operation of the grid and takes all steps necessary to correct any frequency deviation and time error in both normal operations and during both credible and non-credible contingency events. To this end, AEMO utilizes several control schemes and management approaches to manage frequency fluctuations and deviations, which will be discussed in detail in the following sections. Furthermore, AEMO reviews frequency stability and security and publishes an informative periodic report known as the Power System Frequency Risk Review (PSFRR), which will be replaced by the General Power System Risk Review Report in 2023 (it is published now in May 2023) [4]. The continuous assessment of frequency stability and security by AEMO of Australia's power system along with the evaluation of the ancillary services contribute to the AEMC and ESB assessments that update the services and frequency control rules needed to keep the power system frequency operating securely in light of the current uncertainty, variability, and volatility in NEM.

1.3. The NEM’s Frequency Operating Standard

An understanding of the frequency operating standard (FOS) that is currently in place in the Australian power system is crucial for appreciating the significant efforts that are being undertaken by different market bodies to maintain the stability and security of the NEM’s grid. An evaluation of the frequency control of the power system and its effectiveness and challenges is also essential. In Australia, there are two different frequency bands in the FOS, one for the mainland power system and the other for Tasmania’s grid. In fact, HVDC Basslink is the main connection between Tasmania and the mainland system. It is, therefore, partially acceptable as well as technically feasible to have two different FOSs for the time being, although the inconsistency in the FOSs can limit effective collaboration in terms of frequency support in the interconnected power system.

The FOSs in the mainland and TAS power grids contain two essential parts, i) frequency bands and ii) required frequency outcomes as defined by the required time scales for each response [5]. The frequency bands adopted in both the mainland and the TAS systems are given in Table 1.1. The frequency response time scales required based on FOS are depicted in Figure 1.3. It is worth mentioning that in 2021/2022, AEMC and AEMO introduced a mandatory primary frequency response to enhance the frequency stability and power quality by keeping the frequency operating within 49.95-50.05 Hz whenever possible, which will be discussed in the next sections. However, such changes have not yet been reflected in the FOS of NEM.

Table 1.1. Frequency Bands defined in Australian FOS

Frequency Bands in FOS		NOFB (Hz)	NOFB (Hz)	OFTB (Hz)	EFETL (Hz)
Normal	Mainland	49.85 – 50.15	49.75 – 50.25	49.0 – 51.0	47.0 – 52.0
	Tasmania	49.85 – 50.15	49.75 – 50.25	48.0 – 52.0	47.0 – 55.0
Island	Mainland	49.5 – 50.5	49.5 – 50.5	49.0 – 51.0	47.0 – 52.0
	Tasmania	49.0 – 51.0	49.0 – 51.0	48.0 – 52.0	47.0 – 55.0
SC	Mainland	49.5 – 50.5	49.5 – 50.5	48.0 – 52.0	47.0 – 52.0
	Tasmania	N/A	N/A	N/A	N/A

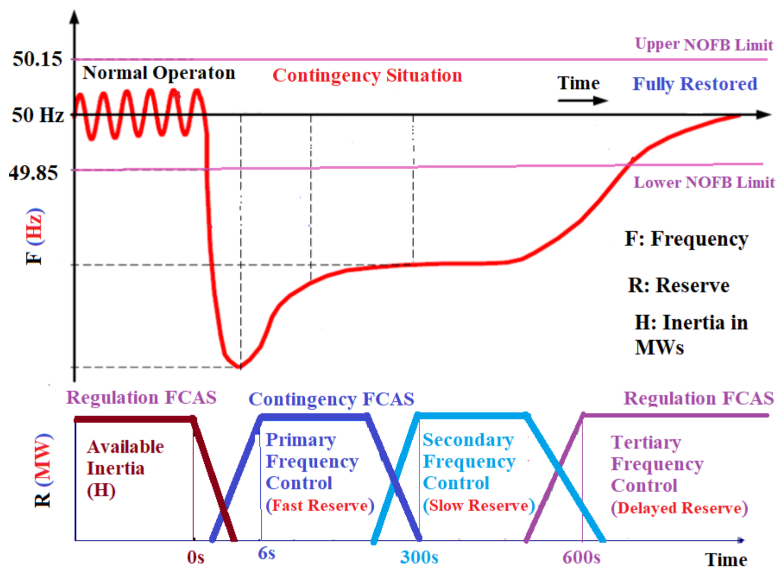

Figure 1.3. Graphical illustration of FOS in NEM with the activation time of each FCAS market

Since it is impossible to avoid the occurrence of disturbances in power system operations, credible or non-credible events, cascading events, and system separations due to natural events or other reasons and due to the unique design of the system in Australia, FOS introduces a large flexibility, known as required frequency outcomes, to the operator to have the required time for correcting the frequency in the system. In fact, the required frequency outcome is a compromise between the system operator capability and the dynamic constraints to achieve best frequency operation in order to maintain overall stability and security with minimum operation costs. The required frequency outcomes defined for Australia's power system are classified based on the event type and are summarised as follows: **i) accumulated time error limit (ATEL):** less than 15 seconds ATEL for both the Mainland and TAS except for island situations, during supply scarcity, or following a multiple contingency event (it is to mention that the ATEL is now removed from the updated FOS [5-6]); **ii) generation event/load event:** the frequency shall not be outside of the applicable normal operating frequency band (NOFB) for more than 5 minutes in the Mainland and 10 minutes in Tasmania, respectively; **iii) network event:** the frequency shall not be outside of the applicable operational frequency tolerance band (OFTB) and NOFB for more than 1 minute and 5 minutes in Mainland, while is allowable to be 10 minutes outside NOFB in Tasmania; **iv) separation event:** the frequency should be operated within the island band and should not be outside the NOFB for more than 10 minutes for both systems; **v) protected event:** the frequency shall be within extreme frequency excursion tolerance limit (EFETL) and should be returned to the NOFB within 10 minutes in both systems while there is no contingency event, however it is worth to mention that AEMO defines a protected event as an event with a low likelihood, high consequence non-credible contingency event, e.g. the loss of multiple transmission elements causing generation disconnection in a power region during periods where destructive wind conditions are estimated, for which AEMO must maintain the frequency operating standards following the occurrence of the event; **vi) non-credible contingency event/multiple contingency event:** the frequency shall be within EFETL and should be returned to the NOFB within 10 minutes in both systems while there is no contingency event. Readers interested in FOS in Australia are referred to [1] and [5].

1.4. Frequency Support Services in the NEM

The services that are provided to Australia's power system that are aimed at keeping the active power balance and frequency within permissible limits include an inertia responsiveness service, primary frequency control, secondary frequency control known as automatic generation control (AGC), and tertiary frequency control. In addition to these main regulatory and ancillary services, emergency services are also being adopted to correct the frequency decline during larger disturbances, including during credible and non-credible events.

The Frequency Control Ancillary Services (FCAS) that are defined for NEM include regulation FCAS and contingency FCAS. The FCAS market is divided into eight different markets, which are summarised in Table 1.2. AEMO controls regulation FCAS, and the generators that provide regulation FCAS should maintain the frequency of between 49.85Hz and 50.15Hz [5], while contingency FCASs are locally controlled and their availability and activation are monitored by AEMO. Measures to correct the frequency in contingency events include generator governor response, load shedding, rapid generation, and rapid unit unloading. Since the battery storage system can take charge and discharge, it can rapidly increase and decrease its power output/input. When there is a contingency event, e.g., a generation deficit due to a generator set accident or a sudden reduction in large-scale loads such as in factories, the electricity system's frequency will suddenly change. The grid can purchase electric energy in the contingency FCAS market to stabilise the frequency. In Australian NEM, different markets can act according to the scale of the crisis of the contingency event. The Contingency FCAS services are provided within the time required by their markets, respectively, such as the immediate raise service will be delivered within 6 seconds of a contingency event. When there is a small deviation in frequency, regulation FCAS can provide frequency regulation services by increasing or decreasing the active power injected into the system. The time response frames of different regulation FCAS and contingency FCAS markets are depicted in Figure 1.2. It is worth mentioning that battery energy storage systems (BESSs), such as Hornsdale Power Reserve BESS, are currently being registered and are contributing to frequency control by participating in the eight FCAS markets defined in NEM. In mid-2019, AEMO has initiated a virtual power plant (VPP) trials, the AEMO's VPP Demonstrations, that are currently being implemented/tested in NEM in terms of their opportunities and challenges in order to officially approve the concept in NEM, which will be important for providing additional support to FCAS during the system transformation. The AEMO VPP Demonstrations are a collaboration between AEMO and the Australian Renewable Energy Agency (ARENA), AEMC, AER, and members of the Distributed Energy Integration Program. However, the main focuses of AEMO's VPP trial are on the contingency FCAS market, and on confirming the concept's capability to support the contingency FCAS market. It should be mentioned that in addition to the eight FCAS markets divided into either contingency or regulation services, there is an expectation that new markets will be introduced, such as inertia and very fast frequency response services. In fact, AEMC has already published National Electricity Amendment, i.e., Fast Frequency Response Market Ancillary Service, on Rule 2021 No. 8, which requires AEMO to set up two markets for very fast frequency responses. The uniqueness of the NEM system, the high levels of RESs and IBRs in the system, and system uncertainties lead to regular reviews of and updates to the FCAS markets.

Table 1.2. FCAS markets and their required outcomes in NEM

FCAS Type	Response Time (Sec)	Market-Type
Contingency	6	Fast Raise
	6	Fast Lower
	60	Slower Raise
	60	Slower Lower
	300 (5min)	Delayed Raise
	300 (5min)	Delayed Lower
Regulation	Continuous	Regulation Raise
	Continuous	Regulation Lower

1.5. Conclusion

This chapter provided a brief introduction about the National Electricity Market System from frequency control view of point. The briefly information introduced in the above sections within Chapter 1 is important for the readers of the next chapters, where an overview of the NEM's topology is provided in addition to an introduction the frequency operating standard that is adopted in the NEM. Furthermore, a brief introduction to the frequency control ancillary services defined for the NEM and a description of their regulation and contingency FCASs are provided. Readers are highly encouraged to go through [1] which provides the necessary information about the Australia's NEM frequency control with focus on the current situation, AEMO's efforts, and the future research directions.

References

[1] H.H. Alhelou, B. Bahrani, J. Ma, D. Hill, "Australia's Power System Frequency: Current Situation, Industrial Challenges, Efforts, and Future Research Directions", In IEEE TechRxiv, 2023.

[2] AEMO, "Integrated system plan for the national electricity market," Australian Energy Market Operator, 2018.

[3] C. E. Council and M. Operator, "Energy security board," Retreived March, vol. 13, p. 2018, 2017.

[4] AEMO, "2022 power system frequency risk review," Australian Energy Market Operator, 2022. [Online]. Available: https://aemo. com.au/en/energy-systems/electricity/national-electricity-market-nem/ system-operations/power-system-frequency-risk-review

[5] AEMC, "Frequency operating standard - effective 1 january 2020," Reliability Panel, The Australian Energy Markets Commission, 2020

[6] AEMC, "Frequency Operating Standard – The updated version effective 9 October 2023", The Australian Energy Markets Commission, 6 April, https://www.aemc.gov.au/market-reviews-advice/review-frequency-operating-standard-2022

2. Chapter 2: Advanced Low-order System Frequency Response Model to Facilize Frequency Support Studies for Power System Transformation

Note: *Part of the work in this chapter is under preparation for a paper.*

The system frequency response model describes the average network frequency response in one power region after a disturbance and has been applied to a wide variety of dynamic studies. There are few attempts in literature to develop the first introduced model by P. M. Anderson in 1990 [1-3]. However, the traditional literature does not provide a generic method for obtaining the system frequency response (SFR) model parameters when the system contains multiple generators; instead, a numerical simulation-based approach or the operators' experience is the common practice to obtain an aggregated model. Likewise, the model developed in literature is for traditional power systems and there is no sophisticated model that consider emerging sources of services combined together to support frequency in modern power systems. Furthermore, there is no SFR model in literature that comprehensively considers future scenarios such as the contribution of EV and combined such contributions to frequency from EVs with other frequency support service providers. Moreover, there is no developed SFR model in literature that considers the combination of interconnectors in such a way to mimic reality. Therefore, the aim of such research is to solve the research gaps and propose a low-order system frequency response model that considers service providers from both demand and generation sides. Likewise, the virtual inertia concept is included in the model. This work also proposes an advanced technique to estimate the parameters' values for SFR model using real-world system measurements and data. In this regard, an advanced subspace system identification technique-N4SD is proposed for estimating the data and identifying the suitable model's dynamic order. The developed low-order SFR model is applicable for multi-machine multi-area interconnected power systems as well. The proposed low-order SFR model has several applications including system frequency control, frequency stability, and dynamic model reduction. The results show the method is promising with broad potential applications. Likewise, the model is useful for identifying challenges and issues related to frequency control and stability and is unique for understanding the requirements of regional inertia and frequency control ancillary services.

2.1. An overview of the proposed SFR and its applications

This Section of the G-PST Topic 6's report covers the research outcomes from the Phase I of the project which focuses on developing a low-order system frequency response (SFR) model. This G-PST project has developed an advanced and effective mathematical system frequency response model that is suitable for developing and validating frequency support services considering the generation and storage mix in today's Australian power systems (especially for NEM system) with ability to extend for future Australia's grids based on the decarbonization 2050 plan and G-PST roadmap. The model provides good benefits for the G-PST project and other ongoing research activities related to frequency support worldwide which is adopted in Topic 6 and has potential applications in other Topics as well for validating the frequency support services from different service providers. It can be used for investigating the frequency stability and frequency control design and validation. The developed new SFR model considers the roadmap of future Australia's power systems especially the consideration of ISP's scenarios, meaning that the SFR is designed in such a way that it can be easily used and modified by G-PST team and AEMO for benefiting both Australian researchers, engineers, and industry stockholders, by making the developed SFR model user-friendly. Furthermore, the model takes into account different frequency service types from RESs and IBRs that are currently available in Australian grid or that would be considered in the future during or after the transformation. Moreover, the model is developed considering different parties in both demand and generation sides that can participate in frequency support services and other services related generation-demand balance services, including demand response programs, ESSs, VPPs, modern flexible semi- dispatchable RESs, and DGs. One of the other advances in the model is the ability to model and consider virtual inertia concept for supporting the frequency and RoCoF in power systems during the energy transition and beyond. It is worth mentioning that AEMO has used a low-order frequency control model to conduct the PSFRR and GPSRR for the past 5 years to determine the impact of non-credible contingencies. It will be useful to model and do analysis for future industry and research reports. This can bring benefits to advance the currently used models by national and international system operators and help including future features such as advanced demand response programs and aggregators such as electric vehicle (EV) aggregators that would be used for frequency support during power system transformation.

As per the project's proposal and to harvest the maximum benefits of the advanced model, the proposed SFR model is developed based of the exact recent topology of electrical connections among the different power regions and states in Australia's national electricity market's power system. The model also considers different types of tie-lines (so-called major interconnectors) and major transmission lines between the different power regions, for example AC major transmission lines, Thyristor Controlled Phase Shifters (TCPSs), and HVDC links. For instance, the belo-mentioned HVDC links in Australia are considered: i) the Basslink which is an HVDC link between Victorian and Tasmanian transmission grids, ii) the Directlink (Terranora) Interconnector which is an HVDC link connecting transmission systems of NSW and Queensland, and iii) Murraylink which is high voltage DC link connecting Victoria and South Australia. It is worth mentioning that modeling these HVDC and other type of links is of great importance for frequency support since some of these links can actively contribute to frequency regulation and support in the National Electricity Market (NEM), while more services are being absorbed from high voltage DC link especially in European grid, which is being operated under European Network of Transmission System Operators for Electricity (ENTSO-E), and North America's power systems. It is worth mentioning that the Basslink interconnector as an HVDC link can help with mainland frequency in the NEM. The other HVDC links in the NEM are parallel to major AC interconnectors and therefore would only transfer more power on to the AC parallel link since generator dispatch targets will not change because of MW changes to the DC link setpoint. During contingencies the generators will respond according to the PFR or FCAS arrangements, meaning the AC interconnector would still transfer frequency response between power regions.

This Phase of the project develops a set of models for different purposes and applications. Nevertheless, the main focus is given to the general model which mimics the National Electricity Market system, i.e. NEM system, which is comprised of five physically connected power regions on the east coast of Australia: Queensland, New South Wales (which includes the ACT), Victoria, Tasmania, and South Australia. Another advantage of the proposed model is the flexibility of modifying the developed topology so that it can be easily modified based on G-PST and AEMO requirements. The obtained results of this Phase confirm the usefulness of the developed SFR model for several frequency support studies including (but not limited to): i) investigating the frequency stability of system under different generation-storage mix; ii) understanding the FCAS requirements of services to support frequency in interconnected systems; iii) understanding the hosting capacity of inertia-free energy sources in modern power systems; iv) understanding the FCAS requirements in different power regions; v) understanding the virtual inertia requirements in each power regions; vi) identifying the requirements of frequency support from neighbour power regions to stabilise frequency in the power region of interest; vii) estimating the frequency response characteristics in different power regions due to credible contingencies; viii) understanding the requirements of interconnectors to stabilise frequency in interconnected power systems ; ix) the usefulness for determining the optimal requirements for supporting the frequency response in different power regions; x) optimal design of frequency controllers for improving frequency response in IBR-dominated power systems.

2.2. The proposed methodology to achieve the advanced SFR

To develop the advanced low-order system frequency response model, a clear and straightforward methodology is proposed in this project. First the full-order dynamic model of synchronous generating units has been carefully studied. The dynamics that have direct impact on the frequency response in the generating unit are carefully considered. In the contrast, the dynamics with no effective impact on the frequency are neglected to reduce the order of the whole model in order to achieve the target model of the developed low-order SFR model. The control loops that have impact of the frequency response are considered. For instance, the governor-turbine system has direct impact on the frequency response in both generating units and the system. However, most of turbine-governor systems are with very high-order dynamic models involving complexities comes from their nonlinearities, such as governor deadband (GDB), generation rate constraint (GRC). It is mandatory to get a suitable low-order model of governor-turbines systems. Therefore, suitable models for different types of power plants, e.g. gas-turbine, thermal-turbine without reheat system, thermal turbine with reheater, hydro turbine, are considered and suggested.

In addition to the major frequency support services that are provided by synchronous generating units, the IBRs have started entering the market for the provision of frequency support services, e.g. FCAS and virtual inertia services. Therefore, there is an urgent need to include them in the developed SFR model. In this regard, suitable low-order frequency response models of IBRs are also considered in this project. In fact, this part of the project is essential to consider future power system transformation scenarios in the developed model and make the developed

SFR model useful for studying the impact of integrated system plan (ISP) scenarios on the frequency during the energy transition and beyond. This is also vital for understanding the possible shortfall of FCAS and inertia services in some regions of the system during the energy transition.

The next stage of the developed methodology to achieve the advanced SFR model is the consideration of the demand-side potentials for providing services to support the frequency in the current power systems and future systems during the transformation and beyond. Since it is expected that the demand-side would play a vital role for supporting the frequency by offering affordable sources of FCAS services, the possibilities for involving the demand-side in the provision of FCAS and inertia services are also considered. In this regard, a suitable frequency response model of demand response is suggested to be integrated to the developed advanced SFR model.

To make the model more suitable for existing interconnected power system topology, the developed methodology proposes using the same exact topology of interconnected power systems. To this end, the power regions of interest can be identified by the system operator based on coherency between a fleet of generating units and IBRs in a specific geographical region. The other way to specify the power regions is to divide the system based on the load centers or state-wise power regions. However, these options give the power system operator the flexibility to choose the most suitable way based on its goals and operation rules. After specifying the number of power regions and their geographical and power borders, each power region is modeled using the suggested low-order system frequency response models of different frequency support service providers, e.g. equivalent synchronous generating units considering different types of them based on the generation mix available at the operation period of interest to the operator, different IBRs providing FCAS and virtual inertia services, and demand-side participants including future scenarios such as potential FCAS services from EVs, etc.

In the last stage of the proposed methodology, the integration between different power regions is made using the exact topology of the interconnected power system. To this end, the tie-lines between different power regions are also modeled considered their frequency response model. It is to mention that the suitable frequency response models of different types of interconnectors are suggested and studied later in this Phase of the project. In some interconnected power systems, HVDC does not fully equipped with primary frequency response control loops, therefore, this fact is also considered and investigated to show the advantage and disadvantage of such operation practice in modern power systems. The AC tie-lines are modeled using their power transfer model and then the system frequency response model of such interconnectors is developed. In the final stage, the AC interconnectors supplied with thyristor controlled phase shifter (TCPS) is also considered in the developed advanced SFR model in this project. In the next subsections, the different stages of the proposed methodology to achieve the advanced SFR model is presented mathematically and discussed in details.

2.3. Full-order frequency response model of synchronous generating units-based power plants

Energy systems are among the most complex systems built by the humankind during the history. The heart of energy systems are power systems. Generally, power systems comprise three major parts including electricity generation, its transfer using transmission and distribution levels (upstream and downstream levels) and the consumption of electricity. Figure 2.1 depicts the generic structure of power systems that can be used for studying their dynamics. The generation-side is responsible for converting the primary energy sources to electricity, where the synchronous generating units are still serving as the backbone in such conversion systems. However, the synchronous generating units will be replaced with inverter-based resources to facilize the integration of renewable energy resources to modern power systems.

In conventional power systems, the demand-side was the sources of uncertainties and variations that could impact the generation-demand balance, where the generation-side was the source of ancillary services (such as FCAS) to support the active power balance and maintain the frequency within permissible limits. However, this fact is being changed by raising the generation-side to be a source of uncertainties and making the demand-side the sources of services by offering affordable ancillary services including FCAS services. These changes need to be considered in the system frequency response models for power systems going through energy transition. However, the synchronous generating units-based power plants are still the source of dominate dynamics the drive frequency response in power systems due to different types of disturbances, contingencies and events. Therefore, their dynamics should be considered carefully when frequency response of interconnected power systems is assessed during the mid-term of future energy transition.

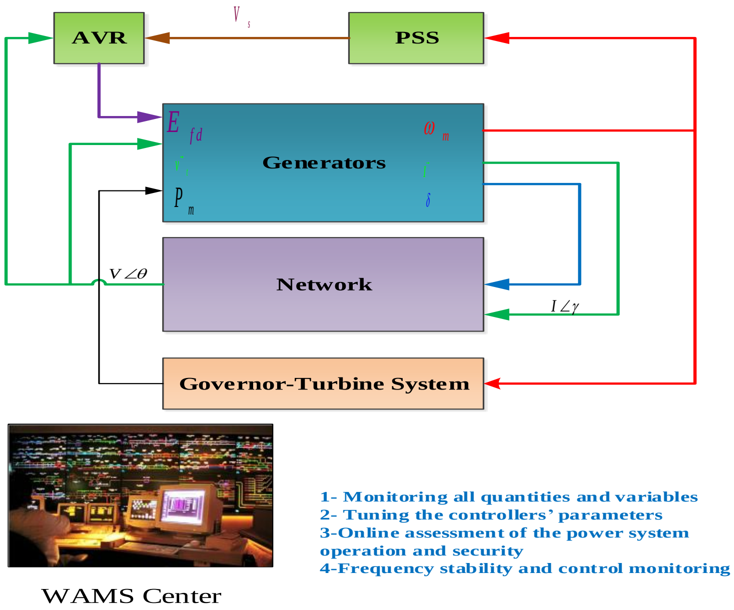

Figure 2.1. The generic structure of power systems

From frequency response's perspective, the power systems can be defined as a combination of mechanical and electrical component integrated together to satisfy the aims of energy system sectors at any country. It is not an easy task to operate a such complex system in safe, reliable, economic and secure modes due to its complexity and high separation over wide geographical areas. Due to complexity and computation burden, many models have been developed over the last decades to study power systems focusing on the issue of interest. Such models have been found effective and useful where low-order SFR model is one of famous models that has several important applications in both academia and industry. The simplification of generation-side model by removing the dynamics that do not have direct impact on the frequency is an important task. Although, there are many models of the generating units based on the aim of the study. In what follows, its detailed dynamic model for studying the frequency dynamics in the system is introduced, then the model is simplified for reducing the order of system frequency response model of synchronous generating units. In the next stage, the low-order frequency response models of different types of governor-turbine systems are driven for integrating them in the developed advanced SFR model.

Let define a power system containing G generators, B buses, and L loads. As this study focus on the operation and control of complex power systems, it is assumed that each generator busbar is supplied with a suitable phasor measurement unit (PMU) or a suitable measurement device to enable online monitoring of the dynamic behavior of the system in the control room at the wide-area measurement system (WAMS) or SCADA center. The generic topology such model is depicted in Figure 2.1. In what follows, we look at the different parts of such model to obtain the low-order system frequency response model.

The sixth-order sub-transient model is considered as one of the full-order models for studying the synchronous generator dynamic behavior under both normal and abnormal operating conditions. This sub-transient model considers 6 dynamic states (state variables), i.e. the frequency which is equal to the rotor speed of the generator in per unit ω, the position of the machine rotor so-called the rotor angle δ, the transient voltage due to the flux in q-axis E'_d, the transient voltage due to field flux linkage E'_q, the sub-transient voltage because of d-axis damper coil ψ_{1d}, the sub-transient voltage because of q-axis damper coil ψ_{2q} [4-7]. The sixth order dynamic model based on the aforementioned variables can be presented as a set of differential-algebraic equations describing the dynamics of the synchronous generators, as follows,

$$\dot{\delta}_i(t) = \omega_{bi}(\omega_i(t) - \omega_{si}) \quad (1)$$

$$\dot{\omega}_i(t)=\frac{\omega_{si}}{2H_i}\left(\begin{array}{l} P_{mi}(t)-(x''_{qi}-x''_{di})i_{di}(t)i_{qi}(t)-D_i\,\omega_i(t)+D_i\,\omega_{si}(t)-\frac{x''_{di}-x_{si}}{x'_{di}-x_{si}}E'_{qi}(t)i_{qi}(t) \\ -\frac{x'_{di}-x''_{di}}{x'_{di}-x_{si}}\psi_{1di}(t)i_{qi}(t)-\frac{x''_{qi}-x_{si}}{x'_{qi}-x_{si}}E'_{di}(t)i_{di}(t)-\frac{x'_{qi}-x''_{qi}}{x'_{qi}-x_{si}}\psi_{2qi}(t)i_{di}(t) \end{array}\right) \tag{2}$$

$$\begin{aligned}\dot{E}'_{qi}(t)&=\frac{1}{T'_{di}}(-E'_{qi}(t)-(x_{di}-x'_{di})(i_{di}(t)-E'_{qi}(t)\\&-\frac{x'_{di}-x''_{di}}{(x'_{di}-x_{si})^2}(\psi_{1d}(t)+(x'_{di}-x_{si})i_{di}(t)))+E_{fdi})\end{aligned} \tag{3}$$

$$\dot{E}'_{di}(t)=\frac{1}{T'_{qi}}(-E'_{di}(t)+(x_{qi}-x'_{qi})(i_{qi}(t)+E'_{di}(t)-\frac{x'_{qi}-x''_{qi}}{(x'_{qi}-x_{si})^2}(\psi_{2q}(t)+(x'_{qi}-x_{si})i_{qi}(t)))) \tag{4}$$

$$\dot{\psi}_{1di}(t)=\frac{1}{T''_{di}}\left(-\psi_{1di}(t)+E'_{qi}(t)-\left(x'_{di}-x_{si}\right)i_{di}(t)\right) \tag{5}$$

$$\dot{\psi}_{2qi}(t)=\frac{1}{T''_{qi}}\left(-\psi_{2qi}(t)-E'_{di}(t)-\left(x'_{qi}-x_{si}\right)i_{qi}(t)\right) \tag{6}$$

The above-presented dynamics describe the dynamics of the ith synchronous generator only. These dynamics in reality are being driven by a set of controllers including active power control loop through the governor-turbine system (control loop), voltage control loop using the automatic voltage regulator (AVR), and damping low-frequency oscillations by external injected control signal to the voltage control loop by the power system stabilizer (PSS). However, not all generating units are supplied with PSS, while all generating units are assumed to be equipped with AVR and automatic generation control (AGC). In term of AGC, there are different control levels (loops) including primary control loop applied locally and directly through the governor droop characteristics, the secondary control loop which is also known as load frequency control loop (LFC) which is a centralized or quasi-decentralized approach requires remote signals/measurements to be implemented, and the tertiary control level which is not a direct control (it is an economic dispatch more than a control mechanism that can impact the frequency response in a power system).

Unlike the synchronous generating units, there are several types and structures of the aforementioned controllers making it as an impossible task to come up with a full-order generic model. The majority of such controllers and their high-order dynamic models are available by IEEE in [5]. However, it is achievable to obtain a low-order model of the full order models of different controllers by using advanced system identification techniques, where we propose and discuss such techniques in the following sections. The full-order model of the well-known and commonly-used types of the above-mentioned controllers are introduced in what follows. For the automatic voltage regulator, AVR-DC4B and AVR-STA1 models are briefly introduced. The block diagrams of the dynamic models of AVRs and PSS are depicted in [4]. The dynamics of the excitation control (AVR system) of IEEE-DC4B are as follows,

$$\dot{E}_{fdi}(t)=\frac{1}{T_{Ei}}\left(-\left(K_{Ei}+A_{xi}e^{B_{xi}E_{fdi}(t)}\right)E_{fdi}(t)+V_{Ri}(t)\right) \tag{7}$$

$$\begin{aligned}\dot{V}_{Ri}(t)&=\frac{1}{T_{Ai}}(-\frac{K_{Ai}K_{Fi}}{T_{Fi}}E_{fdi}(t)-V_{Ri}(t)+K_{Ai}R_{fi}(t)\\&+K_{Ai}\left(V_{refi}-V_{si}(t)-v_i(t)\right))\end{aligned} \tag{8}$$

$$\dot{R}_{fi}(t) = \frac{1}{T_{Fi}}\left(\frac{K_{Fi}}{T_{Fi}}E_{fdi}(t) - R_{fi}(t)\right) \tag{9}$$

$$\dot{E}_{fdi}(t) = \frac{1}{T_{Ri}}\left(K_{Ai}\left(V_{ref} - V_{si}(\mathrm{t}) - \mathrm{v}_i(\mathrm{t})\right) - E_{fdi}(t)\right) \tag{10}$$

It can be seen that there is an external signal, i.e. v_{si}, injected into the above-presented model of IEEE-DC4B excitation system. This signal is the output of an external controller used to stabilize the low-order frequency oscillations using PSS. The goal here is to damp the local and inter-area oscillations to keep the power system operated in a stable mode. The common generic model of the power system stabiliser is given below,

$$V_{si}(\mathrm{t}) = \frac{K_{pi}T_{1pi}T_{3pi}}{T_{2pi}T_{4pi}}(\omega_i(\mathrm{t}) - \omega_{si}) + y_{1p}(\mathrm{t}) + y_{2p}(\mathrm{t}) + y_{3p}(\mathrm{t}) \tag{11}$$

$$\dot{y}_{1pi}(\mathrm{t}) = \frac{1}{T_{wi}}\left(T'_{pi}(\omega_i(\mathrm{t}) - \omega_{si}) - \mathrm{y}_{1pi}(\mathrm{t})\right) \tag{12}$$

$$\dot{y}_{2pi}(\mathrm{t}) = \frac{1}{T_{2pi}}\left(T''_{pi}(\omega_i(\mathrm{t}) - \omega_{si}) - \mathrm{y}_{2pi}(\mathrm{t})\right) \tag{13}$$

$$\dot{y}_{1pi}(\mathrm{t}) = \frac{1}{T_{4pi}}\left(T'''_{pi}(\omega_i(\mathrm{t}) - \omega_{si}) - \mathrm{y}_{1pi}(\mathrm{t})\right) \tag{14}$$

T'_{pi} , T''_{pi}, and T'''_{pi} are as follows,

$$T'_{pi} = \frac{-K_{pi}T_{\omega i}^2 + K_{pi}T_{\omega i}T_{1pi} + K_{pi}T_{\omega i}T_{3pi} - K_{pi}T_{1pi}T_{3pi}}{\left(T_{\omega i} - T_{2pi}\right)\left(T_{\omega i} - T_{4pi}\right)} \tag{15}$$

$$T''_{pi} = \frac{-K_{pi}T_{\omega i}T_{1pi}T_{2pi} + K_{pi}T_{\omega i}T_{1pi}T_{3pi} + K_{pi}T_{\omega i}T_{2pi}^2 - K_{pi}T_{\omega i}T_{2pi}T_{3pi}}{T_{2pi}\left(T_{\omega i} - T_{2pi}\right)\left(T_{2pi} - T_{4pi}\right)} \tag{16}$$

$$T'''_{pi} = \frac{(K_{pi}T_{\omega i}T_{1pi}T_{3pi} - K_{pi}T_{\omega i}T_{1pi}T_{4pi} - K_{pi}T_{\omega i}T_{3pi}T_{4pi} + K_{pi}T_{\omega i}T_{2pi}T_{4pi}^2)}{T_{4pi}\left(T_{\omega i} - T_{4pi}\right)\left(T_{4pi} - T_{2pi}\right)} \tag{17}$$

The above mathematical model of PSS and AVR shows that there is no direct impact of such control loops on frequency control and active power control. In fact, the frequency and active power are controlled using another controller, so-called governor-turbine system, which is responsible of adjusting the generated active power based on the control setting point or the preference of the system operator.

The frequency is controlled in power system to control another important matter which is the active power imbalance between generation and demand. In reality, it is not easy (infeasible task) to determine the active power imbalance directly. Interestingly, the frequency deviation has a relationship with active power imbalance between generation and demand (adding power transfer losses either to generation and demand sides). If the frequency deviation is zero (considering there is no faulty or error measurements), this means that the active generated power exactly matches the demand of active power. If the generation is higher than the demand, then the frequency raises to be above its nominal value, reflecting the fact since the generating active power is higher than the demand, the generators will start accelerating to reach a higher speed than their nominal rotating speed. In the contrast, if the frequency drops below its nominal value, this is a direct reflection of the fact that the active power demand is higher the generation, presenting that the load demands higher power leading to higher loading on the generating units which results on decelerated to reach a lower rotating speed. In per unit system, the rotating speed is equal to the frequency, therefore, the frequency is the electric speed of the generating units while the rotating speed is the mechanical one. The above facts of power systems help developing mechanisms for controlling and maintaining the active power balance and frequency in power systems by measuring the frequency and calculating the frequency deviation. The frequency deviation is used to feed the primary controller so that the mechanical torque (mechanical power) will be controlled using the governor of the mechanical turbine. If the generating unit is selected to provide secondary frequency control (the unit is supposed to maintain secondary reserve), then an additional control signal will be applied. Such a control signal will be generated in the control center based on the area control error (ACE) and sent to the selected unit using the available ICT infrastructure.

The dynamics of the governor-turbine systems are the most impactful dynamics on the frequency of the system. However, such dynamics are slower than those provided by AVRs. The tandem-compound single and double reheat steam thermal turbines with Westinghouse electro-hydraulic governing system is the widely-used system in power plants. The dynamics can be presented as a set of differential equations as given below including the nonlinearities such as GDB and GRC [5-7]. The turbine dynamics are as follows,

$$\dot{P}_{1Ti}(t)=\frac{1}{T_{1Ti}}\left(sat_{\min}^{\max}\left(P_{2gi}(\mathrm{t})-\mathrm{P}_{1Ti}(\mathrm{t})\right)\right) \tag{18}$$

$$\dot{P}_{2Ti}(t)=\frac{1}{T_{2Ti}}\left(P_{1Ti}(\mathrm{t})-\mathrm{P}_{2Ti}(\mathrm{t})\right) \tag{19}$$

$$\dot{P}_{3Ti}(t)=\frac{1}{T_{3Ti}}\left(P_{2Ti}(\mathrm{t})-\mathrm{P}_{3Ti}(\mathrm{t})\right) \tag{20}$$

$$\dot{P}_{4Ti}(t)=\frac{1}{T_{4Ti}}\left(P_{3Ti}(\mathrm{t})-\mathrm{P}_{4Ti}(\mathrm{t})\right) \tag{21}$$

The governor system dynamics including GDB and GRC are as follows,

$$\dot{P}_{1gi}(t)=\frac{1}{T_{1gi}}(K_{1gi}(1-\frac{T_{2gi}}{T_{1gi}})\left(\omega_i(t)-\omega_s(t)\right)-P_{1gi}(t)) \tag{22}$$

$$\dot{P}_{dgi}(t)=\frac{1}{T_{dgi}}(\frac{N_{1dgi}T_{dgi}-N_{2dgi}}{T_{dgi}}(P_{ci}(t)-P_{1gi}(t)$$
$$-K_{1gi}\frac{T_{2gi}}{T_{1gi}}\left(\omega_i(t)-\omega_s(t)\right))-P_{dgi}(t)) \tag{23}$$

$$\dot{P}_{2gi}(t)=Sat_{\min^{\max}}(\frac{1}{T_{3gi}}(\frac{N_{2dgi}}{T_{dgi}}(P_{ci}(t)-K_{1gi}\frac{T_{2gi}}{T_{1gi}}(\omega_i(t)$$
$$-\omega_s(t))-P_{1gi}(t))+P_{dgi}(t)-sat_{\min^{\max}}\left(P_{2gi}(t)\right))) \tag{24}$$

In the synchronous generator's dynamic model presented above, there are two essential inputs to generate electricity, i.e. excitation and mechanical power. The mechanical power (equal to the mechanical torque in per unit) is provided using the turbine modeled above while the turbine is controlled using the governor system. Such governor-turbine system is responsible for delivering the required mechanical power to generate electrical active power based on swing equation given in (2). Therefore, the turbine output mechanical power at time t is calculated from the turbine model as given below,

$$P_{m,i}(t) = P_{m,i}^{op}(t) + K_{1T,i}\,P_{1T,i} + K_{2T,i}\,P_{2T,i} + K_{3T,i}\,P_{3T,i} + K_{4T,i}\,P_{4T,i} \quad (25)$$

It is to emphasis that $P_{m,i}^{op}(t)$ is the determined based on the operating point of the system that determine the dispatching of the corresponding generating unit. Ideally, the operating point can be determined by performing the load flow, which can be done using MATPOWER software package or any other available power flow tools that adopted by the operator.

2.4. Order-reduction of synchronous generating units in a specific power region

In industry and academia, there are needs to convert detailed models to simplified low-order models to reduce the complexity, time, and computational burden. The high-speed dynamics from AVR have neglectable impact on the frequency response because the frequency in a synchronous generator (the rotating speed in per unit) is governed by the governor-turbine system. It is proven that the rotor speed and its angle dynamics drive the frequency in a power plant, therefore, the dynamic model of synchronous generator can be reduced to order 2 if the electric power can be considered accessible and measurable. Modern measurement devices can measure both active and reactive powers at the terminal of synchronous generator with high speed and accuracy. Therefore, the synchronous machine model can be reduced to the well-known swing-equation only when the frequency is the topic of interest. In this case, the equation describing the frequency changes, the rotor speed, given in (1) can be simplified to

$$\dot{\omega}_i(t) = \frac{\omega_{si}}{2H_i}\left(P_{mi}(t) - P_{ei}(t) - D_i\,\omega_i\,(t)\right) \quad (26)$$

The P_{ei} is the electrical power, which can be calculated as follows

$$P_{ei} = (x''_{qi} - x''_{di})\,i_{di}(t)\,i_{qi}(t) + D_i\,\omega_i(t) - D_i\,\omega_{si}(t) + \frac{x''_{di} - x_{si}}{x'_{di} - x_{si}}E'_{qi}(t)i_{qi}(t)$$
$$+ \frac{x'_{di} - x''_{di}}{x'_{di} - x_{si}}\psi_{1di}(t)i_{qi}(t) + \frac{x''_{qi} - x_{si}}{x'_{qi} - x_{si}}E'_{di}(t)i_{di}(t) + \frac{x'_{qi} - x''_{qi}}{x'_{qi} - x_{si}}\psi_{2qi}(t)i_{di}(t) \quad (27)$$

The above swing equation can model the power system dynamic behavior for the frequency studies. Also, all the generating units can be aggregated together to form a system frequency response model for a specific power region.

2.5. Forming A Power Region Swing Equation

It is important to form the control area so called power region for building the advanced system frequency response model. The backbone of the frequency control area model is the equivalent swing equation of all synchronous generating units inside the power region. The most important is to linearize the equation and determine the total available rotating inertia H_{total}, based on which the swing equation can become,

$$2H_{total}\frac{df}{dt} = \Delta P_m(t) - \Delta P_e(t) = \Delta P(t) \quad (28)$$

$$H_{total}S_{total} = \sum_i H_i S_i \quad (29)$$

$$H = H_{total} = \frac{\sum_i H_i S_i}{\sum_i S_i} \quad (30)$$

The total inertia, H_{total}, is calculated from the available inertia provided by different synchronous generating units subjected to the total apparent nominal power in the power region. By the same way, the equivalent change in mechanical power, $\Delta P_m(t)$, and change in electrical power, $\Delta P_e(t)$, in the power region swing equation can be determined as follows

$$\Delta P_m(t) = \sum_i \Delta P_{m,i}\,(t) \quad (31)$$

$$\Delta P_e(t) = \sum_i \Delta P_{e,i}\,(t) \quad (32)$$

In the presented power region swing equation, the total change in the electrical power is calculated from the electrical load and the disturbance, ΔP_d, in the power region.

$$\Delta P_e(t) = \Delta P_d + \Delta P_L(t) \tag{33}$$

Therefore, the total change in the active power imbalance between the generation and demand sides can be determined as follows,

$$\Delta P(t) = \Delta P_m(t) - \Delta P_d - \Delta P_L(t) \tag{34}$$

In case there are sensitive loads to frequency inside the power region, this sensitivity will be presented using the equivalent load damping coefficient, D, (so-called as load frequency relief in Australia), as follows

$$2H\frac{df}{dt} = \Delta P_m(t) - \Delta P_L(t) - \Delta P_d(t) - D\Delta f = \Delta P(t) \tag{35}$$

However, the total change in power is shown in the disturbance term so that the above equation looks at changes online. For simplicity reasons, in what follows, we will use the index i to refer to the ith power region instead of the individual generating units.

2.6. Forming A Power Region SFR Model

It is to simplify the dynamic models of the most important component that directly affect and control the frequency in power systems, which is the governor-turbine system. Mathematically, the high order model of different parts of control loops impact the frequency can be reduced to achieve low-order frequency response model. System identification tools are useful for this purpose. We suggest an algorithm based on Subspace State Space System Identification (N4SID) technique for obtaining the missing models that are not known by the operator of the system, where the proposed algorithm is introduced in the following sections. Either considering the low-order model known or known (which can be identified), the mathematical model presented in the above sections can be represented by two transfer functions, one for modeling the turbine and its reheater and another one for modeling the governor dynamics. In addition to the conventional generation-side modeled above, the demand-side and IBRs can be considered a good source of active power reserves, in which the active consumers and IBRs can provide ancillary services to the power system and participate in controlling the frequency. A such participation from the demand-side can be also modeled using a transfer function with a specific time constant where this transfer function is identifiable and can be driven using the mathematical model of each participant in frequency control services. However, the models of virtual inertia, and EVs will be discussed in the following sections. Figure 2.2 presents a generic simplified frequency response model of the ith area of a power system consisted of an equivalent reheated thermal turbine, governor, aggregated model of electric vehicles as an example of demand side contributions, renewable energy sources, and electric loads presented by their demands.

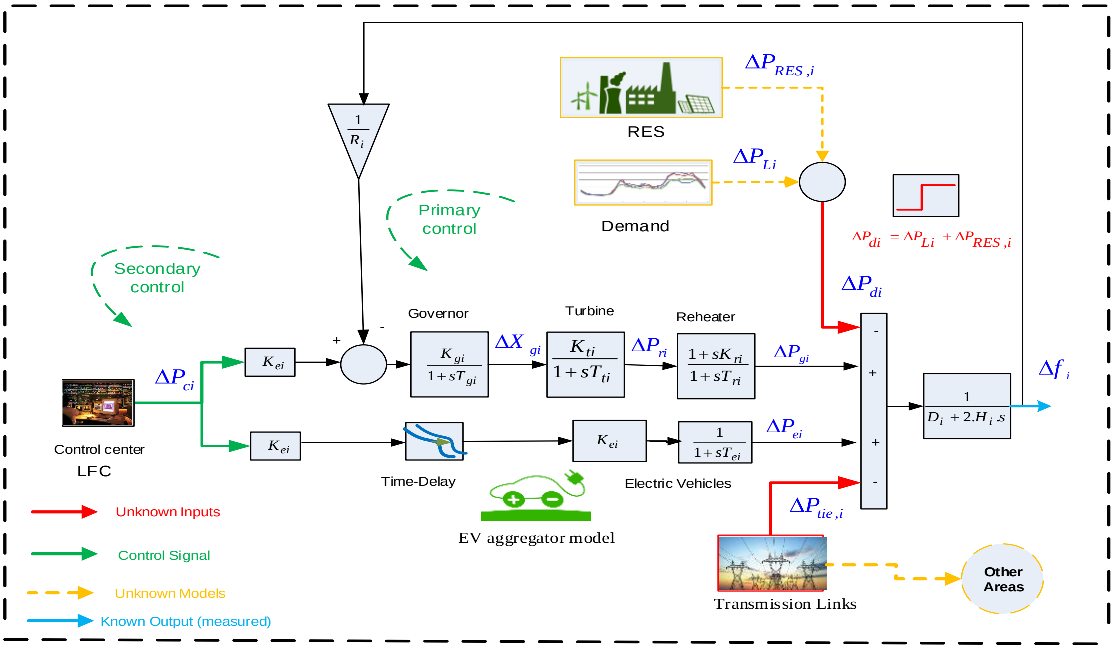

Figure 2.2. The generic SFR model of a power region where frequency supported by thermal power plants and EVs

Based on the aforementioned detailed model and the description on how to reduce the dynamic complexity and order of the system, the differential-algebraic equations of the simplified model are given below:

$$\Delta\dot{f}_i = \frac{1}{2H_i}\Delta P_{mi} + \frac{1}{2H_i}\Delta P_{ei} - \frac{1}{2H_i}\Delta P_{di} - \frac{D_i}{2H_i}\Delta f_i - \frac{1}{2H_i}\Delta P_{tie,i} \tag{36}$$

$$\Delta\dot{P}_{gi} = \frac{K_{ti}K_{ri}}{T_{ti}T_{ri}}\Delta X_{gi} + \frac{T_{ti}-K_{ri}}{T_{ti}T_{ri}}\Delta P_{ri} - \frac{1}{T_{ri}}\Delta P_{gi} \tag{37}$$

$$\Delta\dot{P}_{ri} = \frac{K_{ti}}{T_{ti}}\Delta X_{gi} - \frac{1}{T_{ti}}\Delta P_{ri} \tag{38}$$

$$\Delta\dot{X}_{gi} = -\frac{K_{gi}}{R_i T_{gi}}\Delta f_i - \frac{1}{T_{gi}}\Delta X_{gi} + \frac{K_{gi}\alpha_{gi}}{T_{gi}}\Delta P_{ci} \tag{39}$$

$$\Delta\dot{P}_{ei} = -\frac{1}{T_{ei}}\Delta P_{ei} + \frac{K_{ei}\alpha_{ei}}{T_{ei}}\Delta P_{ci} \tag{40}$$

$$\Delta ACE_i = b_i\Delta f + \Delta P_{tie_i} \tag{41}$$

where i and j are indices for indicating the ith and jth areas, respectively. Δf is the frequency deviation, ΔP_{gi} is the deviation of the output active power of the generators, $\Delta P_{ri}$is the reheater output mechanical power, $\Delta X_{gi}$is the position deviation of the valve, and ΔP_{ei} refers to the participation of the demand side to the frequency control where it refers to the participation of electrical vehicles in this paper. K_{gi}, K_{ri}, K_{ti}, and $K_{ei}$are the gains of the governor, the reheater, the turbine, and the electrical vehicles, respectively. T_{gi}, T_{ri}, T_{ti}, and $T_{ei}$are the constant times of governor, the reheater, thermal turbine, and EVs, respectively [8-9]. H is the inertia constant, which is the most important parameter in frequency response, Drefers to the damping due to the participation of the demand side, and $R$is the primary controller, which is also called the governor droop. The deviation of the area control error, ΔACE_i and the bias of the frequency $b_i$are important parameters in the secondary control of the frequency, which is also called load-frequency control (LFC) or automatic frequency control (AGC).

2.7. Integrating different power regions to form interconnected SFR model

To form the proposed SFR model to create multi-regional (multi-area) multi-machine interconnected power systems, the interconnectors should be modeled using low-order transfer function from frequency viewpoints. In this section, the modelling of interconnectors used to interconnect power regions in power systems is introduced. Let's consider a generic topology of interconnected power system comprising four power areas (power regions) as shown in Figure 2.3, on which the symbols for differentiate between different tie-lines are illustrated. The interconnectors from frequency perspective can be divided into three major types which are:

a) AC interconnectors (AC tie-lines), where the power flow in such interconnectors follows the well-known equation governing the power transfer between two voltage sources. Usually, such types of interconnectors are not supplied with power flow control from frequency perspectives.

b) AC tie-lines with thyristor-controlled phase shifter (TCPS). The power flow in such tie-lines is controlled using the voltage angle differences between the ending-end and receiving-end by the thyristor-controlled phase shifter.

c) HVDC links where most of them contributes to primary frequency control by adding active control loop to their control loops applied to the power electronic devices. However, some of HVDC in reality do not provide frequency support, therefore, there impact on the frequency of both power regions can be neglected and therefore their modeling in SFR can be neglected. This case will be discussed for NEM system later, since NEM has the two types of HVDC interconnectors.

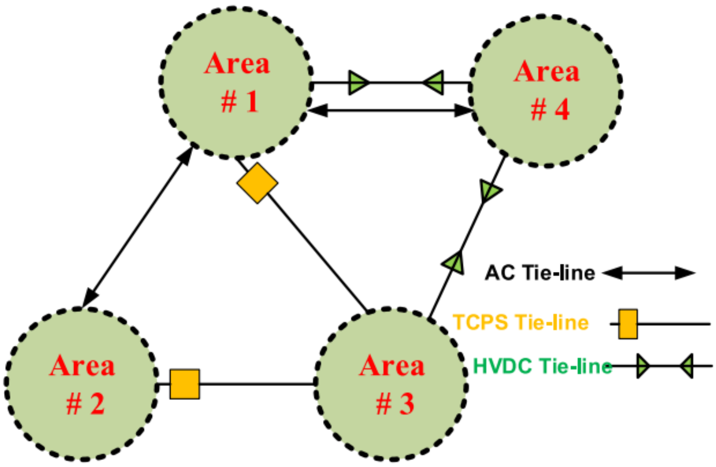

Figure 2.3. The topology of the studied interconnected power system

The system different types of transmission links including AC transmission lines, HVDC links, and AC tie-lines with integrated TCPS to tie the different power areas are modelled as given below.

The transmitted power deviation through AC transmission line between area *i* and *j* is expressed as [8]:

$$\Delta P_{AC_{ij}}(s) = \frac{2\pi T_{ij}}{s}\left(\Delta f_i(s) - \Delta f_j(s)\right) \tag{42}$$

With integrated TCPS, the power deviation is calculated as

$$\Delta P_{AC_{ij}}(s) = \frac{2\pi T_{ij}}{s}\left(\Delta f_i(s) - \Delta f_j(s)\right) + \Delta P_{S_{ij}}(s) \tag{43}$$

where

$$\Delta P_{S_{ij}}(s) = \mathrm{T}_{ij}\frac{K_{S_{ij}}}{1+sT_{S_{ij}}}\Delta f_i(s) \tag{44}$$

Therefore, the AC power deviation of tie-lines connected to area i is determined as

$$\Delta P_{AC_i}(s) = \sum_{j=1, i\neq j}^{N} \Delta P_{AC_{ij}}(s) \tag{45}$$

The power deviation of the HVDC link between areas i and j is determined by the control signal of HVDC, ε_i, with a time constant, T_{DC_i}, as

$$\Delta P_{DC_{ij}}(s) = \frac{1}{1+sT_{DC_{ij}}}\varepsilon_i(s) \tag{46}$$

where,

$$\varepsilon_i(s) = \sum_{j=1, i\neq j}^{N} K_{ij}(\Delta f_i(s) - \Delta f_j(s)) \tag{47}$$

The total deviation of tie-lines power between ith area and other areas can modeled as unknown input to achieve the fully decentralized model is determined as,

$$\Delta P_{tie_i}(\mathrm{s}) = \Delta P_{AC_i}(\mathrm{s}) + \Delta P_{DC_i}(\mathrm{s}) \tag{48}$$

The most important in modeling SFR is to get the values of parameters used for modelling the interconnectors. It is assumed that these parameters are well-known in the control center by the operator. Otherwise, they can be calculated using their mathematical sources. The other solution to get the parameters' values is to estimate them using the suggested system identification technique in this project.

2.8. Systems of systems and state Space Representative of the system frequency response

In reality, power areas are connected together through major transmission lines, i.e. the tie-lines. The frequency deviation in one area would result in fluctuations in the transferred active power from one area to another. The active power deviation through the ith tie-line from its scheduled value at a specific time can be calculated based on (49). This can be considered a useful metric to understand the fluctuations in interconnectors and is an important variable that is being used for issuing the area control error in the international practices of implementing LFC/AGC control systems.

$$\Delta P_{tie,i} = \sum_{j=1}^{m} (\mathrm{P}_{tie,act_{ij}} - \mathrm{P}_{tie,\mathrm{sched}_{ij}}) \tag{49}$$

However, the interconnectors provide good opportunity to divide the bulk power systems into several power regions (control areas) interconnected through major interconnectors. This provides the capability of modeling the system frequency response of an interconnected power system as a systems of systems (SoS). This means that each power region can be modelled separately using a suitable modelling technique, e.g. state space (SS) modelling technique.

If we consider the system a bulk system or we look at a specific power region as a separate system (with the consideration of the transferred power with neighbors as a known input), then the above equations described the simplified model can be rewritten as a combined matrix-vector form called state-space model as follows,

$$\begin{aligned} \dot{x}(t) &= Ax(t) + Bu(t) + Ed(t) \\ y(t) &= Cx(t) \end{aligned} \tag{50}$$

where $\mathrm{x} \in \Re^{\mathrm{n}\times 1}$is the dynamic state vector, $\mathrm{u} \in \Re^{\mathrm{r}\times 1}$is the known input vector, $\mathrm{y} \in \Re^{\mathrm{m}\times 1}$ is the measured output vector, $\mathrm{d(t)} \in \Re^{\mathrm{q}\times 1}$is the disturbance/unknown vector. The matrices $\mathrm{A}, \mathrm{B}, \mathrm{C}, \mathrm{E}$ are the state space matrices, which are considered to be known based on the available data of the power system in the control center.

It is worth mentioning that the number of state variables depends on the requirements of the study and it is flexible. The operator of the system can define the state variables of interest, which results on the dynamic order of the SS model.

It is also worth introducing the detailed synchronous generating units with its controllers in form of compact nonlinear presentative model as follows,

$$\dot{\boldsymbol{x}}_i(\boldsymbol{t}) = \boldsymbol{\Theta}_i\left(\boldsymbol{x}_i(\boldsymbol{t}), \boldsymbol{\nu}_i(\boldsymbol{t}), \boldsymbol{\theta}_i(\boldsymbol{t}), \boldsymbol{P}_{m,i}^{op}(\boldsymbol{t}), \boldsymbol{P}_{c,i}(\boldsymbol{t}), \boldsymbol{E}_{fd,i}(\boldsymbol{t})\right) \tag{51}$$

$$\boldsymbol{u}_i(\boldsymbol{t}) = \begin{bmatrix} \boldsymbol{v}_i(\boldsymbol{t}) \\ \boldsymbol{\theta}_i(\boldsymbol{t}) \\ \boldsymbol{E}_{fd,i}(\boldsymbol{t}) \\ \boldsymbol{P}_{c,i}(\boldsymbol{t}) \end{bmatrix} \tag{52}$$

$$\boldsymbol{y}_i(\boldsymbol{t}) = \begin{bmatrix} \boldsymbol{i}_i(\boldsymbol{t}) \\ \boldsymbol{\gamma}_i(\boldsymbol{t}) \end{bmatrix} = \boldsymbol{\Pi}(\boldsymbol{x}_i(\boldsymbol{t}), \boldsymbol{v}_i(\boldsymbol{t}), \boldsymbol{\theta}_i(\boldsymbol{t})\Big) \tag{53}$$

$\boldsymbol{\Theta}_\mathbf{i}$ and $\boldsymbol{\Pi}$ are known nonlinear functions. Readers are referred to [4] by Alhelou et.al., for more information about detailed modeling of the system for frequency studies, especially for the application of the model in assessing the frequency response and design the secondary frequency controllers.

2.9. Modelling of Generated/Consumed Active Power Variation in Renewable Energy Sources/Demand

One of the issues that need to be considered in power system frequency studies is the impact of variation of generated active power from renewable resources, e.g. Wind and Solar, on the frequency fluctuation. Likewise, the variation (fluctuation) of active power demand on frequency in one power region or whole the baulk system needs to be considered in some studies. Therefore, it is preferable to consider the aforementioned stochastic variations in frequency studies. To this end, the historical data of generated active power from RESs and consumed active power in different busbars are required to achieve their suitable stochastic model. Most of time, the required data is not available or simply the operator has not collected the data during the past, therefore, some widely-accepted models to present such stochastic variation in frequency studies can be used.

To make the suggested SFR model more sophisticated, the models of variations in both generation and demand sides are considered in the developed model based on widely-accepted models. To save the space and avoid excessive descriptions, the models are presented herein by their block-diagrams. Figure 2.4 depicts the system model of wind turbines' fluctuating power for frequency studies [4].

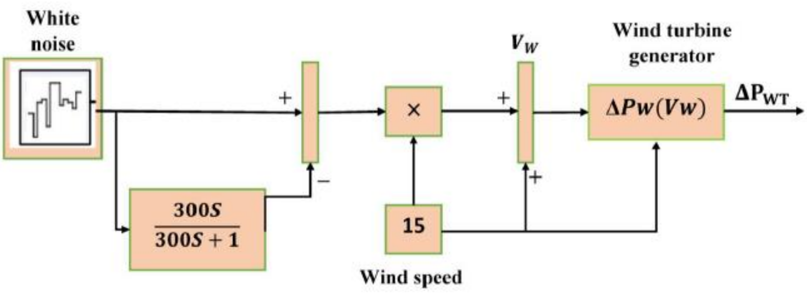

Figure 2.4. Model of Wind turbines' fluctuating active power [10]

Similarly, the solar power fluctuation model is considered for the developed SFR model for studying frequency in modern power systems. The adopted is depicted in Figure 2.5, where its transfer function is clearly presented.

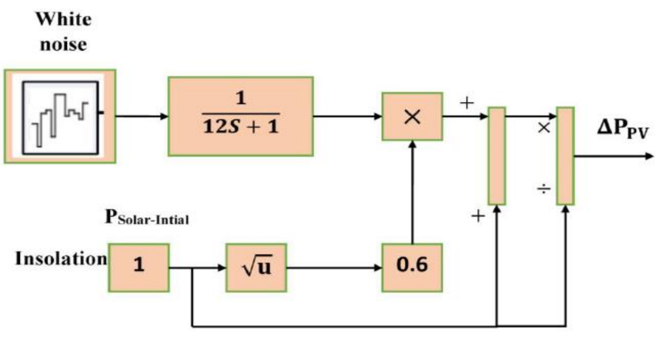

Figure 2.5. Active power fluctuation model for solar energy systems [10]

2.10. Modelling of modern frequency support providers: DR, EV, and Virtual Inertia

In addition to the aforementioned model of the participants in providing frequency services, there are emerging techniques for frequency supports that need attention in modelling. Demand response, services from energy storage systems, virtual inertia, aggregators of electric vehicles, and superconducting Magnetic Energy Storage (SMES) are among the emerging topics that are considered in the developed SFR model. It is worth mentioning that the developed SFR model is structured in a such way new modules can be easily added, which guarantee the flexibility of the suggested SFR model.

Dynamic Demand Response: The widely-adopted and validated models of the emerging techniques and services are considered for SFR model. For instance, it is verified that demand response would take part in supporting frequency future power systems. To model demand response, a generic model that mimic the behaviour of response on the system level is utilised in this work. The demand response has advantage of fast response compared to other frequency support services providers. Its mode can be simplified to a first-order transfer function with a time constant that represent the time response from appliances that provide the frequency support services. It is also essential to model the controller used for managing the demand response based on frequency deviation. However, various control approaches can be considered in reality, therefore, it is up to the operated to specify the control approach that is adopted by the demand response service providers. An approximation can be applied to the transfer function and the controllers to get a simpler model; however, the most critical part of demand response model is the modelling of the time delay due to measurements and communications, which is a hideous task. In literature, extensive efforts have been attempted to get a suitable model for such an issue in demand response studies. It is concluded that the communication delay can be expressed by the exponential function e^{-st_d} where, τ gives the communication delay time. Following a disturbance, the frequency of the system experiences a transient change and the feedback mechanism comes into play and generates appropriate control signal to make generation follow the load demand. For the application of linear robust control techniques in power system, an exponential delay term can be modelled by Padé approximation which is defined as,

$$R_{uv}(e^{-st_d}) = (D_{uv}(e^{-st_d}))^{-1} * \ (N_{uv}(e^{-st_d}))^{uv} \quad (54)$$

N_{uv} and D_{uv} are rational polynomials of order u and v respectively. Generally, the second-order, third-order, and fifth-order Padé approximations are the widely adopted and accepted approximations to be sued for frequency studies. The approximation of fifth-order Padé is as follows,

$$R_{uv}(e^{-st_d}) = \frac{-t_d{}^5s^5+30t_d{}^4s^4-420t_d{}^3s^3+3360t_d{}^2s^2-15120t_d{}^1s^1+30240}{t_d{}^5s^5+30t_d{}^4s^4+420t_d{}^3s^3+3360t_d{}^2s^2-15120t_d{}^1s^1+30240} \quad (55)$$

Dynamic Response from EVs: In addition to traditional dynamic demand response programs, aggregators of electric vehicles are going to be a considerable source in future power systems, during power system transformation and beyond. Therefore, it vital to consider the role of EVs in supporting the frequency in future power systems. For example, the importance of the consideration of EVs for future grids can be verified by the expectations of EV deployment in the future. The different possible scenarios of EVs In Australia for 2030 and 2050 are now accessible through the AEMO's integrated system plan 2022. Similar to DR program, the ability of e-mobility of provision some ancillary services have attracted a considerable attention by both academia and industry. In this regard, the low-order frequency response model of aggregated EV response has been driven from the charging and EV battery models. An advanced model is also developed in this research which can be found in the next chapters, when we discuss the contribution of demand-side to frequency support in modern and future power systems. The generic model of an individual EV that contributes to frequency support is depicted in Figure 2.66.

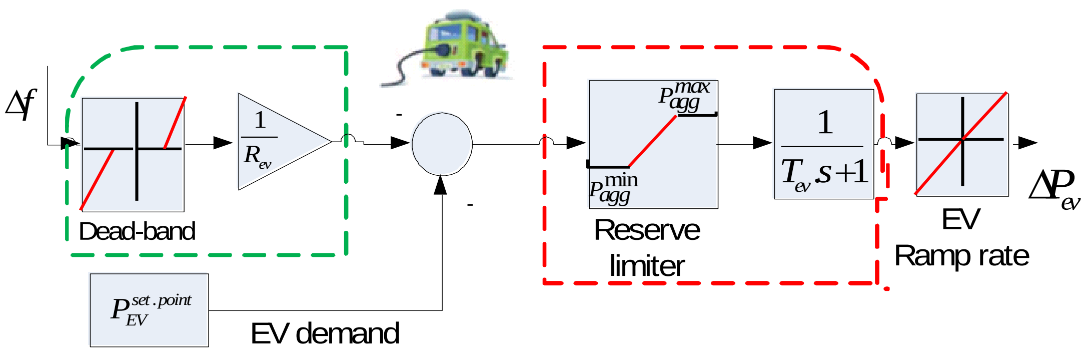

Figure 2.6. The EV battery-charge frequency response model

It is to mention that the EV frequency response is modeled using first-order transfer function, where the time constant plays a vital role in determining the frequency response from EVs. The other important factors are the droop setting and the limits applied to the maximum power absorbed/injected from/to the grid. The transfer function used to model the frequency response from EVs is as follows,

$$TF_{ev,i} = \frac{k_{ev,i}}{1+sT_{ev,i}} \tag{56}$$

The gain, $\mathrm{k_{ev,i}}$, is usually set to be 1, while the time constant which is the most important parameters is determined from the charging system of EV. The time constant, $\mathrm{T_{ev,i}}$, in the EV model can be set as 50 ms, however, it is calculatable using the value of the inductor and resistor of the battery-charge electrical model. The droop coefficient used to implement primary frequency response, $\mathrm{R_{ev,i}}$, is set by the operator based on either on market agreement between the aggregator and the operator, or based on other agreeable approach that is confirmed by the system operator. The model of individual EVs can be aggregated to form an aggregated response from EVs. More information is available on the next chapters.

Dynamic Response from Virtual Inertia: There are a number of methods suggested in literature for implementing and providing virtual inertia services. Therefore, there is a need to develop a generic model that can mimic the inertial frequency response from different inertia implementation methodologies. The generic model presented in this report is based on the concept of virtual inertia that comes from the famous swing equation (See equations (1-2)). To implement virtual inertia concept, a fast-dynamic response energy sources is required, therefore, it is preferred to implement virtual inertia in reality using either SMES or battery energy storage systems by adopting a suitable control method. The main requirements beside the source of the energy, it is vital to accurately measure the frequency at the point of implementation and to accurately calculate the derivative of the frequency, where the derivative of the frequency would be the main input for the control loop to realise the active power response to limit the high RoCoF in power systems, and consequently increasing the overall stability and security of power systems. The transfer function below describes the inertial responsive that could be provided by a suitable implementation of the virtual inertia concept.

$$P_{vir,i} = \frac{k_{vir,i}}{1+sT_{vir,i}} \frac{df(t)}{dt} \tag{57}$$

where the transfer function, $\frac{\mathrm{k_{vir,i}}}{1+s\mathrm{T_{vir,i}}}$, models the source of virtual inertia, meaning that its time constant, $\mathrm{T_{vir,i}}$,and gain, $\mathrm{k_{vir,i}}$, are determined based on the type of the source, e.g. BESSs or SMES.

2.11. A New methodology to identify the parameters of the proposed SFR model

It is to simplify the dynamic models of the most important electrical/mechanical power components that directly affect/control the frequency in power systems, e.g. the governor-turbine systems. Mathematically, the high order models of different parts of control loops impact the frequency can be reduced to achieve low-order frequency response models. System identification tools are useful for this purpose and can help achieving the desirable low order models. In what follows, we describe the proposed methodology for identifying the model parameters in case they are missing or not known by the power system operator. We introduce a new methodology developed based on system identification techniques, where a technique of subspace identification of combined deterministic stochastic systems is developed in this research.

Note: We assume readers of this part have the required knowledge of Advanced Linear Algebra which is basic for postgrad studies in system identification and power system dynamics and stability. Otherwise, readers can refer to [10-12] for familiarise themselves with Advanced Linear Algebra topics. However, we try our best to make this section easy to follow for respected engineers who did not attend postgrad studies with focus on such maths.

Hankel Matrix: The Hankel structure plays a vital in system identification methods especially for the developed, because the suggested subspace identification method forms the input/output signal data and the noises in Hankel structure. We use this unique structure to construct the data/measurements for the developed algorithm to help estimating the missing data and getting the reduced order SFR model.

A square or non-square matrix $A \in \mathbb{R}^{m\times n}$ with Hankel structure is a matrix with constant skew diagonals (anti-diagonals). In other words, in Hankel matrix, the value of (i; j)th entry depends only on the sum i+j. The matrix A with Hankel structure can be created from a vector $\mathrm{a} = (\mathrm{a}_1, \dots, \mathrm{a}_{\mathrm{m+n-1}})$ with $\mathrm{m} + \mathrm{n} - 1$ elements.

$$A = \begin{bmatrix} a_1 & a_2 & \dots & a_n \\ a_2 & a_3 & \dots & a_{n+1} \\ \vdots & \vdots & \dots & \vdots \\ a_m & a_{m+1} & \dots & a_{m+n-1} \end{bmatrix} \tag{58}$$

Each entry of Hankel matrix can be also a matrix. This composition is than called Block Hankel matrix. The matrices with Hankel structure are usually denoted shortly as Hankel matrices, as it will be also used in this work. However, that can be confusing, because Hankel matrix is also a special square matrix $\mathrm{H} \in \mathbb{R}^{\mathrm{n}\times\mathrm{n}}$ defined as

$$h_{ij} = \begin{cases} 0 & if\ i+j-1>0 \\ i+j-1 & otherwise \end{cases} \tag{59}$$

Now let us use the following definitions of row space and column space and null of matrices. The row space of a matrix A, i.e. row(A), is defined as follows,

$$A = \begin{bmatrix} a_{11} & a_{12} & \dots & a_{1n} \\ a_{21} & a_{22} & \dots & a_{2n} \\ \vdots & \vdots & \dots & \vdots \\ a_{m1} & a_{m2} & \dots & a_{mn} \end{bmatrix} = \begin{bmatrix} r_1 \\ r_2 \\ \vdots \\ r_m \end{bmatrix} \tag{60}$$

$$row(A) = \{c_1 r_1^T + c_2 r_2^T + \dots + c_m r_m^T |\ c_i \in \mathbb{R}\} \tag{61}$$

Similarly, the column space of a matrix A, i.e. col(A), is defined as follows,

$$A = \begin{bmatrix} a_{11} & a_{12} & \dots & a_{1n} \\ a_{21} & a_{22} & \dots & a_{2n} \\ \vdots & \vdots & \dots & \vdots \\ a_{m1} & a_{m2} & \dots & a_{mn} \end{bmatrix} = [v_1 \quad v_2 \quad \dots \quad v_n] \tag{62}$$

$$col(A) = \{c_1 v_1 + c_2 v_1 + \dots + c_m v_1 |\ c_i \in \mathbb{R}\} \tag{63}$$

Finally, the null space of the matrix A, i.e. null(A), is defined as follows,

$$null(A) = \{x|\ Ax = 0\} \tag{64}$$

The orthogonal projection of the row space A on the row space of B is defined as follows,

$$\mathrm{P}_B \triangleq B^T(BB^T)^\dagger B \tag{65}$$

$$A/B = AB^T(BB^T)^\dagger B \triangleq A\mathrm{P}_B \tag{66}$$

Note that † is Moore-Penrose pseudo-inverse. Similarly, the projection of the row space A on the orthogonal space to the row space of B is defined as follows,

$$\mathrm{P}_{B^\wedge} = 1 - \mathrm{P}_B \tag{67}$$

$$\mathrm{A}/B^\wedge = A\mathrm{P}_{B^\wedge} = A(1 - B^T(BB^T)^\dagger B) \triangleq A\mathrm{P}_{B^\wedge} \tag{68}$$

The aforementioned projections decompose the matrix A into two matrices, whose row spaces are mutually orthogonal, as follows,

$$A = A/B + A/B^\wedge \tag{69}$$

A numerically efficient and robust computation of the orthogonal projection can be done by LQ decomposition.

$$\begin{pmatrix} B \\ A \end{pmatrix} = LQ = \begin{pmatrix} L_{11} & 0 \\ L_{21} & L_{22} \end{pmatrix} \begin{pmatrix} Q_1 \\ Q_2 \end{pmatrix} \tag{70}$$

Thus,

$$A/B = L_{21} Q_1 \tag{71}$$

$$A/B^{\wedge} = L_{22} Q_2 \tag{72}$$

The oblique projection of the row space A along the row space of B on the row space of C is defined as follows,

$$A/\begin{pmatrix} C \\ B \end{pmatrix} = A\begin{pmatrix} C^T & B^T \end{pmatrix} \begin{pmatrix} CC^T & CB^T \\ BC^T & BB^T \end{pmatrix}^{\dagger} \begin{pmatrix} C \\ B \end{pmatrix} \tag{73}$$

$$A_B/\mathrm{C} = A\begin{pmatrix} C^T & B^T \end{pmatrix} \left[\begin{pmatrix} CC^T & CB^T \\ BC^T & BB^T \end{pmatrix}^{\dagger}\right]_{\text{first r columns}} C \tag{74}$$

Considering that,

$$\begin{pmatrix} C \\ B \\ A \end{pmatrix} = \begin{pmatrix} L_{11} & 0 & 0 \\ L_{21} & L_{22} & 0 \\ L_{31} & L_{32} & L_{33} \end{pmatrix} \begin{pmatrix} Q_1 \\ Q_2 \\ Q_3 \end{pmatrix} \tag{75}$$

Thus, the orthogonal projections can be written as,

$$A_B/C = L_{32} L_{22}^{-1} C = L_{32} L_{22}^{-1} \begin{pmatrix} L_{21} & L_{22} \end{pmatrix} \begin{pmatrix} Q_1 \\ Q_2 \end{pmatrix} \tag{76}$$

Hence, the oblique projection decomposes the matrix A into three matrices

$$A = A_B/C + A_C/B + A/\begin{pmatrix} C \\ B \end{pmatrix} \tag{77}$$

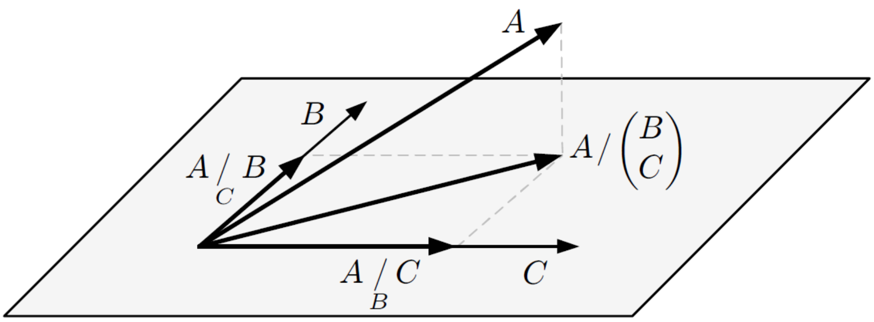

Figure 2.7. Illustration of the oblique projection [11]

It is important to model the statistical properties of projections, which helps considering uncertainties and noises in the estimation of the parameters used in SFR model. To do so, let us assume two general sequences $\mathrm{e_k} \in \mathbb{R}^{\mathrm{n_e}}$ and $\mathrm{e_u} \in \mathbb{R}^{\mathrm{n_u}}$, where $\mathrm{e_k}$ zero mean and independent of $\mathrm{y_k}$, therefore we have,

$$E(e_k) = 0, E(u_k e_k^T) = 0 \tag{78}$$

For the long series of data usual in the estimation and assuming ergodicity, the expectation operator E can be replaced by an average over one, thus we have,

$$E(u_k e_k^T) = \lim_{j \to \infty} \frac{1}{j} \sum_{i=0}^{j} u_i e_i^T \tag{79}$$

If they are structured in row matrices, then we have,

$$u = (u_1 \quad u_2 \quad \cdots \quad u_j) \tag{80}$$

$$e = (e_1 \quad e_2 \quad \cdots \quad e_j) \tag{81}$$

Thus,

$$E(u_k e_k^T) = \lim_{j\to\infty} \frac{1}{j} u e^T \tag{81}$$

Since there is an independency, therefore, we have

$$u e^T = 0 \tag{82}$$

This confirms that the signal u is perpendicular to the signal e.

Assume that y is a vector of the inputs and e is a vector of the additive disturbances. In the geometrical sense and for ($j \to \infty$), the row vectors of the disturbances are perpendicular to the row vectors of the inputs. Using an orthogonal projection of the disturbance on the input, the noise is asymptotically eliminated

$$e/u = 0, \quad (for\ j \to \infty) \tag{83}$$

This feature is used in the estimation to eliminate the noise influence and is among basic concepts of system identification methods.

It is important to structure the system in a specific structure; therefore, we adopt state space model. However, the state space representation of the system can be easily changed to other types, such as modelling the system using transfer functions. In what follows, a state space model of combined deterministic-stochastic system is considered in an innovation form, as follows,

$$x_{k+1} = Ax_k + Bu_k + Ke_k \tag{84}$$

$$y_k = Cx_k + Du_k + e_k \tag{85}$$

In the above form of state space model, $u \in \mathbb{R}^m$ is the input signals, $x \in \mathbb{R}^n$ is the state variables, and $y \in \mathbb{R}^l$ is the output signals. It is worth mentioning that K is the steady state Kalman gain. If we model the process and measurement noises as, $v_k \in \mathbb{R}^m$ and $w_k \in \mathbb{R}^l$, therefore, the above model can be converted to another commonly used stochastic state space model, as follows,

$$x_{k+1} = Ax_k + Bu_k + v_k \tag{86}$$

$$y_k = Cx_k + Du_k + w_k \tag{87}$$

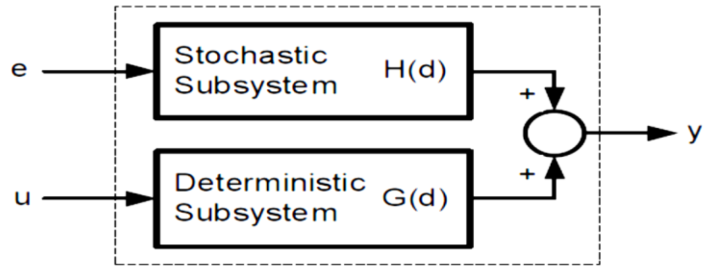

Figure 2.8. Combined deterministic-stochastic system [11]

The output spectral density of stochastic state space model of the aforementioned two state space models as follows,

$$S_{yy} = C(zI - A)^{-1}Q(z^{-1}I - A)^{-T}C^T + R \tag{88}$$

$$S¢_{yy} = [C((zI - A)^{-1}K + I)R_e[C(z^{-1}I - A)^{-1}K + I]^T \tag{89}$$

where

$$R_e = CPC^T + R$$
$$K = APC^T(CPC^T + R)^{-1}$$
$$P = APA^T - K(C^TPC + R)K^T + Q$$

This confirms that the uncertainty contained in the noises can be for the outputs and the states described by the innovations e_k.

To use in subspace estimation technique in estimating the parameters and reducing the order of turbine-governor systems in SFR model, all inputs, outputs and noises are arranged into the Hankel matrices. Assume known set of input/output data samples u_k, y_k. These samples can be arranged into Hankel matrices with i and h block rows and j columns as follows,

$$\begin{pmatrix} U_p \\ \hline U_f \end{pmatrix} = \left(\begin{array}{cccc} u_0 & u_1 & \cdots & u_{j-1} \\ u_1 & u_2 & \cdots & u_j \\ \vdots & \vdots & \ddots & \vdots \\ u_{i-1} & u_i & \cdots & u_{i+j-2} \\ \hline u_i & u_{i+1} & \cdots & u_{i+j-1} \\ u_{i+1} & u_{i+2} & \cdots & u_{i+j} \\ \vdots & \vdots & \ddots & \vdots \\ u_{i+h-1} & u_{i+h} & \cdots & u_{i+h+j-2} \end{array}\right) = \begin{pmatrix} U_p{}^+ \\ \hline U_f{}^- \end{pmatrix} = \left(\begin{array}{cccc} u_0 & u_1 & \cdots & u_{j-1} \\ u_1 & u_2 & \cdots & u_j \\ \vdots & \vdots & \ddots & \vdots \\ u_{i-1} & u_i & \cdots & u_{i+j-2} \\ u_i & u_{i+1} & \cdots & u_{i+j-1} \\ \hline u_{i+1} & u_{i+2} & \cdots & u_{i+j} \\ \vdots & \vdots & \ddots & \vdots \\ u_{i+h-1} & u_{i+h} & \cdots & u_{i+h+j-2} \end{array}\right) \qquad (90)$$

In the above, the U_p is the matrix of past inputs and U_f is the matrix of future inputs. Matrices $U_p{}^+$ and $U_f{}^-$ are created from U_p and U_f by moving the first block row from U_f to the end of U_p. This variation/feature is later used to retrieve the system matrices. Now, we define the combination of U_p and Y_p as W_p which will be used a regressor. Likewise, System state sequence is also used in a matrix form in a specific structure as given below.

$$W_p = \begin{pmatrix} U_p \\ Y_p \end{pmatrix} \qquad (91)$$

$$X_p = (x_0 \quad x_1 \quad \cdots \quad x_{j-1}), \quad X_f = (x_i \quad x_{i+1} \quad \cdots \quad x_{i+j-1}) \qquad (92)$$

The extended observability matrix $\mathrm{G_k}$ is an extension of observability matrix for a number of block rows higher than the system order $\mathrm{k} \geq \mathrm{n}$.

$$\mathrm{G_k} = \begin{pmatrix} \mathrm{C} \\ \mathrm{CA} \\ \vdots \\ \mathrm{CA^{k-1}} \end{pmatrix} \in \mathrm{R^{kl \times n}} \qquad (93)$$

Likewise, if we consider K as the stationary Kalman gain, the reversed extended controllability matrices $\Delta_\mathrm{k}^\mathrm{d}$ and $\Delta_\mathrm{k}^\mathrm{s}$ corresponding to the deterministic and stochastic parts respectively are defined as follows,

$$\Delta_k^d = (A^{k-1}B \quad A^{k-2}B \quad \ldots. \quad B) \in R^{n \times km} \qquad (94)$$

$$\Delta_k^s = (A^{k-1}K \quad A^{k-2}K \quad \ldots. \quad K) \in R^{n \times km} \qquad (95)$$

In the design of the estimator, we also need $\mathrm{H_k^d}$ and $\mathrm{H_k^s}$ which are the Toeplitz matrices composed from the impulse responses (Markov parameters) of deterministic and stochastic subsystems, respectively.

$$H_k^d = \begin{pmatrix} D & 0 & 0 & \dots & 0 \\ CB & D & 0 & \dots & 0 \\ CAB & CB & D & \dots & 0 \\ \vdots & \vdots & \vdots & \ddots & \vdots \\ CA^{k-2}B & CA^{k-3}B & CA^{k-4}B & \dots & D \end{pmatrix} \in R^{kl \times km} \tag{96}$$

$$H_k^s = \begin{pmatrix} I & 0 & 0 & \dots & 0 \\ CK & I & 0 & \dots & 0 \\ CAK & CK & I & \dots & 0 \\ \vdots & \vdots & \vdots & \ddots & \vdots \\ CA^{k-2}K & CA^{k-3}K & CA^{k-4}K & \dots & I \end{pmatrix} \in R^{kl \times kl} \tag{97}$$

It is fact that the very basic and important idea in subspace system identification is that to identify the parameters of a state space model, it is sufficient to known either column space of Extended observability matrix, i.e. $\mathrm{G_h}$, or row space of State sequence matrix, i.e. $\mathrm{X_f}$.

$$\mathrm{G}_h = \begin{pmatrix} C \\ CA \\ \vdots \\ CA^{h-1} \end{pmatrix} \tag{98}$$

$$X_f = \begin{pmatrix} \vdots & \vdots & & \vdots \\ \bar{x}_i & \bar{x}_{i+1} & \dots & \bar{x}_{i+j-1} \\ \vdots & \vdots & & \vdots \end{pmatrix} \tag{99}$$

Assuming the sufficiency of the subspaces for state space model identification, now the problem of estimating invariant subspaces of the extended observability matrix $\mathrm{G_h}$ and the state sequence matrix $\mathrm{X_f}$ from the input/output data will be treated. This estimation is also related to the determination of the system order.

To obtain these subspaces, only the term $\mathrm{G_h X_f}$ is needed and its estimate can be obtained from data by the projections. Let us denote this term as a matrix $\mathrm{O_h}$ and it can be split into the required subspaces by singular value decomposition (SVD).

$$O_h = \mathrm{G}_h X_f \tag{100}$$

For the pure deterministic system, it is a simple task, because the matrix $\mathrm{O_h}$ has the rank equal to the system order with the following SVD factorization, as follows,

$$O_h = USV^T = \begin{pmatrix} U_1 & U_2 \end{pmatrix} \begin{pmatrix} S_1 & 0 \\ 0 & 0 \end{pmatrix} \begin{pmatrix} V_1^T \\ V_2^T \end{pmatrix} \tag{101}$$

$$\mathrm{G}_h = U_1 S_1^{\frac{1}{2}} \tag{102}$$

$$X_f = S_1^{\frac{1}{2}} V_1^T \tag{103}$$

In the presence of the noise, the matrix $\mathrm{O_h}$ will be of the full rank. Thus, all singular values of $\mathrm{O_h}$ will be nonzero, i.e. the diagonal of the matrix S will have nonzero entries in nonincreasing order. The rank of the identified system has to be chosen from the number of significant singular values. This can be tricky task, for which few theoretical guidelines are available. Assuming the system order to be determined, the SVD matrices are partitioned into the 'signal' and 'noise' parts,

$$O_h = \begin{pmatrix} U_s & U_n \end{pmatrix} \begin{pmatrix} S_s & 0 \\ 0 & S_n \end{pmatrix} \begin{pmatrix} V_s^T \\ V_n^T \end{pmatrix} \tag{104}$$

$$\mathrm{G}_h = U_s S_s^{\frac{1}{2}} \tag{105}$$

$$X_f = S_s^{\frac{1}{2}} V_s^T \tag{106}$$

It is also important to develop an estimation of $\mathrm{O_h}$ from the input/output data. The is to estimate the term $\mathrm{G_h}\widehat{\mathrm{X}}_\mathrm{f}$ from the I/O data in the signal matrices by an oblique projection. Let's try an orthogonal projection of the future output $\mathrm{Y_f}$ onto the subspace of past data $\mathrm{W_p}$ and future inputs $\mathrm{U_f}$.

$$Y_f / \begin{pmatrix} W_p \\ U_f \end{pmatrix} = \mathrm{G}_h \hat{X}_f + H_h^d U_f \tag{107}$$

The orthogonal projection eliminated the noise term, because the estimated state sequence $\widehat{\mathrm{X}}_\mathrm{f}$ and the future inputs $\mathrm{U_f}$ lies in the joint row space of $\mathrm{W_p}$ and $\mathrm{U_f}$, but the future noise $\mathrm{E_f}$ is perpendicular to this subspace for the number of samples going to infinity as can be seen in Figure 2.9.

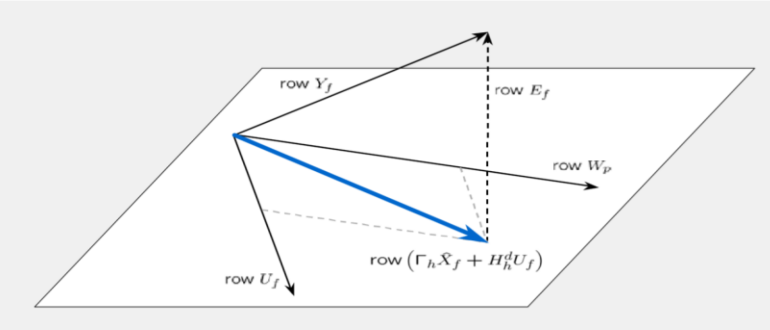

Figure 2.9. Orthogonal projection of input/output data [13]

To proof the above statement, From the above equations, the past states X_p can be expressed as,

$$X_p = G_i^\dagger Y_p - G_i^\dagger H_i^d U_p - G_i^\dagger H_i^s E_p = \left(G_i^\dagger \;\; - G_i^\dagger H_i^d - G_i^\dagger H_i^s\right) \begin{pmatrix} Y_p \\ U_p \\ E_p \end{pmatrix} \tag{108}$$

The future states X_f can be calculated based on the above expression as follows,

$$X_f = A^i X_p + \Delta_i^d U_p + \Delta_i^s E_p = A^i \mathrm{G}_i^\dagger Y_p - A^i \mathrm{G}_i^\dagger H_i^d U_p - A^i \mathrm{G}_i^\dagger H_i^s E_p + \Delta_i^d U_p + \Delta_i^s E_p = \left(A^i \mathrm{G}_i^\dagger \left(\Delta_i^d - A^i \mathrm{G}_i^\dagger H_i^d\right)\left(\Delta_i^s - A^i \mathrm{G}_i^\dagger H_i^s\right)\right) \begin{pmatrix} Y_p \\ U_p \\ E_p \end{pmatrix} \tag{109}$$

These two last equations clearly indicate, that both past states X_p and future states X_f can be obtained as a linear combination of past data Yp, Up, Ep. In other words, they lie in their joint row space. To compute an estimate of X_f the noise term can be replaced by its mean value showing $\widehat{\mathrm{X}}_\mathrm{f}$ to lie in the row space of W_p.

$$\hat{X}_f = \left(A^i \mathrm{G}_i^\dagger \left(\Delta_i^d - A^i \mathrm{G}_i^\dagger H_i^d\right)\right) \begin{pmatrix} Y_p \\ U_p \end{pmatrix} = L_\omega W_p \tag{110}$$

Orthogonal projection helps us to get rid of the noise term, but we need to eliminate also the influence of the future inputs U_f and that is where an oblique projection is the right tool,

$$Y_f /_{U_f} W_p = \mathrm{G_h} \hat{X}_f \tag{111}$$

Making the oblique projection of the future outputs Y_f onto the row space of past data W_p along the row space of future inputs U_f will give exactly the term we are looking for $\mathrm{G_i}\widehat{\mathrm{X}}_\mathrm{f}$. An illustrative of this fact is shown in Figure 2.10.

It is worth mentioning that the oblique projection of every term will be also considered in the projection and estimation process, which is,

$$Y_f /_{U_f} W_p = (\mathrm{G}_h X_f + H_h^d U_f + H_h^s E_f) /_{U_f} W_p = (\mathrm{G}_h X_f /_{U_f} W_p + H_h^d U_f /_{U_f} W_p + H_h^s E_f /_{U_f} W_p \tag{112}$$

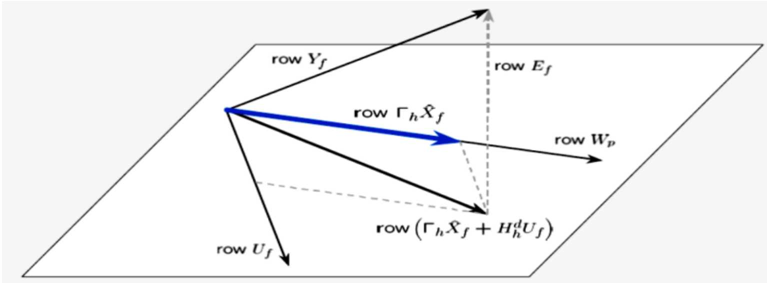

Figure 2.10. Oblique projection of input/output data [13]

Now, by applying the previous mathematical backgrounds, it is evidence that the the matrix O_h is already known. Now it can be used to get the state space model parameters by splitting it into the required subspaces by SVD as was illustrated in the previous discussion. The parameters can be basically obtained from the extended observability column space col (G_h) or the state sequence matrix row space row $(\hat{X}_f)$.

To estimate the state space model including the required parameters that used in SFR model, we suppose that the outputs and the state sequences are now available as follows,

$$\hat{X}_i = (\hat{x}_i, \dots, \hat{x}_{i+j-1}) \tag{112}$$

$$\hat{X}_{i+1} = (\hat{x}_{i+1}, \dots, \hat{x}_{i+j}) \tag{113}$$

$$U_i = (u_i, \dots, u_{i+j-1}) \tag{114}$$

$$Y_i = (y_i, \dots, y_{i+j-1}) \tag{115}$$

Then in the presence of no feedback the parameters of the innovation model can be consistently estimated from the following matrix equation relating all data by the state space model.

$$\begin{pmatrix} \hat{X}_{i+1} \\ Y_i \end{pmatrix} = \begin{pmatrix} A & B \\ C & D \end{pmatrix} \begin{pmatrix} \hat{X}_i \\ U_i \end{pmatrix} + \varepsilon \tag{116}$$

The solution can be obtained by least squares or total least squares. Denoting:

$$\mathrm{Q} = \begin{pmatrix} \mathrm{A} & \mathrm{B} \\ \mathrm{C} & \mathrm{D} \end{pmatrix}, \mathrm{C} = \begin{pmatrix} \hat{\mathrm{X}}_\mathrm{i} \\ \mathrm{U}_\mathrm{i} \end{pmatrix}, \mathrm{U} = \begin{pmatrix} \hat{\mathrm{X}}_{\mathrm{i}+1} \\ \mathrm{Y}_\mathrm{i} \end{pmatrix} \tag{117}$$

the least squares solution can be obtained as,

$$\mathrm{Q} = \mathrm{UC}^{\dagger} = \mathrm{UC}^{\mathrm{T}}(\mathrm{CC}^{\mathrm{T}})^{-1} \tag{118}$$

$$R_e = \mathrm{S}_{22}, \qquad K = \mathrm{S}_{12}\mathrm{S}_{22}^{-1} \tag{119}$$

$$\mathrm{S} = \begin{pmatrix} \mathrm{S}_{11} & \mathrm{S}_{12} \\ \mathrm{S}_{21} & \mathrm{S}_{22} \end{pmatrix} = \frac{1}{j-(n+m)} (\mathrm{U} - \mathrm{QC})(\mathrm{U} - \mathrm{QC})^{\mathrm{T}} \tag{120}$$

The other way to estimate the parameters and the state space model is to complete the estimation from Estimating parameters from col(G_h). The first step is to determine matrices A and C, as follows,

$$\underline{G_h} = \begin{pmatrix} C \\ \vdots \\ CA^{k-2} \end{pmatrix} \in R^{l(h-1)\times n} \tag{121}$$

$$\overline{G_h} = \begin{pmatrix} C \\ \vdots \\ CA^{k-1} \end{pmatrix} \in R^{l(h-1)\times n} \tag{122}$$

$$\underline{G_h} = A\overline{G_h} \tag{123}$$

This equation is linear in A and can be solved by LS or TLS.

The next step is to determine the matrices B and D. Generally determining matrices B and D needs more efforts compared to matrices A and C. Multiplying the I/O equation from the left by $G_h^{\wedge}$ and from the right by $U_f^{\dagger}$ and applying some liner algebra space operations yields to

$$G_h^{\wedge} Y_f U_f^{\dagger} = G_h^{\wedge} . H_h^d \tag{124}$$

Denote i-th column of LHS as M_i and ith column of $G_h^{\wedge}$ as L_i, then we have,

$$(M_1 \quad M_2 \quad \dots \quad M_h) = (L_1 \quad L_2 \quad \dots \quad L_h) \begin{pmatrix} D & 0 & 0 & \cdots & 0 \\ CB & D & 0 & \dots & 0 \\ CAB & CB & D & \cdots & 0 \\ \vdots & \vdots & \vdots & \ddots & \vdots \\ CA^{h-2}B & CA^{h-3}B & CA^{h-4}B & \cdots & D \end{pmatrix} \tag{125}$$

Applying some mathematical operations, one can get,

$$\begin{pmatrix} M_1 \\ M_2 \\ \vdots \\ M_h \end{pmatrix} = \begin{pmatrix} L_1 & L_2 & \dots & L_{h-1} & L_h \\ L_2 & L_3 & \dots & L_h & 0 \\ L_3 & L_4 & \cdots & 0 & 0 \\ \vdots & \vdots & \vdots & \ddots & \vdots \\ L_h & 0 & 0 & \dots & 0 \end{pmatrix} \begin{pmatrix} I_l & 0 \\ 0 & \underline{G_h} \end{pmatrix} \begin{pmatrix} D \\ B \end{pmatrix} \tag{126}$$

The above form presents an overdetermined set of linear equations in the unknowns B and D and it can be solved by LS or TLS. In this way, the model will be estimated including the required parameters by knowing some set of measurements. This will help getting the missing data and reducing the order of some models to be used in the advanced SFR model. The steps required for implementing the above suggested algorithm to get the model of some components and their parameters are demonstrated in Algorithm 1.

Algorithm 1: the suggested subspace estimation technique to obtain missing parameters for SFR model

Step	*The process applied through the estimation*
01	***Pre-process***: *arrange the input/output data into Hankel signal matrices U_p, U_f, Y_p, Y_f and their respective +/- modifications.*
02	***Oblique Projections***: *calculating the Oblique Projections to determine O_h*
03	***Applying SVD***: *Compute SVD of the weighted oblique projection*
04	***System Order***: *Determine the system order by inspecting the singular values of S and partition the SVD accordingly to obtain U1 and S1*
05	***Calculation***: *Determine different types of G_h*
06	***Obtain states***: *Determine the state sequences*
07	***Estimation***: *Estimate the parameters A, B, C and D form a set of linear equations*
08	***Estimation***: *Estimate the stochastic parameters R_e and K from the covariance estimate of the residuals as*
09	***End the process***

2.12. Validation of the proposed methodology for Obtaining SFR Data

Several scenarios have been considered to validate the developed methodology of obtaining SFR model. To avoid excessive results presentation, only the important results would be included in this section. As seen in the previous sections, the design of SFR model relies on the accuracy of the data of the system. However, most of time some data is either missing/unavailable or inaccurate. Therefore, there is a need to get an accurate data that can result in acceptable accuracy of the developed system frequency response model.

In this section we validate the ability and accuracy of the proposed estimation methodology in estimating the required data from the available measurements. Since the most important parameters for frequency studies are the inertia, damping coefficient (known as load relief), and time constants of governor-turbine systems, they need to be accurately obtained for building a useful SFR model. Considering the fact that the inertia is the most difficult to estimate, especially is the passive inertia delivered by loads and fluid coupling of generator turbines are included, therefore this section will focus on briefly introducing the obtained accuracy of inertia estimation for different scales of power systems.

Let us consider a generic SFR model of a power system to test the proposed SFR data estimation tool based on subspace estimation techniques. It is well-known that to estimate the inertia, a frequency response of a large disturbance is required. This means the operator should wait until occurrence of a large disturbance, the measure the frequency with high accuracy to estimate the available inertia. This also assumes that the operator has accurate knowledge of the amount of disturbance. In reality, such method to obtain the inertia is not practical since it is not efficient. However, the proposed technique in our work allow the operator to estimate the parameters including inertia at any time without need of waiting for a large disturbance of knowledge of the disturbance amount. The method can trigger healthy modes by injecting low power high frequency signals and based on which the data can be estimated. In case of estimating the inertia for using it in SFR model, Figure 2.11 presents the estimation error in case of different scenarios of injecting the signal. The scenarios are defined as follows: 1) Scenario 1 is where a 0.01 p.u. disturbance occurs in the system; 2) Scenario 2 is where a pseudorandom binary sequence (PRBS) signal with power 0.01 p.u. is injected into the system; 3) Scenario 3 shows results for injecting white noise into the system; and 4) scenario 4 presents the results for the injection of a multisinusoidal signal. The results confirm that the estimation error does not exceed 0.5% for inertia higher than 5 sec. Similarly, the results confirm that scenario 2 has the best estimation accuracy.

The results confirm that the proposed subspace state space system identification (N4SID) method is sufficient for obtaining most of the required data for SFR model and other data might be needed by the operator of the grid. It worth mentioning that the method is applied to different parameters and get a suitable estimation accuracy. However, in this work, we limit the presentation of results on the most influence parameters, such as the total inertia in power systems.

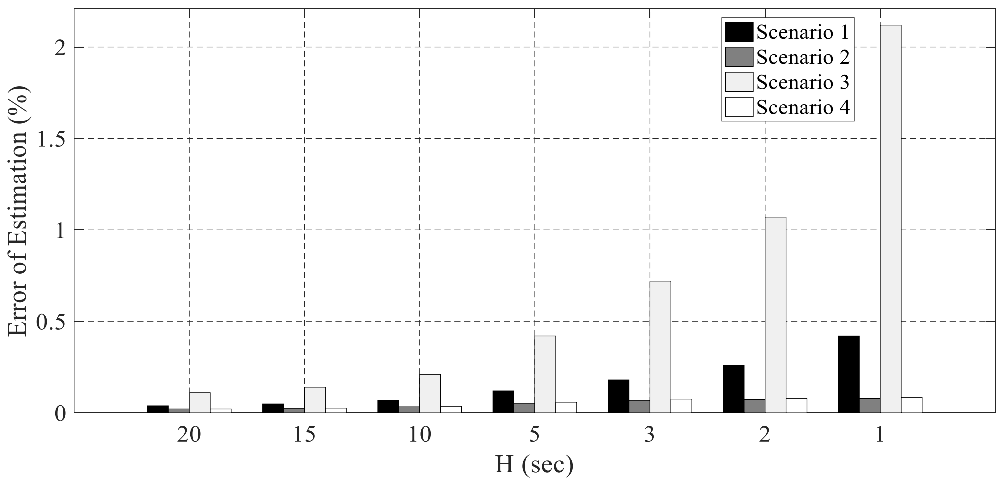

Figure 2.11. The estimation error of inertia in a generic power system model

In addition to testing the estimation on a generic model to validate the accuracy of the estimation of data that used for SFR model, the developed method is also applied to large-scale systems, e.g. IEEE 39-bus test system. In this regards, Table 2.1 presents the proposed method estimation results in case where there is a 0.1 p.u. disturbance in the demand-side. The results are obtained from the system when one of the loads suddenly is increased by 0.01 p.u. The results confirm the ability of the proposed method for estimating the parameter values for usage in SFR model. To validate the ability of estimation using ambient noise or injected PRBS signal into one of generators only, a PRBS signal is injected in G1 in IEEE 39-bus test system and the method is applied to get the parameters' values. The results given in Table 2.2 verify that the proposed method can accurately estimate the parameters that effect the frequency response in power systems.

It can be seen from Table 2.1 and Table 2.2 that the method is able to estimate the inertia in different locations in IEEE 39-bus system with high accuracy. It is worth mentioning that the worst case is considered in the previous scenarios where the damping was set to zero, making the estimation as a challenging case. The results confirm that even in such a case, the estimation accuracy is preserved.

Table 2.1. The estimation results of IEEE 39-bus system in case of a 0.1 p.u. disturbance in demand-side

Gen #	Actual H	Estimated H	Error of H-estimation (%)	Actual D	Estimated D
G1	50	50.0592	0. 12	0	0.0011
G2	3.03	3.0271	0. 0945	0	0.000038
G3	3.58	3.5802	0. 0578	0	0.000061
G4	2.86	2.8609	0. 0299	0	0.000051
G5	2.6	2.6015	0. 0570	0	0.000048
G6	3.48	3.4786	0. 0393	0	0.000053
G7	2.64	2.6402	0. 0596	0	0.000045
G8	2.43	2.4311	0. 0465	0	0.000045
G9	3.45	3.4494	0. 0183	0	0.000055
G10	4.2	4.2019	0. 0447	0	0.000077

Table 2.2. The estimation results of IEEE 39-bus system in case of injecting PRBS in G1

Gen #	Actual H	Estimated H	Error of H-estimation (%)	Actual D	Estimated D
G1	50	50.0139	0.0277	0	0.029000
G2	3.03	3.0327	0.0899	0	0.000775
G3	3.58	3.5831	0.0857	0	0.000703
G4	2.86	2.8615	0.053	0	0.000665
G5	2.6	2.6016	0.0628	0	0.000737
G6	3.48	3.4827	0.0776	0	0.000902
G7	2.64	2.6416	0.0614	0	0.000634
G8	2.43	2.4319	0.0791	0	0.000474
G9	3.45	3.4522	0.0635	0	0.000878
G10	4.2	4.2049	0.12	0	0.000953

The impact of sampling and location of estimation on the estimation accuracy has been also analysed. Table 3 gives the results of such analysis. It can be seen that the sampling rate of measurements has high impact on the estimation accuracy of the dynamic parameters used in SFR model. However, most of measurements are now available with high sampling rates from PMUs preserving the estimation accuracy in real-world applications. Similarly, this table also presents how we can solve data missing issues in measurements in control centre to avoid impacting the estimation accuracy of the proposed method. It is suggested that the data would be estimated using polynomial fitting technique. The results confirm that the proposed estimation technique suggested for obtaining SFR model data preserves good accuracy of estimation under different possible practical issues and operation cases.

Table 2.3. The estimation results of IEEE 39-bus system in case of a disturbance

Multisine injection							
No. of generator	Sample of measurement	Sample of fitting	H_{actual}	$H_{estimation}$	% Error of H	D_{actual}	$D_{estimation}$
G1	1/5	1/10	50	50.8857	-1.7713	0	0.13682
		1/30	50	50.5053	-1.0106	0	0.03300
		1/60	50	50.4334	-0.8667	0	0.01101
		1/120	50	50.4149	-0.8297	0	0.00717
	1/10	1/30	50	50.3673	-0.7346	0	0.03947
		1/60	50	50.3111	-0.6222	0	0.01599
		1/120	50	50.2878	-0.5755	0	0.00441
	1/30	1/60	50	50.3164	-0.6328	0	0.01840
		1/120	50	50.2922	-0.5845	0	0.00652
	1/60	1/120	50	50.2023	-0.4046	0	0.00738
No. of generator	Sample of measurement	Sample of fitting	H_{actual}	$H_{estimation}$	Error of H	D_{actual}	$D_{estimation}$
G10	1/5	1/10	4.2	4.3364	-3.2469	0	0.00498
		1/30	4.2	4.3343	-3.1977	0	0.00085
		1/60	4.2	4.3251	-2.9778	0	0.00007
		1/120	4.2	4.2685	-1.6320	0	0.00004
	1/10	1/30	4.2	4.3097	-2.6118	0	0.00134
		1/60	4.2	4.2654	-1.5577	0	0.00009
		1/120	4.2	4.2526	-1.2525	0	0.00004
	1/30	1/60	4.2	4.2577	-1.3577	0	0.00006
		1/120	4.2	4.2446	-1.0619	0	0.00002
	1/60	1/120	4.2	4.2363	-0.8646	0	0.00004

2.13. Validation of the proposed SFR Methodology: Time-Domain Analysis

It is crucial to validate the proposed methodology for obtaining low-order SFR model in order to build SFR model for a specific power system, such as NEM system. In what follows, we validate the proposed method for obtaining low-order models of different parts of SFR model using time-domain analysis. In this regard, the time-domain simulation results of both the original models and reduced obtained models using the proposed method are presented.

It is well-known that the frequency response after a disturbance is impacted by several elements/parts in power systems. The most influence parts are the swing equation modelling (the total rotating inertia + the load-frequency relief) and the dynamic model of governor-turbine systems. In addition to the aforementioned parts of the system that directly impact the frequency response, the disturbance magnitude has direct impact on the frequency as well. In the previous section, the estimation of important data has been found accurate enough to build an accurate model of power systems to study the frequency response. In fact, it is a novel contribution to estimate data such as inertia using the developed methodology (as an additional work to the project scope). Now, since it is validated the parameters used for modelling swing equation can be obtained accurately, it is important to obtain the dynamic model of a very challenging part for study the frequency response, which is the governor-turbine system model. In reality, it is not easy to get the model for such complex mechanical systems that directly impact the frequency response, therefore we developed a method to determine the suitable dynamic order and how to determine the model and its parameters' values.

In what follows, we apply the proposed subspace system identification method suggested in the previous sections for obtaining and validating the governor-turbine model. Also, the time-domain simulation results would be introduced to verify the accuracy of the obtained low-order model. Let's consider a power system operated in a critical operation situation with inertia shortfall, (the inertia H=2 Sec and load damping coefficient D=1 p.u.). Now, only the thermal with reheat turbine systems are considered to provide ancillary services (primary frequency support) with a speed governor droop characteristic R=0.05. In addition to the thermal power plant, it is considered that an aggregator of EVs would provide some services for supporting the frequency. However, we will focus on validating the governor-turbine models for SFR studies.

The original model of the turbine in the simulation is considered to be as, $\mathrm{TF}=\frac{1}{0.3s+1}\times\frac{2.1s+1}{7s+1}$, while the speed governor is modeled using a first-order transfer function as, $\mathrm{TF}=\frac{1}{0.2s+1}$. The nonlinearities such as Governor-deadband and Generation Rate Constraint have been also taken into account. At time t=1sec, the system is subjected to a disturbance $\mathrm{P_d}=0.1\ \mathrm{P.u.}$ Figure 2.12 presents the frequency response after the disturbance, where the sufficient primary frequency support services from thermal power plant and EVs have rescued the frequency and kept it in a stable situation. The rate of change of frequency due to the mentioned disturbance is depicted in Figure 2.13.

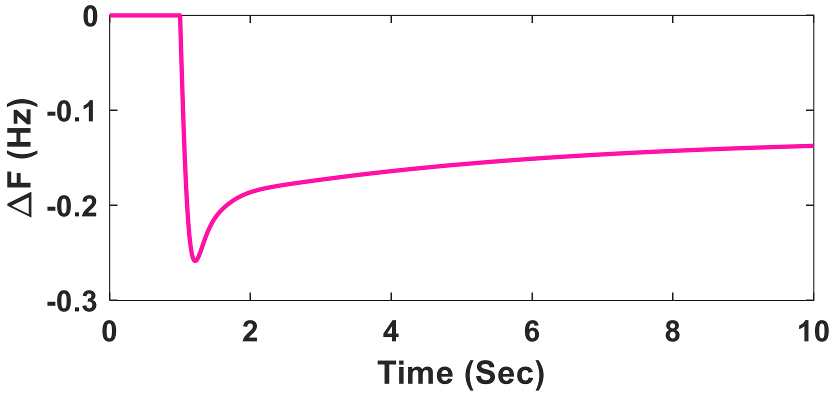

Figure 2.12. The frequency response due to a 0.1 p.u. disturbance.

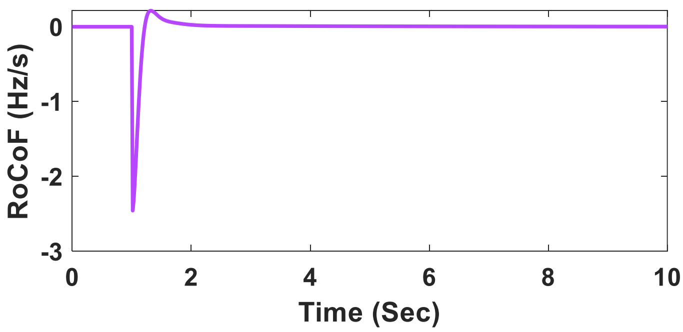

Figure 2.13. The RoCoF due to a 0.1 p.u. disturbance.

To perform the estimation of the low-order model of the original governor-turbine system model, the input and output of the governor-turbine system are measured and depicted in Figure 2.14. It is worth mentioning that the input is directly measured after the droop coefficient and before entering the governor, while the output is measured as the mechanical output power from the turbine. It is worth mentioning that the proposed N4SD method is able to obtain an accurate model to model the governor-turbine system. The dominator of the obtained accurate model can be modelled using [1.0000 9.0294 19.1316 2.5362], while the numerator polynomial parameters [5.3737 2.5411]. To verify the accuracy, the time-domain simulation results of both original model and the obtained one using the proposed method are depicted in Figure 2.15. This figure shows the output of the estimated model compared to output of the original model. The results clearly confirm the high accuracy of the obtained model using the suggested subspace system identification technique, verifying its ability to be adopted for estimating the different parts for SFR model.

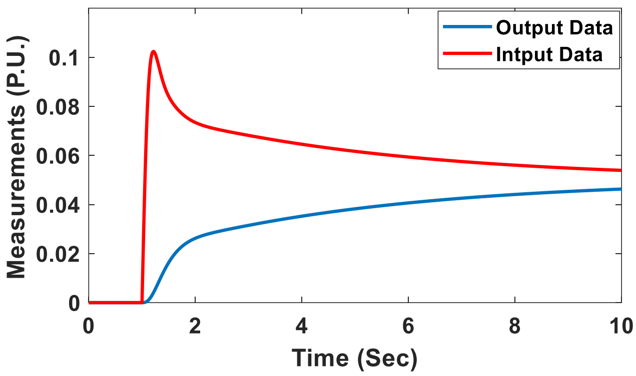

Figure 2.14. The measurements of the input and output of the original governor-turbine system

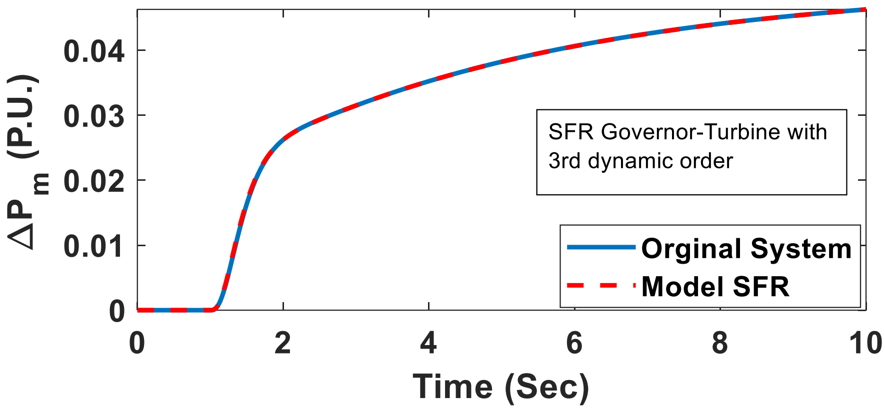

Figure 2.15. Validating the estimated governor-turbine model against the original model

In addition to the previous case study that confirmed the capability of the proposed N4SD method for estimating the dynamic models for SFR model usage, different scenarios for obtaining low-order models of the original model have been also investigated. In Scenario 1, a model of 3rd dynamic order (3 poles) is obtained without considering any zeros, where the results are depicted in Figure 2.16. It can be seen that the obtained model has accurate and identical response compared with the original model, which is another evidence of the capability of the proposed method.

To challenge the proposed method, a lower-order dynamic model (2ed order with a zero; i.e. a model with two poles and one zero) is obtained using the proposed method. The simulation results are also given in Figure 2.16, as scenario 2. One can see that the results of the lower-order model is almost identical with the original model, confirming the capability for practical usage of the proposed method. The dominator of the obtained accurate model can be modelled using [1.0000 9.0294 19.1316 2.5362], while the numerator polynomial parameters [5.3737 2.5411]. To verify the accuracy, the time-domain simulation results of both original model and the obtained one using the proposed method are depicted in Figure 2.15. This figure shows the output of the estimated model compared to output of the original model. The results clearly confirm the high accuracy of the obtained model using the suggested subspace system identification technique, verifying its ability to be adopted for estimating the different parts for SFR model.

In the final scenario, the proposed subspace system identification technique is highly challenged to get the lowest dynamic order model, 1st dynamic order model, of the governor-turbine system. The results are depicted in Figure 2.17 under Excessive Order reduction scenario. The results confirm that the proposed method is able to obtain the lowest dynamic order preserving acceptable dynamic performance of the obtained low-order governor-turbine model compared with the original model. It is worth mentioning that the lowest order model obtained under the Excessive Order reduction scenario is $\mathrm{TF}=\frac{0.2872}{s+0.3713}$. The results presented in this subsection in addition to the results discussed in the previous subsection serve as an evidence for the capability of the proposed methodology and validate it. Therefore, the proposed methodology is capable to capture the important dynamics that considered in SFR model.

Therefore, a low-order SFR model exists for any power systems, and it can be built once the required data are required. In case of that the data are not available, we have also provided a solution to estimate the data and models in order to construct the low-order SFR model.

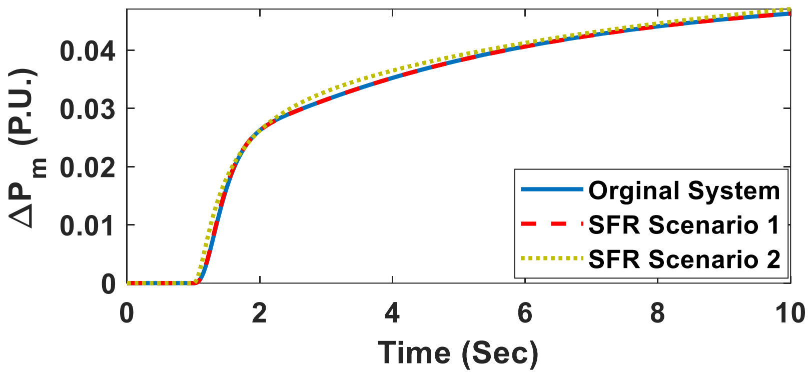

Figure 2.16. Validating the estimated low-order governor-turbine model for SFR model usage

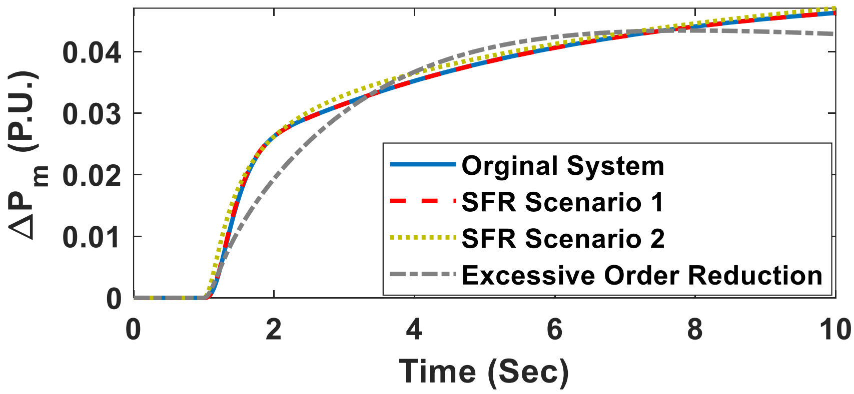

Figure 2.17. Validating the estimated excessively low-order governor-turbine model for SFR model usage

2.14. Application to NEM system

The aim of this section is to construct an advanced low-order SFR model for the National Electricity Market-NEM system. Before constructing the SFR for the NEM topology, it is worth introducing NEM system based on its description by its operator and the Australian department of energy. They define NEM as one of the largest interconnected electricity systems in the world. It covers around 40,000 km of transmission lines and cables, supplying around 9 million customers. The NEM is a wholesale market through which generators and retailers trade electricity in Australia. It interconnects the six eastern and southern states and territories and delivers around 80% of all electricity consumption in Australia. It is worth mentioning that Western Australia and the Northern Territory are not connected to the NEM. They have their own electricity systems and separate regulatory arrangements. The NEM facilitates the exchange of electricity between generators and retailers. Retailers resell the electricity to businesses and households. High voltage transmission lines transport the electricity from the generators to electricity distributors, who deliver it to homes and businesses on lower voltage ‘poles and wires. The wholesale market is where generators sell electricity and retailers buy it to on-sell to customers. There are lots of generators and retailers participating, so it’s highly competitive. The wholesale market operates around a common pool, or spot market, for wholesale trading in physical electricity. This process determines an electricity spot price which reflects physical supply and demand across the NEM. This spot price is an important price signal for investors. Financial markets sit alongside the wholesale market and involve retailers and generators entering into contracts to buy and sell electricity at an agreed price. The financial markets enable retailers to manage the risk of volatile wholesale prices for their customers.

The NEM system comprises five power regions, i.e. New South Wales (NSW), Victoria (VIC), Queensland (QLD), South Australia (SA) and Tasmania (TAS) power regions, as shown in Figure 2.18. The four power regions in the mainland, i.e. NSW, VIC, SA, and QLD, form the Mainland power system that is connected with TAS through an undersea HVDC cable so called Basslink. QLD is connected with NSW through two major interconnectors, i.e. an HVDC link named as Terranora interconnector and AC tie-line named as Queensland-NSW interconnector (QNI). SA is connected to VIC using two interconnectors as well, i.e. HVDC Murraylink link and AC Heywood tie-line. VIC is connected to NSW using only one AC interconnector, i.e. VNI. The topology and the main interconnectors are clearly depicted in Figure 2.18.

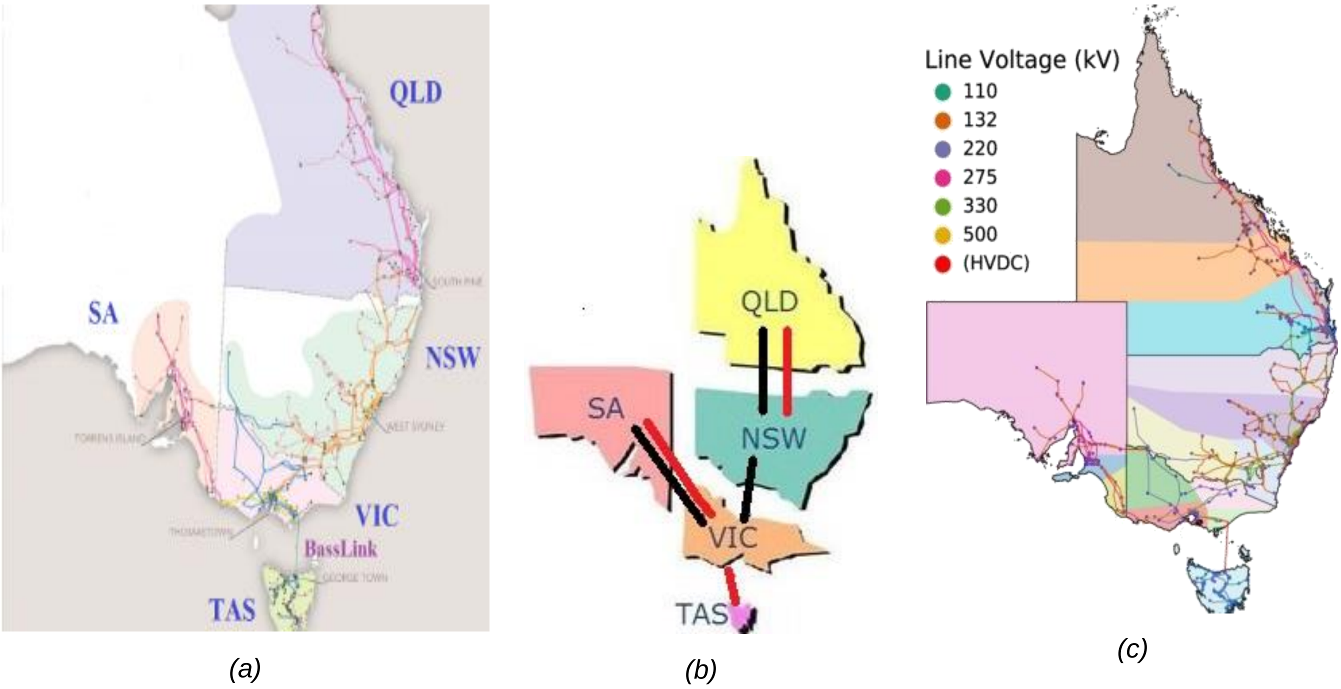

Figure 2.18. The National Electricity Market System: a) state-wise power regions and their geographical locations, b) type of interconnectors between different power regions (red-line= HVDC; black-line=AC tie-line), and c) transmission network in different power states with different voltage levels

To build an advanced SFR model, the SFR model for NEM is constructed to have the exact topology of the system from frequency response perspective. This means that we build the main low-order SFR model using the exact topology of NEM, i.e. five power regions. The type of interconnectors is also kept same to the reality. However, it worth mentioning that not all HVDC interconnectors provide frequency response services during contingencies. The confirmed information is that only Basslink provides primary frequency response. To achieve accurate modelling more information about interconnectors and the way of implementation of their primary frequency control is required. Therefore, we build a set of models, one of them we consider the international common practice, i.e. assuming that all HVDC interconnectors providing frequency support services, while in another model we develop the model to mimic reality. Also, to make the model more useful for different types of frequency and future planning about frequency studies, we build a set of SFR models from AC tie-lines view of point, that is a model with normal AC interconnectors, and another one with TCPS AC tie-lines.

The aim of this research is to develop an advanced low-order system frequency response model for research use purposes especially for studies of the system frequency situation under and beyond power system transformation. The developed model is suitable for developing and validating frequency support services considering the generation and storage mix in today’s power systems with ability to extend for future systems based on the energy transition plan, scenarios (like ISP), and G-PST scenarios for future systems, if any. In addition to the different possible scenarios, the model is developed to consider the different types of RESs and IBRs from frequency support perspective that are available in Australian and international grids or that would be considered in the future during or after the power system transformation. Moreover, the model is designed considering different parties in both demand and generation sides that can participate in frequency support services and other services related generation-demand balance services, including demand-side management (DSM), DR programs, ESSs, VPPs, modern flexible semi- dispatchable RESs (if any), and DGs. One of the other advances in the model is its ability to model and consider virtual inertia for supporting the frequency and RoCoF in power systems during energy transition. It is worth mentioning that the model is also advanced by adding demand0-side aggregator for supporting the frequency, for example electric vehicle aggregators for providing frequency services to future systems, especially NEM based on ISP's scenarios. Figure 2.19 depicts the MATLAB user-interface of the developed advanced low-order system frequency response model for National Electricity market system. It can be seen from the figure that the same topology of the current NEM system is preserved. This model can be validated based on the real-world data from the current NEM system once the data/measurements of NEM is available. Based on the real-word data, the parameters values for the developed low-order SFR model can be calculated.

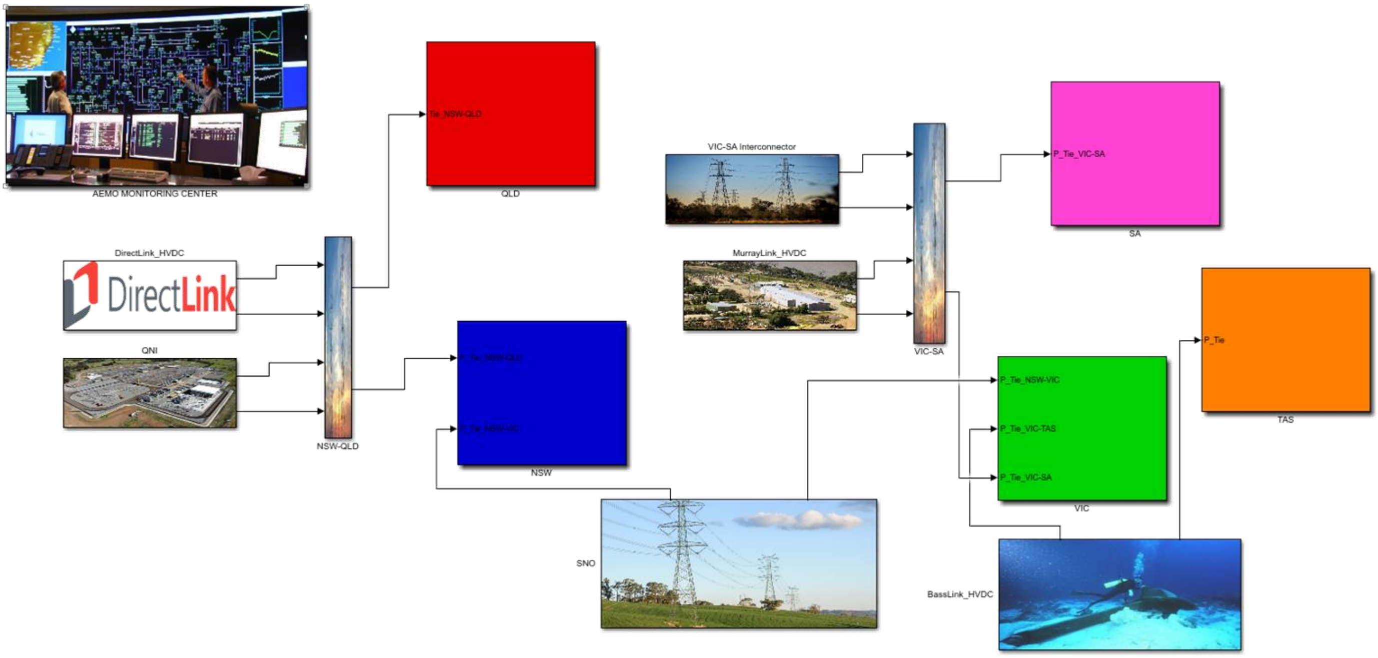

Figure 2.19. The topology of the main SFR model built for the system

As mentioned-above, the aim of this research is to build an advanced low-order system frequency response model. Therefore, the potential ancillary service sources for supporting the frequency control in future power systems need to be incorporated to make the model sophisticated enough to assess the frequency in future power systems during and beyond energy transition. In this research, we consider the capability of demand side for supporting the frequency in future power system, therefore, the aggregators of electric vehicles have been considered in the model. In this regard a suitable frequency response model of EV is developed and added to each power region. The data setting for such EV model can be set based on the future scenarios, i.e. ISP's scenarios. This gives the operator and researchers the source for evaluating the impact of EVs' demand on the frequency and the capability of their aggregators for supporting the frequency. In modern power systems including NEM system, there are several trial programs for implementing virtual inertia from IBRs, e.g. BESS-based virtual inertia service. Therefore, the model of virtual inertia is also considered in each power region of SFR model. The demand response model is also considered for frequency support. Additionally, the sources of variations such as solar and wind have been considered in the modelling, where their models have been described in the previous sections. A sample of model of one power region to be considered in SFR model is shown in Figure 2.19. Likewise, Figures 2.20 and 2.21 shows a sample of output power variation from wind and solar, respectively.

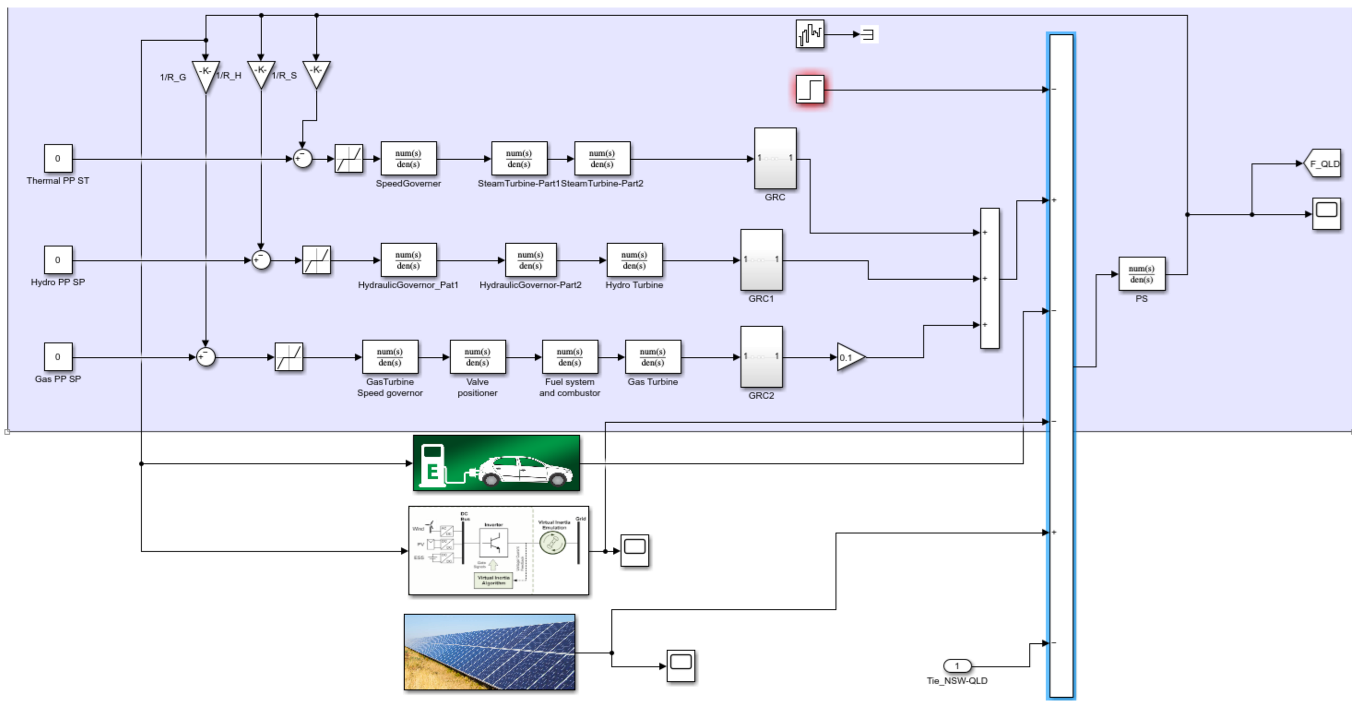

Figure 2.19. Sample of power region model showing the generation mix and the sources of frequency support services and the sources of variations

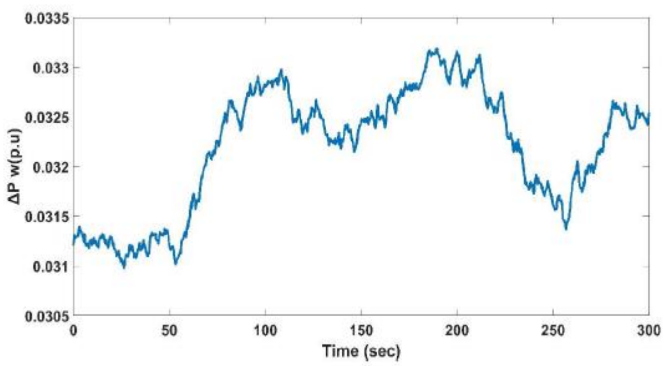

Figure 2.20. Sample of the active power fluctuation from wind power [9]

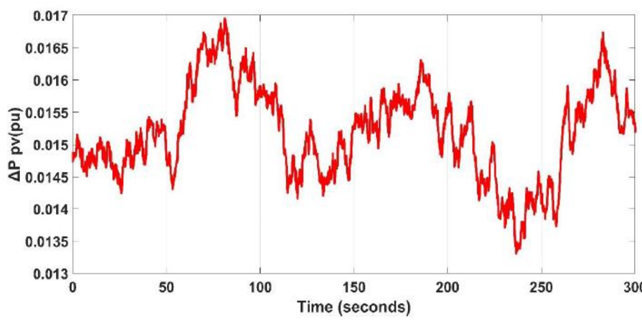

Figure 2.21. Sample of the active power fluctuation from solar power [9]

In case typical values considered for the parameters of the developed SFR Model of NEM system, we would be to perform some scenarios to test and evaluate the frequency response in such system. However, the parameters are subjected to change once the real-data is obtained from the operator, therefore, it might be some minor changes in the trend of frequency response if data would be changed. Let us consider that the system is being operated with sufficient reserve and without any large disturbances, Figures 2.21-2.22 show the frequency deviations and RoCoF in each power region, under normal operation, where the system is subjected to variations from renewable energy sources and demand only. Figure 2.23 shows the power flow deviation in interconnectors due to acceptable frequency fluctuation in different power regions.

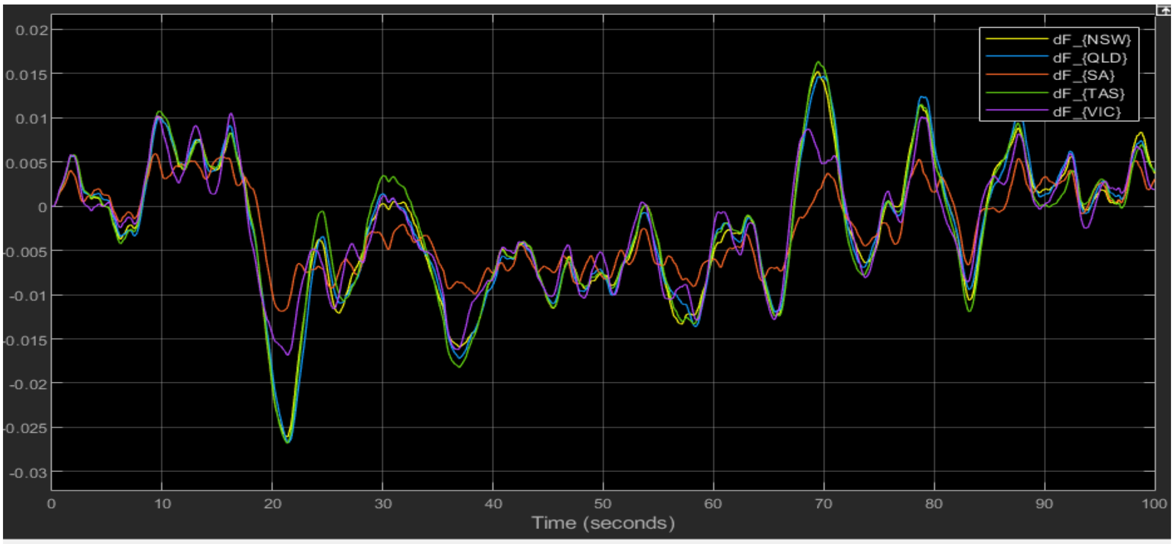

Figure 2.21. Frequency deviations in different power regions during normal operation

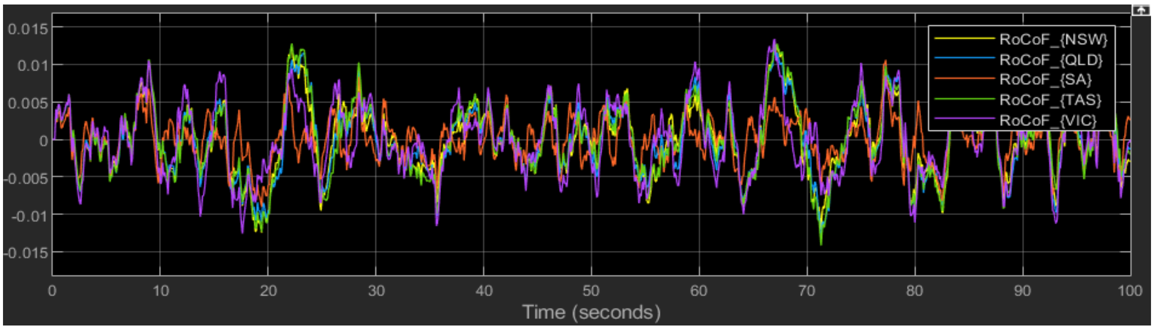

Figure 2.22. RoCoF in different power regions during normal operation

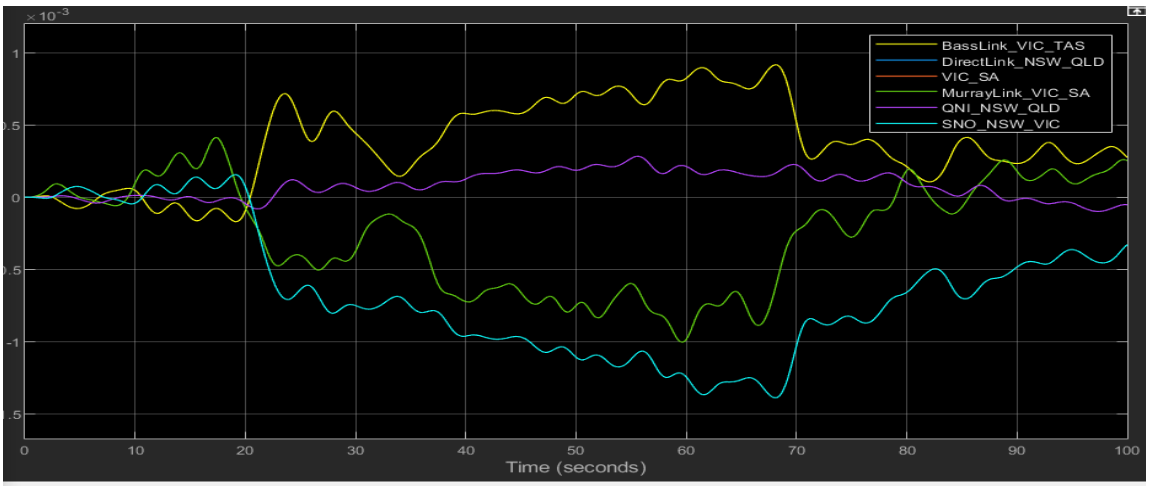

Figure 2.23. Tie-line power deviations in different power regions during normal operation

Further to the testing of the model for normal operation cases, the model is also has been tested for large disturbance (abnormal operation situation of the system. In this case, it is assumed that 0.1 p.u. step disturbance is occurred in VIC power region. Figures 2.24-2.25 show the simulated frequency deviations and RoCoF in each power region, under abnormal operation, where the system is subjected to a large disturbance occurred in VIC power region. Figure 2.26 shows the power flow deviation in interconnectors due to acceptable frequency fluctuation in different power regions (This is due to the fact that interconnectors power flow deviation is not involved with the current approach for calculating the area control errors and therefore such deviation will not be corrected by AGC system quickly).It is worth mentioning that this section is only to present the results, where the analysis and the lessons to be learnt will be discussed in details in next chapters of this report. The instruction on how to get parameters for the model, how to restructure SFR model for a specific power system, etc are clearly provided through the methodology developed in this report. This chapter has provided above a straightforward methodology to get data and model SFR.

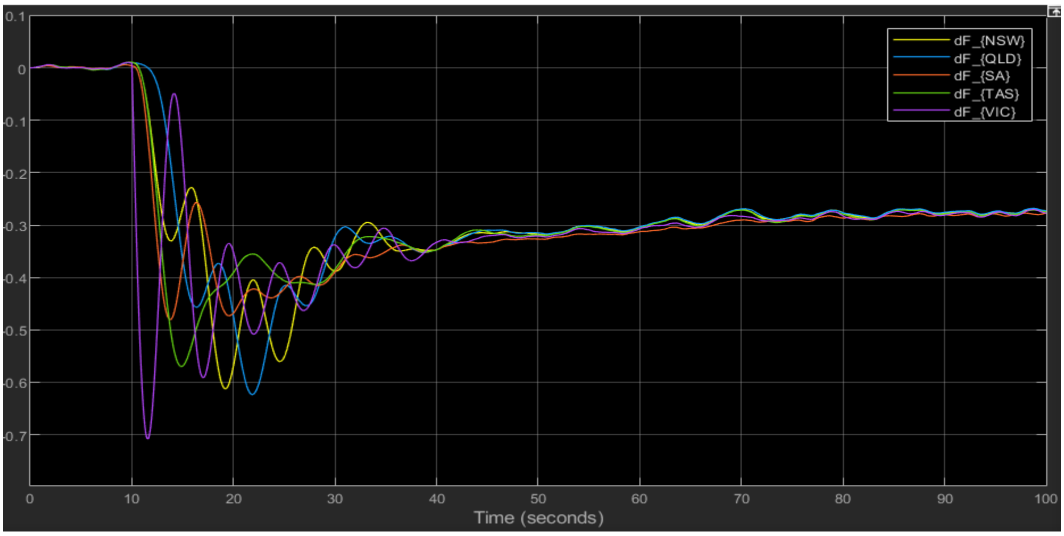

Figure 2.24. Frequency deviations in different power regions during abnormal operation

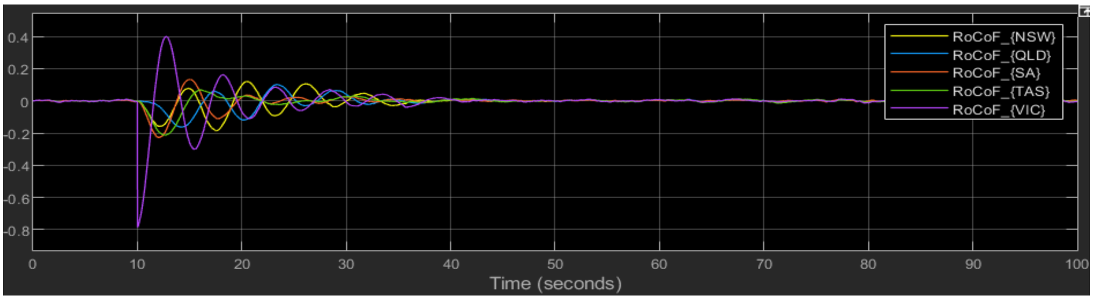

Figure 2.25. RoCoF in different power regions during abnormal operation

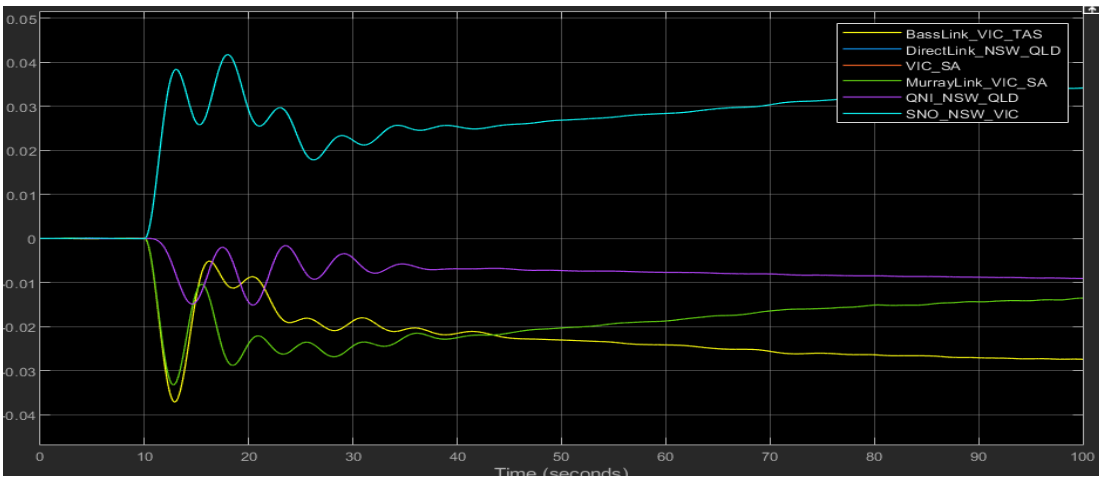

Figure 2.26. Tie-line power deviations in different power regions during abnormal operation

2.15. Insights and Outstanding Outcomes:

The system frequency response model describes the average network frequency response in one power region after a disturbance and has been applied to a wide variety of dynamic studies. However, the traditional literature does not provide a generic, analytical method for obtaining the SFR model parameters when the system contains multiple generators; instead, a numerical simulation-based approach or the operators' experience is the common practice to obtain an aggregated model. Likewise, the model developed in literature is for traditional power systems and there is no sophisticated model that consider emerging sources of services combined together to support frequency in modern power systems. Furthermore, there is no SFR model in literature that consider future scenarios such as the contribution of EV and combined such contributions to frequency from EVs with other frequency support service providers. Moreover, there is no developed SFR model in literature that consider the combination of interconnectors in such a way to mimic reality. Therefore, the aim of such research was to solve the research gaps and propose a sophisticated low-order system frequency response model that considers service providers from both demand and generation sides. Likewise, the virtual inertia concept is included in the model. This work also proposes an advanced technique to estimate the parameters' values for SFR model using real-world system measurements and data. In this regard, an advanced subspace system identification technique-N4SD is proposed for estimating the data and identifying the suitable model's dynamic order. The developed low-order SFR model is applicable for multi-machine multi-area interconnected power systems as well. The proposed low-order SFR model has several applications including system frequency control, frequency stability, and dynamic model reduction. The results show the method is promising with broad potential applications. Likewise, the model is useful for identifying challenges and issues related to frequency control and stability and is unique for understanding the requirements of regional inertia and frequency control ancillary services. The insights and outstanding outcomes of the above research are listed below:

1. A sophisticated low-order system frequency response model considers RESs, VPPs, DSM, ESSs, and FCAS services providers. The model is, therefore, more efficient from the computing and real-time implementation requirements.
2. Considering the high-level system topology and modelling the different types of interconnectors/tie-lines, providing the capability to understand the limitation and boundaries for transferring FCAS between different power regions. The model is, therefore, useful for understanding the requirements for FCAS regionalization.
3. The model considers future scenarios of the power systems during the energy transition and transformation. It is, therefore, useful for understanding the requirements from FCAS and frequency control perspectives for enabling the power system transformation and achieving future scenarios, e.g. ISP's scenarios.
4. The developed model is beneficial for identifying the challenges and issues that would encounter energy transition from the frequency control view of point; it is, therefore, useful for power system operators and planners by divining the required insights for enabling energy transition.
5. The model is capable for identifying the research gaps and technical issues related to frequency support in modern and future power systems going through energy transition.
6. The is capable for testing and validating frequency control methods and frequency support services techniques.
7. The model is applicable for understanding, designing, and analysing the UFLS techniques for power systems, therefore, the model is useful for power system frequency protection studies.
8. The model is useful for determining the requirements of services in a specific power region of an interconnected power system. This means the model is useful for understanding the requirements for frequency control ancillary services regionalisation.
9. The model is capable for determining the required minimum rotating synchronous inertia in a specific power region, considering the interconnectors and their capability to transfer the inertial response from one region to others.
10. The model is useful for coordination between different frequency service providers to achieve the optimal frequency response; this means the model can be useful for coordinating between primary frequency control, secondary frequency control, and inertia response in order of obtaining a satisfactory frequency response after a disturbance.
11. The model is unique for determining the optimal setting of frequency controllers and service providers to get a stable and secure frequency response.
12. The model can be useful for assessing and evaluating the frequency risk in modern and future power systems under different possible scenarios.

2.15. References

[1] P. M. Anderson and M. Mirheydar, "A low-order system frequency response model," in *IEEE Transactions on Power Systems*, vol. 5, no. 3, pp. 720-729, Aug. 1990, doi: 10.1109/59.65898.

[2] Q. Shi, F. Li and H. Cui, "Analytical Method to Aggregate Multi-Machine SFR Model With Applications in Power System Dynamic Studies," in *IEEE Transactions on Power Systems*, vol. 33, no. 6, pp. 6355-6367, Nov. 2018, doi: 10.1109/TPWRS.2018.2824823.

[3] Denis Lee Hau Aik, "A general-order system frequency response model incorporating load shedding: analytic modeling and applications," in *IEEE Transactions on Power Systems*, vol. 21, no. 2, pp. 709-717, May 2006, doi: 10.1109/TPWRS.2006.873123.

[4] H. Haes Alhelou, M. E. H. Golshan and N. D. Hatziargyriou, "A Decentralized Functional Observer Based Optimal LFC Considering Unknown Inputs, Uncertainties, and Cyber-Attacks," in *IEEE Transactions on Power Systems*, vol. 34, no. 6, pp. 4408-4417, Nov. 2019, doi: 10.1109/TPWRS.2019.2916558.

[5] P. W. Sauer and M. Pai, Power System Dynamics and Stability. Upper Saddle River, NJ, USA: Prentice-Hall, 1998.

[6] P. Kundur, N. J. Balu, and M. G. Lauby, Power System Stability and Control, vol. 7. New York, NY, USA: McGraw-Hill, 1994.

[7] IC Report, “Dynamic models for steam and hydro turbines in power system studies,” IEEE Trans. Power App. Syst., vol. PAS-92, no. 6, pp. 1904–1915, Nov. 1973.

[8] H. Haes Alhelou, M. E. Hamedani Golshan and N. D. Hatziargyriou, "Deterministic Dynamic State Estimation-Based Optimal LFC for Interconnected Power Systems Using Unknown Input Observer," in *IEEE Transactions on Smart Grid*, vol. 11, no. 2, pp. 1582-1592, March 2020, doi: 10.1109/TSG.2019.2940199.

[9] H. Haes Alhelou, M. Hamedani Golshan, and P. Siano. "Frequency response models and control in smart power systems with high penetration of renewable energy sources." Computers & Electrical Engineering, 2021.

[10] M. Khudhair, et al. "Robust control of frequency variations for a multi-area power system in smart grid using a newly wild horse optimized combination of PIDD2 and PD controllers." Sustainability 14.13 (2022): 8223.

[11] P. Overschee, and B. De Moor, “Subspace Identification of Linear Systems: Theory, Implementation, Applications”, Springer Publishing: 1996.

[12] L. Ljung, “System Identification: Theory for the User”, Second Edition, pp. 132–134. Upper Saddle River, NJ: Prentice Hall PTR, 1999.

[13] I. Jamaludin, et al. "N4SID and MOESP subspace identification methods." 2013 IEEE 9th International Colloquium on Signal Processing and its Applications. IEEE, 2013.

3. Chapter 3: An advanced frequency control and FCAS activation technique for power systems

Note: *Part of the work in this chapter has been prepared based on the following preprint: H.H. Alhelou, B. Bahrani, J. Ma, D. Hill, "Australia's Power System Frequency: Current Situation, Industrial Challenges, Efforts, and Future Research Directions", In IEEE TechRxiv, 2023.*

3.1. An overview

This section discusses real-challenge related to secondary frequency control and proposes a novel advanced frequency control system for the Australian National Electricity Market (NEM) power system considering the special design of its current automatic generation control system, which does not involve interconnectors between different power regions, which might result in technical challenges from scientific view of point for both stability and security of the system. The proposed new method converts the NEM centralised frequency control system to a fully decentralised one with virtually consideration of interconnectors' power, thus the stability and security would be improved and the high fluctuations in interchanged power smoothed without extra costs of infrastructure and procurement of frequency control ancillary reserves (FCASs). The novel idea is to model the interconnectors' power deviation as unknown input to operator in each power regions, like load disturbances and renewable power variations, using dynamic observation techniques, for enabling the proposed method capabilities. The method is theoretically verified that it can enhance stability and security and stabilise both local frequencies and power exchanges. The experiment results confirm the capability of the proposed method for the NEM system and its superiority over the existing adopted approaches in industries since the proposed approach models the interconnectors as unknown inputs resulting in less control complexity and enhanced cybersecurity and stability of the system.

3.2. A statement of the problem, a review of related literature, and a highlight of research gaps

Advanced energy systems are direct reflections of prosperous economies and developments in their nations. For more than a century, energy systems have been relatively operated in stable and reliable modes with no prominent global instability issues due to their high rotating inertia and synchronous machine units-based power generation. Due to environmental concerns and energy security risks, many countries around the world including Australia have moved forward to adopt new energy concepts, i.e. smart grid and deregulation, enabling high penetration of renewable energy sources (RESs) and inverter-based resources (IBRs) and loads (IBLs), which highly affect the rotating inertia and load-frequency relief [1]. The incentive programs adopted in Australia have led to the high capacity installation of distributed energy resources (DER), e.g. rooftop photovoltaic systems, in the distribution level and grid-scale integration of RESs, e.g. wind and solar energy sources, where the grid is not yet capable for such high penetrations. The aforementioned changes have highly reduced the rotating inertia and load-frequency relief putting the overall stability and security of the system in danger, and the problem would be more obvious in Australia after the approval of the 2050 Australian decarbonisation plan which accelerates the deployment of RESs through the grid. In addition to the aforementioned challenges that exist in most of the developed Countries like Australia, the Australian National Electricity Market (NEM) system does not adopt the common international practices in controlling the frequency. Its frequency control system does consider the power flow deviations in its automatic generation control system, which theoretically might lead to higher local frequencies and power fluctuations in interconnectors which affect its stability and security. These real-world industry challenges and issues concisely present the problem statement and motivate this research work, supported by CSIRO and G-PST project, for providing suitable and affordable solutions for this uniquely-designed massive power system located in the eastern and south-eastern states of Australia.

According to IEEE/CIGRE joint task-force (TF) on stability terms and definitions, power system stability can be divided into three categories, i.e. Frequency, rotor angle, and voltage stabilities [2]. Maintaining frequency stability is considered as the most important task in power system operation and control centers because frequency is a relatively global variable in power systems. Likewise, the frequency in different power regions should be maintained with specific standards in order to link these regions together through major transmission links and tie-lines, known as interconnectors in the Australian NEM system. Any deviation in the frequency in one area compared to others would lead to high deviation and fluctuation in the transferred power between the different power areas which might trigger the protection relays resulting in separated areas/regions from each other in which each area would be operated as an island after the separation with the possibility of blackouts due to higher or lower new frequency and imbalanced operation situations, e.g. Queensland (QLD) and South Australia (SA) power regions separation on 25 August 2018 in Australian NEM system. For instance, a recently severe nation-level blackout has occurred in Pakistani power system [3], and a severe separation in ENTSO-E to two islands, one with higher frequency and the other with lower frequency, occurred in European power system [4], indicating the need for taking the network topology especially major transmission links in the stability studies for modern and future smart power systems. However, the situation in Australia's system is different since NEM does not include the interconnectors in frequency control approach, operating the system under continuous stress from frequency instability viewpoint.

To maintain their stable operation, power systems are equipped with different frequency control and protection schemes. Frequency control is generally divided into three levels, i.e. primary, secondary, and tertiary control levels [5-6]. The primary control is responsible for intercepting the frequency decline before triggering the under-frequency load shedding (UFLS) relays which is a local controller implemented using the governor-droop characteristic in traditional power systems. In this regard, new concepts have been recently suggested that consider more dynamical demand response for providing such ancillary services for future power systems [7-8]. However, network topology and major transmission lines, i.e. tie-lines, have not been considered in the design of primary frequency control which is a practical issue that needs to be considered in order to enhance the dynamic performance of modern power systems with high renewable energy shares. The secondary frequency control loop, which is also known as load frequency control (LFC) or automatic generation control (AGC), aims to maintain the frequency and power flow in a permissible level, however, the NEM system does not follow the international practice in involving interconnectors power deviation in the calculation of area control error (ACE). In fact, the whole system in NEM, comprising 5 large power regions, is operated as a single control area posing great technical and research challenges.

Great research efforts have been devoted in literature for improving the international practice of secondary frequency control and AGC systems, where different control approaches and methods, such as model-based control approaches [9-10], evolutionary optimization-based control techniques [11], and sliding-mode control methods [12], have been suggested for controlling the small frequency and tie-line power variations due to variation of renewable power generation and the small demand changes occurring because of the stochastic behavior of end-users. Furthermore, emerging technologies such as energy storage systems (ESSs) [13], virtual inertia [14], virtual power plant (VPP) [15], Superconducting magnetic energy storage (SMES) systems [16] have been suggested for frequency control in modern power systems. Interested readers are referred to the comprehensive review, by Alhelou et al., [5, 17] for more details in the different methods and their challenges and opportunities.

In general practice of frequency control, the real-time measured power deviation through tie-lines in addition to the center of inertia frequency measured in each area are used to generate the AGC control signals that can diminish both frequency and power flow variations in a specific operating point. Additionally, the different types of tie-lines/interconnectors can be effectively involved in frequency response provision and LFC services using specific mechanisms. For instance, advanced HVDC and Thyristor Controlled Phase Shifter (TCPS) can provide more efficient frequency and power flow services once they are supplied with sufficient and advanced control approaches, if they are compared to AC tie-lines [18]. However, the aforementioned general practice is different from Australian practice in the implementation of secondary frequency control, where the tie-line power deviation is completely ignored and replaced by the time error, posing challenges to its system frequency stability and security, presenting limitations in uptaking the installed capacity of interconnectors/tie-lines, and increasing the local frequencies phenomena [19].

This paper solves the following industry concerns and research gaps, where by which it contributes to both industry and research bodies of knowledge:

- How to effectively involve tie-lines'/interconnectors' power flows in frequency control of Australian NEM's system and similar ones without much extra investment cost in information and communication technology (ICT) infrastructure; where successful involvement of them would highly improve the frequency stability and security and enhance the uptake of invested interconnectors/tie-lines.

- How to convert the centralised secondary frequency control in the Australian NEM power system to fully decentralised one without additional complexities. Such conversion would improve the operation security of whole system and fairly allocate FCASs in different power regions.
- How to convert the quasi-decentralised frequency control systems in the international practices to fully decentralised one. Successful conversion would be a tremendous contribution to the currently adopted LFC/AGC with tie-line consideration in international real-world systems; where a fully-decentralisation would highly reduce the requirements in LFC/AGC implementation in international practices, improve the stability and security, and reduce the complexities of implementation.

By solving the above-mentioned research gaps, this work contributes to the body of knowledge by presenting a novel frequency control method for the Australian National Energy Market power system considering current issues and challenges in the implementation of the AGC system in comparison with international practices. However, an economic study and analysis are needed to understand the final cost associated with converting AGC systems to fully decentralised one, which is out of the scope in this work. The method is extended to international practices to successfully and affordably convert the quasi-decentralised LFC approaches to fully-decentralised ones, for the first time, unleashing their potential capabilities. To this end, this work employs a novel dynamic observation technique known as known input observation (UIO) for virtually decoupling the different power regions from each other, leading to several benefits including i) the ability to model interconnectors as unknown input to each power region, ii) the possibility to better controlling the frequency in power regions with high variations and uncertainties, like SA region which is enriched with RESs, and iii) the ability to handle different uncertainties, disturbances, deviations in imported/exported powers from/to other power regions since they would become unknown inputs to the system dynamics. The results confirm the superiority of the proposed technique since it solves existing industry challenges, not only in Australia but also internationally by making quasi-decentralised systems be converted to fully-decentralised one, and improves the overall stability and security of the power systems' frequency.

3.3. Discussion on the problem and the needs to address it

Secondary frequency control is crucial, especially for interconnected power systems, yet is the most challenging control system in modern power systems due to several technical issues that will be discussed in this section. The necessity of LFC control is to compensate the area control error in each power region and/or ACE of the whole system in order to enable safe and stable interconnection between different systems and/or power regions. Conventionally, this crucial system was implemented as a centralized one, but due to its impact on the overall stability and security of the systems, several efforts have been made to convert it to a quasi-decentralized one. However, the fully-decentralization of this control system was not feasible due to several technical challenges including the need for remote signals which limits its decentralization, which is a real-world industry challenge.

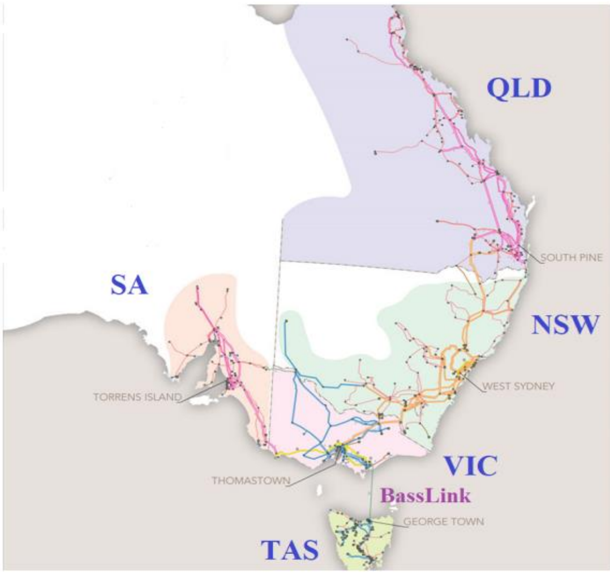

Figure 3.1. General topology under investigation and its sub topologies

The Australian National Electricity Market power system comprises 5 power regions, namely VIC, NSW, QLD, SA, and TAS. This system is spilt into two subsystems, i.e. mainland system comprising VIC, NSW, QLD and SA which is connected to another subsystem, i.e. TAS, via an undersea HVDC cable known as BassLink as shown in Figure 3.1. The BassLink does not currently provide sufficient frequency response and frequency regulation services due to technical challenges and due to the fact that both subsystems are being operated using different frequency operating standards (FOSs), especially during credible/non-credible events. It is worth mentioning that there are two ACE signals, i.e. one is determined for the mainland interconnected system and the other is calculated for the TAS system. In fact, both systems are currently separated from each other from the frequency control view of point, while the BassLink interconnector supports the power deficit in TAS system since the power dispatch of both systems is done simultaneously based on one spot market each 5 minutes.

The aforementioned operation facts of the NEM system present two main challenges, from frequency control and stability perspectives, which are:i) TAS system is being operated as an isolated system from frequency stability and security perspectives even though it is connected to VIC region in the Mainland system using BassLink, which highlights known concerns about frequency stability and security in isolated systems; and ii) the Mainland interconnected system frequency is being controlled based on one ACE meaning that the secondary frequency control is strictly centralized one which raises concerns about its stability and security.

Due to its importance, it frequency stability and security, LFC systems have been converted to quasi-decentralized ones with no more efforts in implementing them as fully-decentralised one due to the implementation feasibility issues of fully decentralized ones, which is one of the main challenges in international practices of secondary frequency control systems. In (1), the LFC is internationally implemented as a quasi-decentralized one because it requires local frequency deviation, F_i, and remote measurements of tie-line power flow, $P_{tie,i}$, while the NEM practice of LFC implementation is modelled using (2). The NEM practice presents the fact that whole the Mainland system frequency is controlled using one ACE which does not involve the tie-line power flow deviations between different power regions, which presents technical challenges and stability and security issues.

$$ACE_{int} = \beta \times \Delta F_i + \Delta P_{tie,i} \quad (1)$$

$$ACE_{NEM} = 10 \times \beta \times (F - FN - FO) \quad (2)$$

where ACE_{int} and ACE_{NEM} are the calculated area control error in international practices using quasi-decentralised control methods and calculated one for the NEM system. F_i is the frequency in the ith power region, F is the actual frequency measurement, F_O is the time error which is also known as the frequency offset representing accumulated frequency deviation, and β is the frequency bias which is a tuned value that represents the conversion ratio between MW and 0.1 Hz of frequency deviation.

The aforementioned facts verify that there are real-world challenges in the international practice of the fully-decentralized implementation of AGC/LFC that need to be solved and industry challenges in NEM system due to centrally implementing AGC system and the inconsideration of interconnectors' power flow in NEM AGC system. These real-world technical challenges prevent the utilization of several decentralized control methods and the uptake of their advantages in improving the stability and security of frequency in the NEM system and international power systems as well. Thus, this CSIRO funded G-PST research is devoted to solving the aforementioned technical challenges.

3.4. The Developed Novel Methodology

In what follows, we develop novel dynamic state estimators that can track dynamic systems in any power system/power region enriched with uncertainties, variations, and unknown inputs, like the Australian NEM system. Since the aim is to virtually decouple power regions from each other, for the first time, by a novel concept presented here known as unknown inputs between regions, therefore a unique dynamic state estimator is designed for each power region. In each power region, the term unknown input (UI) refers to the short-term deviations in imported/exported real power through the interconnectors including HVDC and AC tie-lines, and variation in the generated power from RESs, e.g. solar and wind, and fluctuation in load demand in each region.

A. *Generic Dynamic State Estimator Considering UIs:*

Let's consider an interconnected power system comprising N power regions, i.e. $N_{NEM} \in$ {VIC, NSW, QLD, SA, TAS}. In the such a whole system, the ith power region system can be modelled as,

$$\dot{x}_i(t) = A_i x_i(t) + f_i(x_i, t) + B_i u_i(t) + E_i d_i(t) \quad (3)$$

$$y_i(t) = C_i x_i(t) + D_i u_i(t); \qquad i \in \mathrm{R}^N, \quad (4)$$

where $x_i \in \mathrm{R}^{n\times1}, u_i \in \mathrm{R}^{r\times1}$, $d_i \in \mathrm{R}^{q\times1}, y_i \in \mathrm{R}^{m\times1}$ are ith power region vectors of dynamic states, known/control inputs, unknown inputs, and measurable output variables, respectively. $f_i(x_i, t)$ models the nonlinearities.

Without losing the generality and considering the fact that u(t) is known in real-time in control center resulting in $y_{i,new}(t) = y_i(t) - D_i u_i(t) = C_i x_i(t)$ and the term $f_i(x_i, t)$ can be involved in x_i and d_i based on an efficient linearization technique, therefore, the above model can be written as a generic differential-algebraic compact form, sufficient for AGC/LFC studies, as,

$$\dot{x}_i(t) = A_i x_i(t) + B_i u_i(t) + E_i d_i(t), \quad (5)$$

$$y_i(t) = C_i x_i(t); \qquad i \in \mathrm{R}^N, \quad (6)$$

where A, B, C, and E are the system matrices with appropriate sizes known to the system operator.

Let us now define a new virtual dynamic observation system, given in (7-8), as a dynamic system effectively designed to accurately track the inaccessible/accessible variable states in the physical power system, given in (5-6), in a real-time manner.

$$\dot{z}(t) = Fz(t) + TBu(t) + Ky(t) \quad (7)$$

$$\hat{x}(t) = z(t) + Hy(t). \quad (8)$$

where $z_i \in \mathrm{R}^{n\times1}$ is the virtual states of the virtual system, that is the observer, $\hat{x}_i \in \mathrm{R}^{n\times1}$ is the observed/real-time estimated state variables of the system (\ref{eq2}). F, T, K, H are matrices that need to be well-designed/selected for guaranteeing asymptotically stability of dynamic estimation error.

The system (7-8) can observe the system state variables regardless $d_i(t) \in$ {P_{RESs}, P_d, P_{tie}}. Thus, the proposed system would track the dynamic states of the power systems without any knowledge of real-time variations and fluctuations in the active power generated by RESs, consumed by demand, and imported/exported from/to other power regions through real interconnectors, i.e. tie-lines, which is a great feature would build a novel concept of frequency control involving interconnectors' power without knowledge of it and handling uncertainties in demand and generation sides without pre-knowledge of their magnitude and stochastic probability.

Theorem: Given a power system (5-6) with relatively known system matrices. The system (7-8) is a dynamic observer of the original system (5-6), if the dynamics of estimation error e(t) is asymptotically stable. Thus, there exists a Hurwitz matrix F; i.e. a square matrix is a Hurwitz matrix if every eigenvalue of F has a strictly negative real part, that is, Re [λ] < 0; such that, $\dot{e}(t) = Fe(t)$, where e(t) is the observation/estimation error of x (t) in (5) regardless of d(t), and $\dot{e}$ is the estimation error dynamic.

Proof: Assume the estimation error is e(t)=x(t)-ẋ(t), hence taking the first derivative, and considering $K=K_1+K_2$, yields,

$$\begin{aligned}\dot{e}(t) &= (A - HCA - K_1C)e(t) + [F - (A - HCA - K_1C)]z(t) \\ &+ [K_2 - (A - HCA - K_1C)]y(t) \\ &+ [T - (I - HC)]Bu(t) + (HC - I)Ed(t)\end{aligned} \quad (9)$$

The above mathematical expression of the error dynamics (9) presents an attractive fact that the error dynamic can be asymptotically stable if and only if the first term of the right-hand side of (9), that is A-HCA-K_1C is a Hurwitz matrix and let us named as F, and the other terms should be zeros. Thus, the state estimation error dynamic $\dot{e}(t)$ will be stable if and only if the matrix F is a Hurwitz matrix and if the conditions given in (10) are strictly stratified.

$$\begin{aligned} &(HC - I) = 0 \\ &T = I - HC \\ &F = A_2 - K_1 C \\ &K_2 = FH \\ &K = K_1 + K_2 \\ &A_2 = A - HCA \end{aligned} \tag{10}$$

$$\dot{e}(t) = F\,e(t) \tag{11}$$

If the above conditions (10) hold true, then (7-8) becomes a stable observer of (5-6); that is $\dot{e}(t) = F\,e(t)$. This completes the proof.

For illustrative purposes, the proposed dynamic observer in (7-8) that can estimate the state variables regardless unknown inputs, disturbances and uncertainties is illustratively depicted in Figure 3.2. One can see the main matrices that need to be optimally determined before making such an advanced observer feasible. In what follows, we will work on developing a straightforward method for obtaining the matrices in order to design an advanced observer that can benefit the system operator for several applications in monitoring and control rooms.

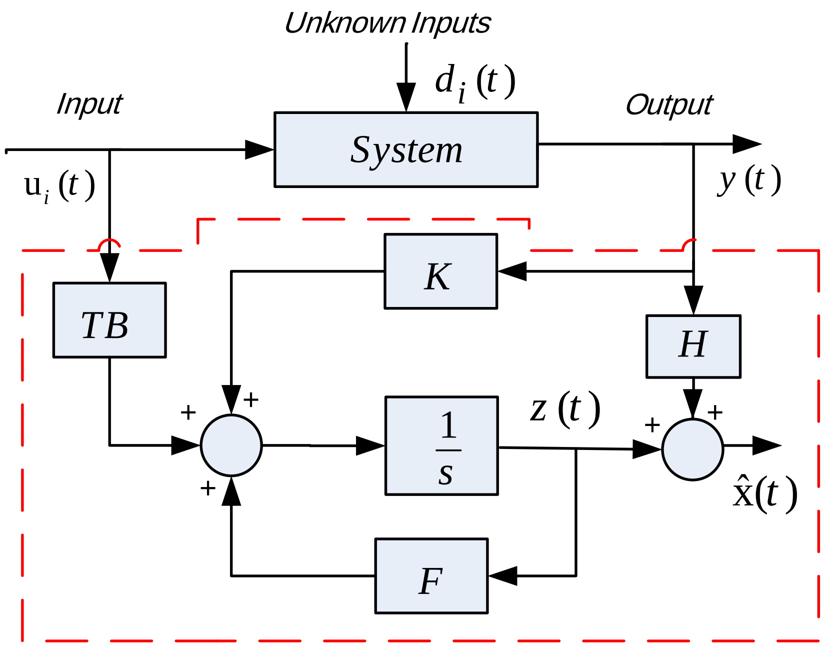

Figure 3.2. The block diagram of the proposed observer in (7-8)

Equation (11) shows that the state estimation error, e , approaches asymptotically zero, if the matrix F is stable. As a consequence, the matrix K_1 should be assigned such that the matrix F is Hurwitz.

By mathematically analysing the system and the proposed observer using controllability and observability techniques, it is evident that the state estimation is decoupled from unknown input vector, d . It is proven that the sufficient and necessary conditions for the dynamic system given in (7-8) to be an UIO system for the ith area of the power system defined in (5-6) are:

i) $rank(CE) = rank(E)$ (12)

ii) The pair (C, A_1) is detectable (13)

$$A_1 = A - \Theta \tag{14}$$
$$\Theta = E[(CE)^T CE]^{-1}(CE)^T CA \tag{15}$$

Also, it has been proven that the disturbances modelled as unknown inputs, can be estimated using (16).

$$\hat{d} = (CE)^{\dagger}\left[\dot{y} - CA\hat{x} - CBu\right] \tag{16}$$

B. UIO observer producer

In this section, a straightforward procedure for designing an UIO dynamic system for each power area in interconnected power systems is provided. The first step is to determine the power areas' matrices, in which the output matrix, C, is determined based on the available measurements. The second step is to check the existence of UIO by checking the rank condition, $rank\ (CE) = rank\ (E)$ and the detectability of the pair (C, A_1). If the rank condition is not met, then the UIO does not exist. To overcome this problem, the rank of matrix C can be changed by selecting new virtual outputs to satisfy the rank condition. The next step is to check the observability of the system by evaluating the detectability of the pair (C, A_1). Once these conditions are satisfied, the matrix K_1 can be easily computed using a mathematical method called pole placement. Otherwise, if the pair (C, A_1) is not detectable, a transformation matrix P should be calculated by performing observable canonical decomposition on the pair (C, A_1), as illustrated in (17) and (18).

$$PA_1P^{-1} = \begin{bmatrix} A_{11} & 0 \\ A_{12} & A_{22} \end{bmatrix} \quad where\ A_{11} \in \Re^{n_1 \times n_1} \tag{17}$$

$$CP^{-1} = \begin{bmatrix} C^* & 0 \end{bmatrix} \quad where\ \ C^* \in \Re^{m \times n_1} \tag{18}$$

n_1 is the rank of the observability matrix for the pair (C, A_1) in which the pair (C^*, A_{11}) is observable. The unobservable modes are combined in the eigenvalues of A_{22}. More details about the observable canonical decomposition method can be found in [18].

C. Further Advantages and Contributions

The proposed method has the potential for further contributions in addition to its core item of modelling interconnectors as unknown inputs to each power region, resulting in sophisticated frequency control and a substantial enhance in frequency approach adopted in Australian National Electricity Market System. Since the introduced dynamic estimator is able to track dynamic states in different regions in a real-time manner, it can be used as an alarm for the unhealthy operation of the frequency control system in NEM and international systems by structuring residual signals r(t) and threshold σ, as given in (19-21), based on the needs in the mentoring/control rooms, so that the residual signals can online detect faulty measurements, faculty controllers, incorrect measurements, and physical or cyberattack to the system.

$$r(t) = e_y = y(t) - \hat{y}(t) = (I - CH)y(t) - Cz(t) \tag{19}$$

$$\hat{y}(t) = Cz(t) + CHy(t) \tag{20}$$

$$\exists \sigma\colon \left|\left|r\right|\right| > \sigma \rightarrow Abnormal; \left|\left|r\right|\right| \leq \sigma \rightarrow Normal \tag{21}$$

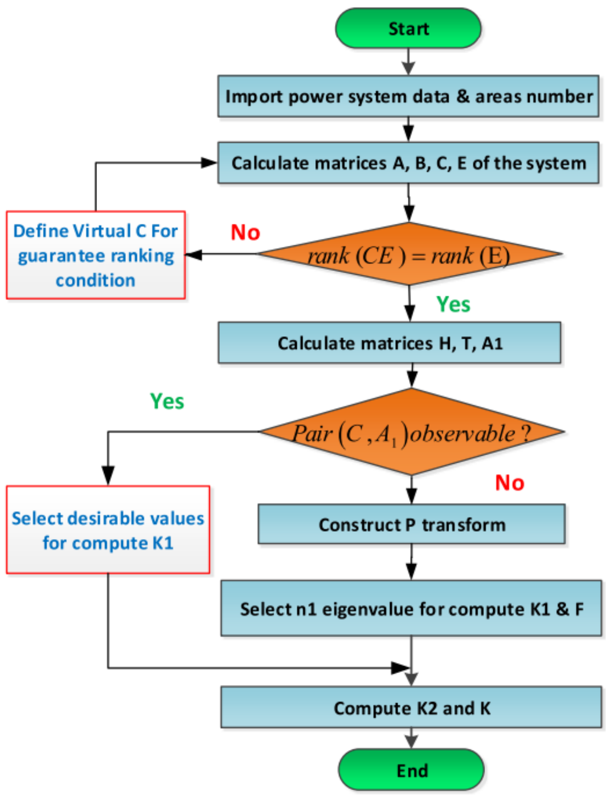

Figure 3.3. The suggested procedure for designing the observer

In fact, all the aforementioned features can be achieved without extra design modification of the proposed technique. Additionally, the classification of the fault type and localization of its sources can be done without extra effort by adding a set of the suggested above observer. Furthermore, the uncertainties, unknown inputs, and equivalent real-time variation in both demand and generations side, e.g. due to solar and wind powers. The method is capable of continuously tracking disturbances in each power region, which can provide great knowledge to the operator so that they can be involved in advanced frequency control, such as disturbance-rejection approaches, where their implementation has not been feasible due to unavailability of real-time tracking of the overall disturbance in modern power systems, which would be a potential future work. Finally, the above-introduced procedure for designing the observer and obtaining it optimal matrices is depicted in Figure 3.3 as flowchart. In this flowchart, all the steps are discussed mathematically in the above subsections. Once the observability of the system and feasibility of the observer existing are proven, the operator can utilise the proposed technique for different applications including power system control, monitoring or detection of physical and cyber failures and attacks.

3.5. *Generic Multi-Area & Interconnectors Frequency Response Models*

To generalise the proposed affordable frequency control method, a generic graph theory is used to represent interconnected power systems. Let us consider a power system consisting of G generators, B buses, TL transmission lines, and L loads. Based on the coherency of synchronous generating units, a new topology can be obtained from a such system based on dividing it into N power regions linked together using I interconnectors, i.e. tie-lines. Thus, the system is defined by a graph $(\mathrm{N}, \varepsilon)$, where $\mathrm{N} = \{1, 2, \ldots, |\mathrm{N}|\}$ denotes the set of power regions, i.e. control areas, in which $|\mathrm{N}| = \mathrm{A}$ and $\varepsilon \subseteq \mathrm{N} \times \mathrm{N}$ represents a set of interconnectors/tie-lines connecting the control-areas together. Let us take the Australian NEM power system as an example, there are G=200 generators, B=000 buses, TL=000 lines, and L=000 loads. This system is divided into 5 control areas, i.e. $\mathrm{A} = |\mathrm{N}| = 5$, (VIC, NSW, QLD, SA, TAS), and 6 major interconnectors, i.e. I=6. It is worth mentioning that the interconnectors are classified based on their type as HVDC link, $\mathrm{I}_{\mathrm{HVDC}}$, $\mathrm{ACtie-line}$, I_{AC}, and Interconnector with TCPS, i.e. I_{TCPS}, and the generation source is categorized as RES-based, G_{RES}, thermal turbine-based, G_{THR}, gas turbine-based G_{GAS}, and hydro turbine-based G_{HYDRO}. In what follows, sufficient dynamic models of both control areas (power regions) and major tile-lines (interconnectors) are introduced for assessing the frequency and power flow deviations in different regions and through different interconnectors in Australia's power system and for validating the proposed affordable frequency control method.

A. Power-Areas Dynamic Model:

In industry, it is crucial to equivalise each area to a single bus model, due to several technical and computation challenges, in order to assess frequency response and its control, where such model is found to be sufficient in NEM studies and its response match the detailed models in PSS/E and PSCAD. An equivalent generator and equivalent load are connected to a single busbar. The dynamics of the equivalent synchronous generating unit in area i is modelled using swing equation as follows,

$$2H_i\Delta\dot{\omega}_i + D_i\Delta\omega = P_i^m - P_i^e - P_i^{loss} \quad (22)$$

where H_i is the total rotating inertia in area i, D_i is the damping coefficient, which is known as load-frequency relief, in area i, P_i^m represents the total mechanical power converted to electricity by generators inside the ith power area, P_i^e models the equivalent loads, and P_i^{loss} models the power losses inside the power area where their major amount is a loss in the local electrical network due to power flow.

In (22), the total rotating inertia, and total mechanical and electrical powers can be determined as follows,

$$H_i = \frac{\sum_j^{N_{G,i}} H_j S_j}{\sum_j^{N_{G,i}} S_j} \quad (23)$$

$$P_i^m = \sum_j^{N_{G,i}} P_j^m;\ P_i^e = \sum_j^{N_{G,i}} P_j^e \quad (24)$$

where $N_{G,i}$ is the number of generating units in area i, and S is the apparent power of generating unit j in area i.

Since this paper focuses on frequency stability, it is crucial to model the dynamic responses due to changes in the frequency where such responses increase/decrease the total mechanical power due to governor-turbine systems. There are different types of dynamic models for governor-turbine systems. Here, we introduce the dynamic models of reheated thermal turbine systems as follows,

$$\Delta\dot{P}_{gi} = \frac{K_{ti}K_{ri}}{T_{ti}T_{ri}}\Delta X_{gi} + \frac{T_{ti}-K_{ri}}{T_{ti}T_{ri}}\Delta P_{ri} - \frac{1}{T_{ri}}\Delta P_{gi} \quad (25)$$

$$\Delta\dot{P}_{ri} = \frac{K_{ti}}{T_{ti}}\Delta X_{gi} - \frac{1}{T_{ti}}\Delta P_{ri} \quad (26)$$

$$\Delta\dot{X}_{gi} = -\frac{K_{gi}}{R_i T_{gi}}\Delta f_i - \frac{1}{T_{gi}}\Delta X_{gi} + \frac{K_{gi}\alpha_{gi}}{T_{gi}}\Delta P_{ci} \quad (27)$$

$$\Delta\dot{P}_{ei} = -\frac{1}{T_{ei}}\Delta P_{ei} + \frac{K_{ei}\alpha_{ei}}{T_{ei}}\Delta P_{ci} \quad (28)$$

$$\Delta P_{tie,i} = \sum_{j=1}^{N}\left(P_{tie,act_{ij}} - P_{tie,sched_{ij}}\right) \quad (29)$$

where Δf_i, ΔP_{gi}, ΔP_{ri}, ΔX_{gi}, and ΔP_{ei} denote the deviations of frequency, mechnical power, the output mechanical power of the reheater section, the valve position, and the response power of demand side programs, respectively; $K_{\{gi,ri,ti,ei\}}$ and $T_{\{gi,\ ri,ti,ei\}}$ are set of gains and time constants for the governor, the reheater, the thermal turbine, and the demand response, respectively; R and b_i is governor droop and frequency bias, respectively. $\Delta P_{tie,i}$ is the deviation in the transferred power from its scheduled value.

B. Tie-line frequency response Dynamic Model:

This paper solves an industry problem related to the involvement of interconnectors in AGC/LFC in Australia's power systems by suggesting an affordable frequency control method applicable for international practices as well by its contribution to converting the real-world centralized or quasi-decentralized LFC approaches to fully decentralized ones. Therefore, the different types of transmission systems, i.e. AC transmission links, AC transmission lines with power flow controllers, e.g. AC tie-lines with integrated TCPS, and HVDC transmission links with/without active power control equipment are in-depth analysed and their suitable frequency response model are presented in what follows.

The transmitted power deviation through an AC interconnector between power regions i and j is expressed as,

$$\Delta \dot{P}_{AC_{ij}}(t) = T_{ij}\left(\Delta\omega_i(t) - \Delta\omega_j(t)\right) = 2\pi T_{ij}\left(\Delta f_i(t) - \Delta f_j(t)\right), \tag{30}$$

where,

$$T_{ij} \backslash triangleq 3 \frac{|v_i||v_j|}{x_{ij}} \cos\left(\theta_i^0 - \theta_j^0\right) \tag{31}$$

therefore, it can be rewritten as,

$$\Delta P_{AC_{ij}}(s) = \frac{2\pi T_{ij}}{s}\left(\Delta f_i(s) - \Delta f_j(s)\right). \tag{32}$$

In addition to AC transmission links and to mimic reality, tie-line equipped with TCPS is also considered in this paper. The power deviation of tie-lines with TCPS can be determined as,

$$\Delta P_{AC_{ij}}(s) = \frac{2\pi T_{ij}}{s}\left(\Delta f_i(s) - \Delta f_j(s)\right) + \Delta P_{S_{ij}}(s) \tag{33}$$

where,

$$\Delta P_{S_{ij}}(s) = T_{ij}\frac{K_{S_{ij}}}{1+sT_{S_{ij}}}\Delta f_i(s) \tag{34}$$

Based on the above models, the total power deviations through AC tie-lines connected to ith area is calculated as follows,

$$\Delta P_{AC_i}(s) = \sum_{j=1, i\neq j}^{N} \Delta P_{AC_{ij}}(s) \tag{35}$$

Nowadays, there are prominent research and industrial activities for motivating the deployment of DC transmission links, especially after the recent developments in power electronics that made them cost-efficient in comparison with AC transmission links, especially for underwater cables to link offshore wind farms to national energy networks. From the power system frequency control viewpoint, there are two types of HVDC links, namely controllable and non-controllable transmission links. The first type, i.e. controllable ones, changes their transferred power from one area to others based on the frequency changes in the connected areas or due to changes in the voltage angles of their terminals, while the second one, non-controllable DC links, transfer a specific power between areas regardless the frequency situation in the connected areas which means that the non-controllable type does not provide frequency response services. The power deviation of the HVDC link, in the first type, between areas i and j is determined by the control signal of HVDC, ε_i,with a time constant, T_{DC_i}, as,

$$\Delta P_{DC_{ij}}(s) = \frac{1}{1+sT_{DC_{ij}}}\varepsilon_i(s) \tag{36}$$

$$\varepsilon_i(s) = \sum_{j=1, i\neq j}^{N} K_{ij}\left(\Delta f_i(s) - \Delta f_j(s)\right) \tag{37}$$

The total deviation of tie-lines power flows between the ith area and other areas can be modelled as an input to the ith area as follows,

$$\Delta P_{tie_i}(s) = \Delta P_{AC_i}(s) + \Delta P_{DC_i}(s) \tag{38}$$

C. LFC Control Scheme

The suggested affordable LFC control scheme for the NEM system is to convert the existing centralised one to a fully decentralised one without need for extra investment in infrastructure and additional procurement of FCAS reserves. Similarly, the new control schemes are able to solve the international challenges of adopting fully-decentralised methods instead of implementing quasi-decentralised LFC schemes.

The virtual dynamic system, the observer given in (7-8), is proposed and designed to be able to estimate internal dynamic states in each power region (control area) including the ACE in each control area without the need of further measurements. This means that the physical links, i.e. the interconnectors, are modelled as unknown inputs to each power region, yet the observer makes the required coordination between different power regions. Therefore, the implementation of LFC control can be implemented as a fully-decentralised scheme for the first time.

Since the area control error of the ith power region is estimated, the operator can implement any desired control method for diminishing the frequency deviations in each power region and the power flow fluctuation through different interconnectors. For instance,

$$\hat{\upsilon}_{c,i}(t) = -\Upsilon_{c,i}\ \hat{x}_i(t) \tag{39}$$

The control vector, $\hat{\upsilon}_{c,i}(t)$, is designed using optimal control. To achieve suitable control performance, the quadratic performance index, $J_i = \int_0^\infty (x_i{}^T Q x_i + u_i{}^T R u_i)dt$, is selected as an objective function for designing the controller of the ith power region, considering that its matrix Q should be a semidefinite one and the matrix R should be totally positive matrix, i.e. $Q \geq 0\ \&\ R > 0$.

Since this paper focuses on the real-world challenges in NEM power system, the existing controllers adopted in industries including NEM system, i.e. proportional-integral (PI), can be also extended and adapted with the new ACE defined in this paper to construct the control signal in the ith power region as follows,

$$\hat{\upsilon}_{c,i}(t) = [K_{P,i} \quad K_{I,i}] \begin{bmatrix} AC\hat{E}_i(t) \\ \int AC\hat{E}_i(t)d(t) \end{bmatrix} \tag{40}$$

Figure 3.4. The system topology under investigation

3.6. *Numerical Results and Discussions*

To validate the proposed affordable frequency control method for the NEM system, the same topology with exact connectivity between different power regions is considered. Figure 3.1 and Figure 3.4 present the structure of the NEM system, which comprises 5 power regions, namely SA, VIC, NSW, QLD, and TAS. It is worth mentioning that TAS is being operated based on a different FOS in comparison with the rest of regions, i.e. the mainland system. To confirm the superiority of the proposed dynamic estimator in tracking internal dynamics in different power regions, the estimation error is directed in Figure 3.5 for different severe cases. Figure 3.5a shows the results for SA power regions which is a region with high uncertainties due to high penetration of renewable energies especially Rooftop solar power presenting some challenges to controlling the frequency in NEM and Figure 3.5b presents the estimation error for QLD power region. The high accuracy shown in the results confirms the superiority of tracking the required variables for controlling the frequency of NEM system.

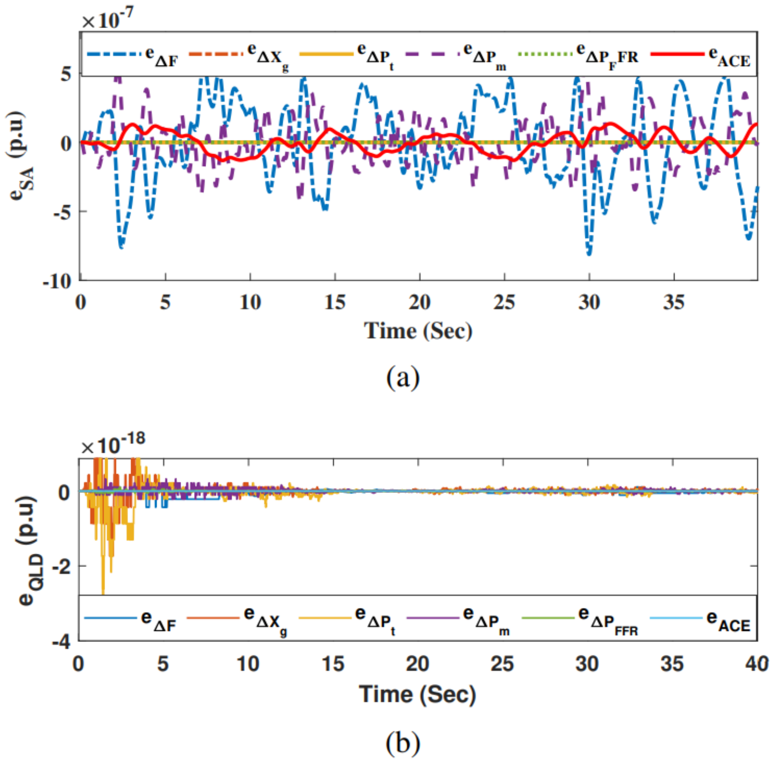

Figure 3.5. Estimation error of different dynamic states due to RES disturbances in SA and 0.015 pu step disturbance in NSW: a) SA and b) QLD power region.

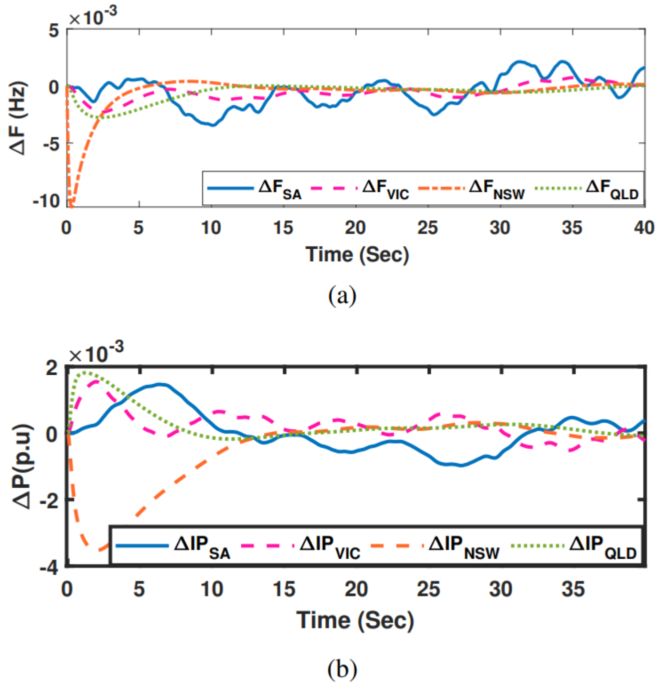

Figure 3.6. Dynamic responses due to RES disturbances in SA and 0.015 pu step disturbance in NSW: a) the frequency deviation and b) the power deviation through interconnector

The same scenarios of disturbances, i.e. high RES power variation in SA and simultaneously a 0.015 p.u step disturbance in NSW power region, are used to test the applicability of the proposed frequency control based on modelling tie-lines, i.e. the interconnectors, as unknown inputs. The results depicted in Figure 3.6 verify the ability of the proposed optimal control method in maintaining the frequency within acceptable limits and converges the interconnectors' power to its scheduled values within a few seconds even in case of continuous active power variations from RESs in SA power regions, presenting the capability of the proposed method for practical power systems.

To confirm the proposed method's capability in controlling both frequency and interconnectors' power deviations in an acceptable manner, several scenarios that present the different operation scenarios of the NEM system are considered and tested. For instance, Figure 3.7 depicts the dynamic performance of both frequency and interconnectors' power flow due to different step disturbances considered in different power regions simultaneously, i.e. 0.03 p.u in SA and 0.015 p.u in NSW. The superiority of the proposed control method for handling these variables and improving their dynamic performance is an index of its practicability and implementation feasibility. The results show that the novel control method could bring both interconnectors' power and regions' frequency back to its scheduled values even if it is a challenging task because of the unique design of NEM system. It is to point out that the NEM system is a highly challenging one for controlling its frequency and interconnectors' power at the same time due to the fact that it is a radial system. Although of the mentioned challenges, the successful operation and implementation of the proposed method in the NEM system, makes it a suitable solution for international practical power systems to convert their quasi-decentralized to fully decentralised ones by modelling the interconnectors, i.e. tie-lines, as unknown inputs which reduce the complexity and improves the dynamic performances and stability.

To show the real need for the aforementioned novel frequency control method to improve the NEM system frequency dynamics, NEM practice for implementing frequency control is considered and implemented in the same system. Figure 3.8 depicts both frequency deviation in different power regions and active power deviations through different interconnectors between NEM power regions, due to disturbance scenarios including 0.03 p.u step disturbance in SA, 0.015 p.u step in NSW, -0.02 p.u step in QLD and 0.01 p.u step in TAS power region. Although the current control practice of the frequency in NEM can bring the frequency deviation to an acceptable level after 20 seconds, there are concerns about the frequency fluctuation and its oscillation that might lead to higher wear and tear in governor-turbine systems. Another technical issue is the different frequency responses in the different power regions after the disturbances raising a new problem known as local frequencies which might affect the power system stability and security.

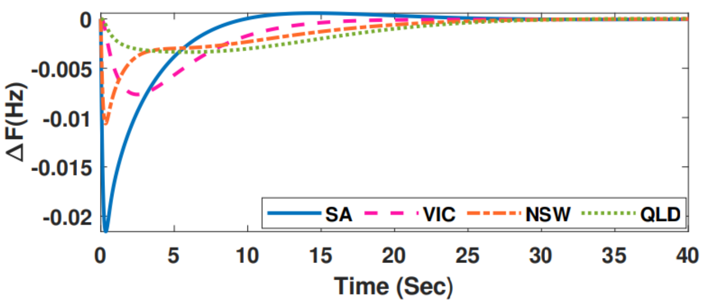

(a)

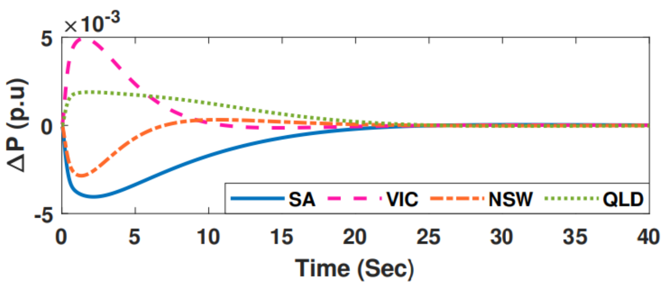

(b)

Figure 3.7. Dynamic responses due to 0.03 pu in SA and 0.015 p.u step in NSW: a) the frequency deviation and b) the interconnector power deviation

The real challenge and great industry issue in NEM frequency practice relates to interconnectors' power flow as shown in Figure 3.8. These concerns are captured and depicted in Figure 3.8b, where after the aforementioned disturbance scenario, the interconnectors' power deviations through different tie-lines do not converge and have not been removed. In fact, there are oscillations as shown in the same figure which present stability and security concerns about the system operation and its capability to be operated with higher RESs penetrations in the future especially after adopting the Australian decarbonization plan that would accelerate the increase of RES power share in NEM. This high deviation through interconnectors due to normal and continuous disturbances from both demand and generation sides would be highly increased in the future putting the system stability in danger. However, our proposed method tackles this industrial challenge in NEM, as shown in the previous results, e.g. Figs Figure 3.7.

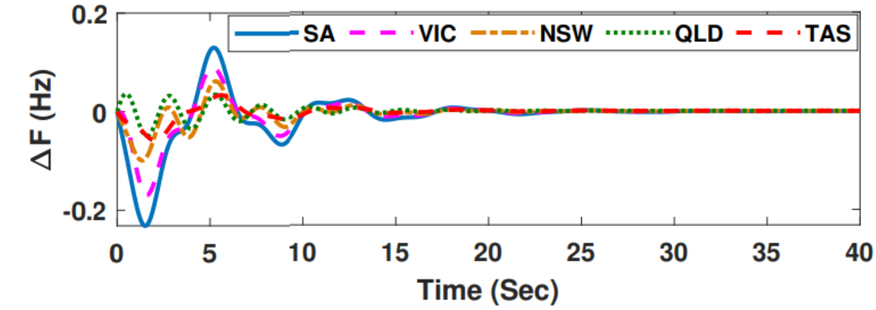

(a)

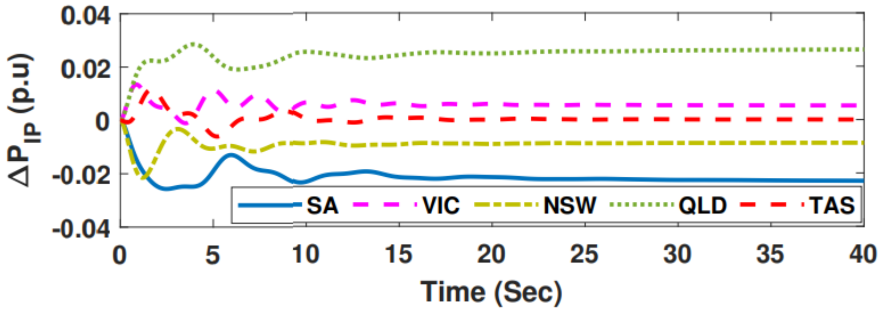

(b)

Figure 3.8. Dynamic responses due to 0.03 pu in SA and 0.015 pu step in NSW, -0.02 pu QLD and 0.01 pu TAS with NEM practice-based controller: a) F and b) power deviation in tie-lines

To show the superiority of the proposed method of the current control practices either in the National electricity market-NEM in Australia or ENTSO-E in Europe, the proposed method and its performances are compared to dynamic performances based on NEM and ENTSO-E control practices. Figure 3.9 depicts the comparative study results. It is clear that the proposed method can improve the frequency control if compared to the national and international current control practices. It is worth pointing out that the ENSTO-E frequency control practice is better than the NEM practice since ENTSO-E considers tie-lines' power in its area control error and thus for issuing its frequency control signals. However, the proposed control method in this paper is superior to ENTSO-E practice since it converts the quasi-decentralized approach adopted in international systems to a fully decentralized one for a practical system for the first time.

Figure 3.9b shows one of the main accomplishments of the proposed novel method, which is the well-controlling and diminishing of active power oscillation through different interconnectors in the NEM system. While the current NEM practice of implementing the frequency control leads to high deviation in transferred active powers and oscillations as well, the proposed control method can highly dampen the oscillations and remove the power deviation within a few seconds as shown in Figure 3.9b. Similarly, the proposed method can improve the dynamic performance of active power response through interconnectors after a disturbance if compared to the current practices in international real-world power systems, e.g. ENSTO-E.

The comparative study with actual practices of implementing frequency control in NEM and ENSTO-E confirms the main advances of our novel affordable frequency control method. We solved a technical issue in the NEM system and international systems. For the NEM system, we involved the interconnectors' power in ACE without the need for further investment of infrastructure and provided an enhanced frequency and power flow dynamics which highly improve the stability and security of NEM system operation. For international current practices, we could, for the first time, convert the quasi-decentralised frequency control approaches to fully decentralised ones by modelling tie-lines as unknown inputs, resulting in less complexity and higher efficiency of implementing different control methods for controlling both frequency and tie-line power.

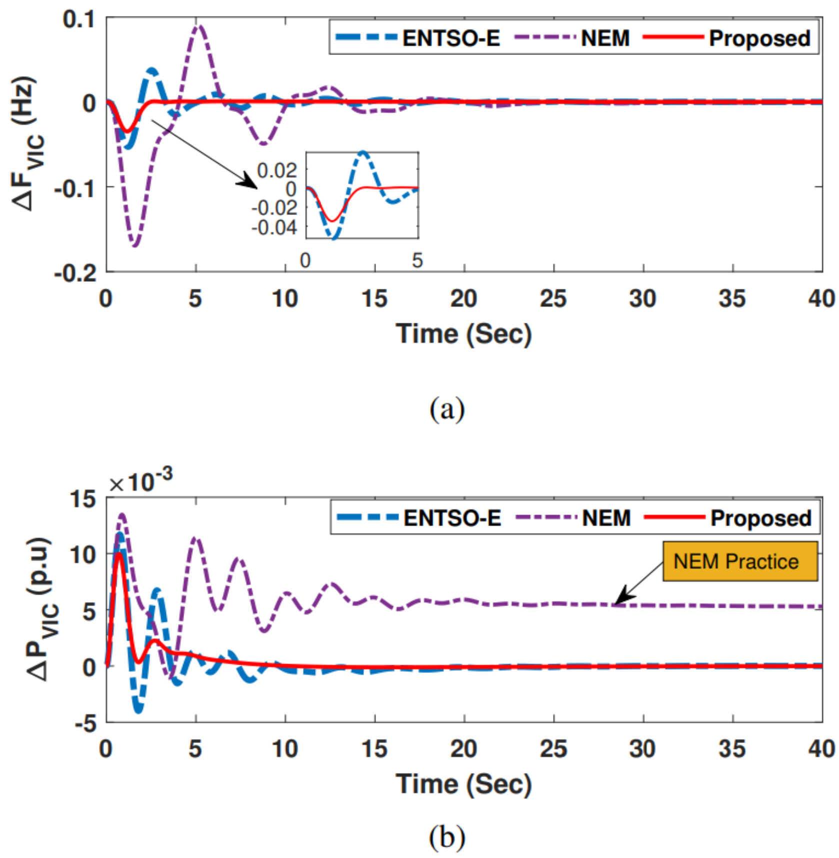

Figure 3.9. Compassion of dynamic responses due to 0.03 pu in SA and 0.015 pu step in NSW, -0.02 pu QLD and 0.01 pu TAS with ENTSO-E, NEM and proposed controllers: a) F and b) Power deviation through tie-lines

3.7. *Remarks, Conclusions, main insights and outcomes*

In alignment of GPST's goals of enabling energy transition and power system transformation, there are several technical challenges in modern power systems related to frequency control and the activation of the services required for supporting the frequency in IBR-dominated power systems. The underway research in this project has highlighted several challenges either based on the comprehensive literature review completed in the first phase of this project or by research outcomes from phases I-III of Topic 6. One of the highlighted issues is the need for a sophisticated load frequency control (advanced/new automatic generation control (AGC)) system that can handle uncertainties, RES variability, and unknown inputs in IBR-dominated power systems. Likewise, it has been found that there is a need for considering the power system topology and the regionalization of regulation FCAS in order to enhance the dynamic and frequency performances in modern power systems. Furthermore, the different types of the interconnectors should be considered in such modelling and studies to improve the dynamic response. This part of the project is developed to solve industry concerns and research gaps by answering the following critical research questions:

- How to effectively involve tie-lines'/interconnectors' power flows in frequency control of Australian NEM's system and similar ones without extra investment cost in information and communication technology (ICT) infrastructure; where successful involvement of them would highly improve the frequency stability and security and enhance the uptake of invested interconnectors/tie-lines.

- How to convert the centralised secondary frequency control in the Australian NEM power system to fully decentralised one without additional complexities. Such conversion would improve the operation security of whole system and fairly allocate FCASs in different power regions.
- How to convert the quasi-decentralised frequency control systems in the international practices to fully decentralised one. Successful conversion would be a tremendous contribution to the currently adopted LFC/AGC with tie-line consideration in international real-world systems; where a fully-decentralisation would highly reduce the requirements in LFC/AGC implementation in international practices, improve the stability and security, and reduce the complexities of implementation.

It is to emphasis that the NEM system has been considered as the main case for this part of the project since NEM is in the forefront of the systems that face challenges in frequency control due to high power share from RESs and IBRs. The work, that has been completed in this part of the project, proposes a novel frequency control method for the Australian National Energy Market power system (and power systems going under transformation and energy transition) considering current issues and challenges in the implementation of the AGC system in comparison with international practices. The method is extended to international practices to successfully and affordably convert the quasi-decentralised LFC approaches to fully-decentralised ones, for the first time, unleashing their potential capabilities. To this end, this work employs a novel dynamic observation technique known as known input observation (UIO) for virtually decoupling the different power regions from each other, leading to several benefits including: **i)** <u>the ability to model interconnectors as unknown input</u> to each power region, **ii)** <u>the possibility to better controlling the frequency in power regions with high variations and uncertainties</u>, like SA region which is enriched with RESs, and **iii)** <u>the ability to handle different uncertainties, disturbances, deviations in imported/exported powers from/to other power regions</u> since they would become unknown inputs to the system dynamics.

The results confirm the superiority of the proposed technique since it solves existing industry challenges, not only in Australia but also internationally by making quasi-decentralised systems be converted to fully-decentralised one, and improves the overall stability and security of the power systems' frequency.

<u>Insights and Outstanding Outcomes:</u>

1. A novel frequency control method for NEM and international power systems based on advanced dynamic state estimation method.
2. Modelling interconnectors and renewable power variation as unknown inputs, resulting in great advantages for power system modelling, operation, and control.
3. The ability to convert the centralised or quasi-decentralised frequency control structure to fully decentralised control structure, for the first time, bringing tremendous advantages to the system stability and security with ability to enable FCAS regionalisation.
4. Improving the frequency response in IBR-dominated power systems which enable power system transformation by making power systems more resilient against disturbances, uncertainties, and variability during energy transition.

To conclude, this industry-oriented research proposes a novel sophisticated frequency control system for the Australian National Electricity Market (NEM) power system considering the special design of its current automatic generation control approach, which does not involve interconnectors between different power regions, resulting in technical challenges for both stability and security of the system. The proposed new method converts the centralised frequency control system to a fully decentralised one with virtually consideration of interconnectors' power flow, thus the stability and security would be improved and the high fluctuations in interchanged power smoothed without extra costs of infrastructure and procurement of frequency control ancillary reserves (FCASs). It models the power flow deviation as unknown input to the operator in each power region, like the disturbances and renewable power variations using dynamic observation techniques, for enabling the proposed method capabilities. The method is theoretically verified that it can enhance the stability and security and stabilise both local frequencies and power exchanges. The experiment results confirm the capability of the proposed method for the NEM system and its superiority over the existing approach.

3.7. *References*

[1] S. F. Aliabadi, S. A. Taher, and M. Shahidehpour, “Smart deregulated grid frequency control in presence of renewable energy resources by evs charging control,” IEEE Transactions on Smart Grid, vol. 9, no. 2, pp. 1073–1085, 2016.

[2] N. Hatziargyriou, J. Milanovic, C. Rahmann, V. Ajjarapu, C. Canizares, I. Erlich, D. Hill, I. Hiskens, I. Kamwa, B. Pal et al., “Definition and classification of power system stability–revisited & extended,” IEEE Transactions on Power Systems, vol. 36, no. 4, pp. 3271–3281, 2020.

[3] F. M. Mirza, S. B.-U.-H. Rizvi, and O. Bergland, “Service quality, technical efficiency and total factor productivity growth in pakistan’s post-reform electricity distribution companies,” Utilities Policy, vol. 68, p. 101156, 2021.

[4] Entso-e: System separation in the continental europe synchronous area on 8 january 2021 – update. [Online]. Available: https: //www.entsoe.eu/news

[5] H. H. Alhelou, M.-E. Hamedani-Golshan, R. Zamani, E. HeydarianForushani, and P. Siano, “Challenges and opportunities of load frequency control in conventional, modern and future smart power systems: a comprehensive review,” Energies, vol. 11, no. 10, p. 2497, 2018.

[6] H. H. Alhelou, M. H. Golshan, and J. Askari-Marnani, “Robust sensor fault detection and isolation scheme for interconnected smart power systems in presence of rer and evs using unknown input observer,” International Journal of Electrical Power & Energy Systems, vol. 99, pp. 682–694, 2018.

[7] W. Mendieta and C. A. Canizares, “Primary frequency control in ˜ isolated microgrids using thermostatically controllable loads,” IEEE Transactions on Smart Grid, vol. 12, no. 1, pp. 93–105, 2020.

[8] T. Tao, S. Roy, and S. Baldi, “Stable adaptation in multi-area load frequency control under dynamically-changing topologies,” IEEE Transactions on Power Systems, 2020.

[9] R. Lu, J. Wang, and Z. Wang, “Distributed observer-based finite-time control of ac microgrid under attack,” IEEE Transactions on Smart Grid, vol. 12, no. 1, pp. 157–168, 2020.

[10] O. Stanojev, U. Markovic, P. Aristidou, G. Hug, D. S. Callaway, and E. Vrettos, “Mpc-based fast frequency control of voltage source converters in low-inertia power systems,” IEEE Transactions on Power Systems, 2020.

[11] H. Haes Alhelou, M. E. Hamedani Golshan, and M. Hajiakbari Fini, “Wind driven optimization algorithm application to load frequency control in interconnected power systems considering grc and gdb nonlinearities,” Electric Power Components and Systems, vol. 46, no. 11-12, pp. 1223–1238, 2018.

[12] S. Biricik, H. Komurcugil, H. Ahmed, and E. Babaei, “Super twisting sliding mode control of dvr with frequency-adaptive brockett oscillator,” IEEE Transactions on Industrial Electronics, 2020.

[13] W. Liu, G. Geng, Q. Jiang, H. Fan, and J. Yu, “Model-free fast frequency control support with energy storage system,” IEEE Transactions on Power Systems, vol. 35, no. 4, pp. 3078–3086, 2019.

[14] H. Golpˆıra, A. Atarodi, S. Amini, A. R. Messina, B. Francois, and H. Bevrani, “Optimal energy storage system-based virtual inertia placement: A frequency stability point of view,” IEEE Transactions on Power Systems, vol. 35, no. 6, pp. 4824–4835, 2020.

[15] J. Chen, M. Liu, and F. Milano, “Aggregated model of virtual power plants for transient frequency and voltage stability analysis,” IEEE Transactions on Power Systems, vol. 36, no. 5, pp. 4366–4375, 2021.

[16] A. S. Mir and N. Senroy, “Adaptive model predictive control scheme for application of smes for load frequency control,” IEEE Transactions on Power Systems, 2017.

[17] H. Haes Alhelou, M. E. Hamedani-Golshan, T. C. Njenda, and P. Siano, “A survey on power system blackout and cascading events: Research motivations and challenges,” Energies, vol. 12, no. 4, p. 682, 2019.

[18] H. H. Alhelou, M. E. H. Golshan, and N. D. Hatziargyriou, “Deterministic dynamic state estimation-based optimal lfc for interconnected power systems using unknown input observer,” IEEE Transactions on Smart Grid, vol. 11, no. 2, pp. 1582–1592, 2019.

[19] H.H. Alhelou, B. Bahrani, J. Ma, D. Hill, “Australia’s Power System Frequency: Current Situation, Industrial Challenges, Efforts, and Future Research Directions”, In IEEE TechRxiv, 2023.

4. <u>Chapter 4:</u> Demand-side Based Frequency Support Services

Note: *part of the work in this chapter is under preparation for a journal paper.*

4.1. An overview

For enabling energy transition, especially its power system transformation, it is crucial to seek new advanced, reliable, affordable, and flexible sources for providing frequency control ancillary services to power systems during the transformation and beyond. This is necessary due to the fact that power systems are changing, where such services where have been provided from generation-side in conventional power systems. The transition pushes operators to move to demand-side for harvesting more flexible services such as primary and secondary frequency control. Therefore, building aggregators of smart appliances that can participate in frequency support is important for both modern and future power systems. Not all appliances in demand-side can be considered for the provision of services. In fact, only those that can not impact the customers comfort should be carefully considered. In this regard, we categorise the appliances at the demand side that can provide frequency services into two main groups, that is,

i) Thermostatically-controlled loads, e.g. water heaters, inverter-based air conditioners, …, etc.

ii) eMobility, e.g. electric vehicles (EVs), electric buses, public transport sector, …, etc.

We develop estimation tools for estimating the demand at system-level of such smart demand-side appliances that can provide some frequency services. To make them more sophisticated and useful, the tools would be also developed to estimate the available reserve not only at the system level, but also at the power region level making them useful for real-world applications, especially for implementing the ancillary services regionalisation concept. Therefore, this research contributes to the body of knowledge by,

a) developing a system-level and power region-level estimation of EV demand and EV active power reserve to support frequency. The estimation will be useful to understand the impact of future scenarios, such as ISP scenarios and the opportunities and challenges that bring;

b) developing an advanced frequency response model-based EV aggregation for studying and analysing the frequency support from EVs in future systems under different possible scenarios, such as ISP scenarios;

c) developing an aggregator of thermostatically-controlled loads for understanding the available frequency control services from such loads;

d) developing a model to understand the impact of the participation of thermostatically controlled loads in frequency control in modern and future power systems.

The rest of this chapter of research is organised as follows. Subsection 4.2 introduce the developed EV estimations tools that can estimate the available frequency support services from EVs at the system level and power region-levels. Section 4.3 introduces a novel method to aggregated EVs for supporting the frequency in a power system, followed by a novel advanced frequency response model of the aggregated EV response to study the frequency in future power systems. Section 4.4 introduce a developed tool for estimating the electric demand of thermostatically controlled loads based on an advanced estimation model suggested by CSIRO. Section 4.5 introduce a dynamic frequency response model to investigate the impact of thermostatically controlled ability of such smart appliances at demand side for providing services and to analysis their impact on frequency stability and frequency response after large disturbances, e.g. credible events.

4.2. Estimating the available frequency control reserve from EVs at system level

This part of research looks at how the operator of the system can understand the situation in its future system under different possible scenarios of eMobility, e.g. EVs, deployment and integration with the grid. The main aim is to understand the potential opportunities for providing the required frequency control ancillary services in future systems from demand-side, especially from EV. To this end, the active power demand of EVs under different possible future scenarios need to be estimated. The estimated electric demand of EVs in future, e.g. in 2030 and

2050, will be useful for future planning of system ancillary services. This would help understand the opportunities that could help solve the challenges associated with energy transition and power system transformation, especially from frequency stability, security and its required services view of points.

A. ***Estimating the active power demand for an individual EV***

To estimate the EV demand and EV reserve at the region-level and the whole system level, the demand of each EV should be first stochastically estimated. To this end, the estimation requires using suitable probabilistic distribution functions based on the available EVs on the market and based on the behaviour of customers. This is in fact a challenge where such information usually is not available in public, however, the system operators should be able to obtain such information. Therefore, this research develops a generic tool while the selection would be subjected to the fitting of suitable distribution functions based on the information that the operator of the system has. In the adopted methodology, the estimation is divided into several stages, that are,

i) Categorisation of electric vehicles

ii) Selecting the suitable distribution functions

iii) Estimating the active power demand for an individual electric vehicle

iv) Aggregation of estimation of EV demand on a power region-level

v) Aggregation of estimation of EV demand on the whole system-level

In what follows, the aforementioned items are briefly introduced, where the detailed description will be provided in the final report.

A.1 Categorisation of electric vehicles

The transportation sector is an important sector for each country. Therefore, it is usually regulated to ensure it is well-managed in the national level. Such sector has different regulations in different countries. Likewise, the life style of people directly impacts the usage of transport sector nowadays and in the future as well once all cars would be replaced by electric vehicles.

In Australia, the vehicles can be classified based on their use as follows,

i) Vehicles owned by individuals who work and are essentially considered as home-based work vehicles. For such groups of vehicles, there is a specific trend of usage during working days and holidays.

ii) Vehicles owned by individuals who do not work and are essentially considered as home-based non-work vehicles. A suitable distribution function can be obtained based on the data of such vehicles' usage.

iii) Vehicles owned by companies and are essentially considered as company-based work vehicles. For such group of vehicles, a specific distribution can be obtained to describe their trips during day and night.

Another type of classification could be done based on the type of electric vehicles. It is to emphasis that each country has a specific policy that allow specific types of vehicles to be imported and usage by individuals. Generally, the electric vehicles can be classified as: 1) L7e: Quadricycle-four wheels, used essentially for carrying goods; 2) M1: Passenger vehicle, up to 9 seats; 3) N1: Goods-carrying vehicle, with a maximum laden mass of 3500 kg; 4) N2: Goods-carrying vehicle, with a maximum laden mass of 12000 kg.

The above classification is important, because the charging trend follows a specific pattern for a specific type of vehicles. In addition to the classification of types of electric vehicles, the technology used to construct the batteries is of importance and impact the demand since the charging trend will be also impacted by the type of battery. In addition to the battery, the type of charger is also important where it impacts the available frequency control ancillary services from EVs. Figure 4.1 shows the charging pattern for different EV battery technologies. It can be observed from this figure that the type of battery impacts the electric demand of individual EVs and therefore the total electric demand of EVs at power region or system levels. As a consequence, the type of EV would impact the available reserve for supporting the frequency, especially if the type of battery chargers is carefully considered. The EV battery charger can be classified into,

i) Unidirectional battery charger; for EV with such charger, it can contribute to frequency support by stopping its charging power only.

ii) Bidirectional battery charger; for EV with such charger, it can contribute by both stopping its charging power and injecting power back to the grid, if needed.

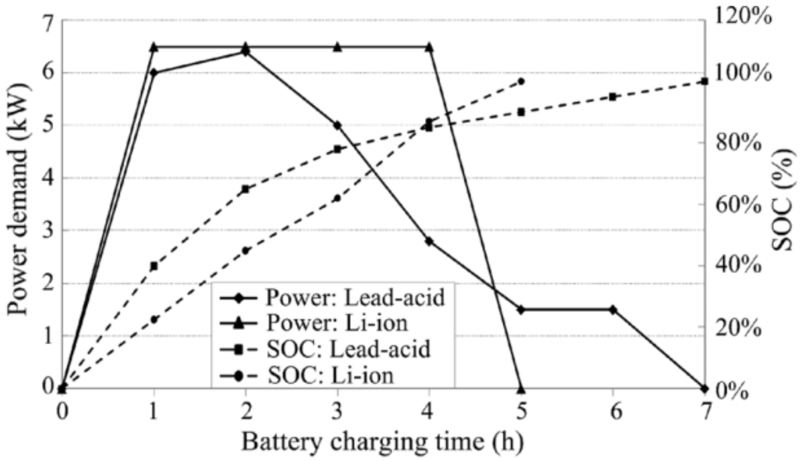

Figure 4.1. the charging pattern for different types of vehicles' batteries [8]

A.2 Selecting the suitable distribution functions

The selection of suitable probabilistic distribution function is of importance to estimate the future electric vehicle demand on power region and system levels with a suitable accuracy enabling the power system operator to understand the future possible scenarios of how to utilise EV to provide services such as frequency support services.

Generally, statistical data is required to select the most suitable distribution functions. For this research, the typical distribution functions verified in literature to be suitable for estimation are used. However, the developed method is built in a such way to provide flexibility for easy modifying the algorithm to adapt any change in the distribution functions due to change of the technology of EVs in the future or due to the change in classification and pattern of using EVs in a specific region.

For this research, the following main distribution functions have been adopted,

i) Normal distribution, where its probability density function (pdf) is given in (1) as follows,

$$g(\chi;\mu,\sigma) = \frac{1}{\sigma\sqrt{2\pi}}\, e^{-(\chi-\mu)^2/2\sigma^2} \quad (1)$$

ii) Gamma distribution, where its probability density function (pdf) is given in (2) as follows,

$$f(\chi;\alpha,\beta) = \frac{1}{\beta^{\alpha}\Gamma(\alpha)}\chi^{\alpha-1}\, e^{-\chi/\beta} \quad (2)$$

The parameter setting for the aforementioned distribution functions will be different based on their usage. For instance, the normal distribution function is suitable for determining the starting time of the next trip, however its μ and σ are set based on statistical data or best on typical values for such a task. The usage of the aforementioned distribution functions for different purposes in this work has been described in the following section.

A.3 Estimating the active power demand for an individual electric vehicle

In order to get the estimation of EV power demand on power region level or system level, the electric active power demand of each individual EV needs to be obtained. The following steps in the developed algorithm need to be done,

i) The battery capacity, C, of each individual EV should be determined. This can be done based on a suitable probabilistic distribution function. For this purpose, the above-mentioned distribution functions are used. Based on the available data and studies, the gamma distribution function is found to be suitable for L7e and M1 type of vehicles, while normal distribution function is more suitable for N1 and N2 type of vehicles. Therefore, (1-2) can be rewritten as follows,

$$g(C;\mu,\sigma) = \frac{1}{\sigma\sqrt{2\pi}}\, e^{-{(C-\mu)^2}/{2\sigma^2}} \qquad (3)$$

$$f(C;\alpha,\beta) = \frac{1}{\beta^{\alpha}\Gamma(\alpha)} C^{\,\alpha-1}\, e^{-{C}/{\beta}} \qquad (4)$$

ii) The maximum allowable distance travel per day, D_max, needs to be determined in the next step. This can be determined based on statistical data. However, it has found that there is a linear relationship between the EV battery capacity and the maximum trip per day. Another way to determine is to construct a distribution function based on the available statistical data. The normal distribution function for the maximum distance trip per day is given as,

$$g(D\_max;\mu,\sigma) = \frac{1}{\sigma\sqrt{2\pi}}\, e^{-{(D\_max-\mu)^2}/{2\sigma^2}} \qquad (5)$$

iii) The km daily travel, D, can also be probabilistically determined using a suitable distribution function, by the same way the state of charge before the first trip, SoC_0 is stochastically determined.

iv) Now, we determine the state of charge of battery at the charging start time, SoC_ts, which can be easily determined from SoC_0 and the travel distance per day, D, considering that the SoC is decreased linearly with the travel distance.

v) One of the important factors in the estimation is the determination of the starting time of the trip, arrival time, charging time, and finish charging time. All these times can be determined based on the above information if the trip stating time is estimated. For trip starting time, the normal distribution function can be used to determine the staring of the next trip based on statistical data.

vi) Finally, the charging type is important. There are several possible charging modes: i) dump charging mode where EV starts charging once it gets back to the home which is the worst charging mode because it adds more load to the peak demand; ii) off-peak charging mode; and iii) smart controlled charging model based on pricing signals. The EV demand and the EV available reserve can be obtained for different charging modes. However, the worst-case scenario is the most important case for the operator which determine what arrangements are needed to support the frequency in the worst-case scenario.

A.4 Aggregation of estimation of EV demand on a power region-level

In the next step of the estimation algorithm is to estimate the EV charging demand for different power regions within a power system. For the ith power region, the total regional active power demand of EVs can be obtained as follows,

$$P(t) = \sum_i^N P_i(t) \qquad (6)$$

where N is the number of EVs for a specific power region.

It is worth mentioning that the active power demand and SoC for each individual electric vehicle within the power region would be estimated by the developed algorithm. Based on the estimation, the available active power reserve to support the frequency in the ith power region can be determined as follows,

$$R(t) = \sum_i^N R_i(t) \qquad (7)$$

where,

$$R_i(t) = \begin{cases} 0 & if\ EV\ does\ not\ participate \\ P_i(t) & If\ EV\ has\ unidirectional\ charger \\ 2\ P_i(t) & If\ EV\ has\ bidirectional\ charger \end{cases} \quad (8)$$

A.5 Aggregation of estimation of EV demand on the whole system-level

In the final stage, the active power demand of EVs at the system level and the available reserve for supporting the frequency can be determined as follows,

$$P_{sys}(t) = \sum_i^{N_{sys}} P_i(t) \quad (9)$$

$$R_{sys}(t) = \sum_i^{N_{sys}} R_i(t) \quad (10)$$

where $\mathrm{N_{sys}}$ is the number of power regions in a power system.

More description on the above methodology will be provided in the final report.

A.6 Results from the developed algorithm

Typical values and data for Australian transportation sector is used to perform the above described algorithm, resulted in an estimation of EV demand at power region and system levels. The data used as an input for the algorithm can be provided upon a reasonable request. The estimation result for VIC power region in 2030 and 2050 are depicted in Figure 4.2. To make the figure more illustrative the estimated demand is combined with a typical 2022 daily electric demand in VIC power region, considering that no huge change will be occurred in the typical electrical demand except growth in a specific rate. It is worth mentioning the depicted results show the estimation of EV demand in red colour for 2030 and 2050 in VIC power region for the worst-case scenario, which is the most important scenario for frequency studies. The worst-case scenario assumes that EVs follow the dump charging mode. This means that EVs start charging once they arrive after a daily trip. The results would be changed if the off-peak charging is adopted in the estimation. Likewise, the price-based charging mode will also change the estimation. As mentioned-above, the worst-case scenario, the dump charging mode, is the most important for our study, therefore, we limit result presentation to the case of interest to the study. One can observe that a huge peak in specific scenarios will occur around 8 pm after arriving vehicles from trip where the majority of vehicles are home-based work vehicles. The results show the estimation of EVs based on AEMO's ISP scenarios, i.e. Slow-Change Scenario (SCS); Step-Change Scenario (STCS); Progress-Change Scenario (PSC); and Super hydrogen Power Scenario (HSPS).

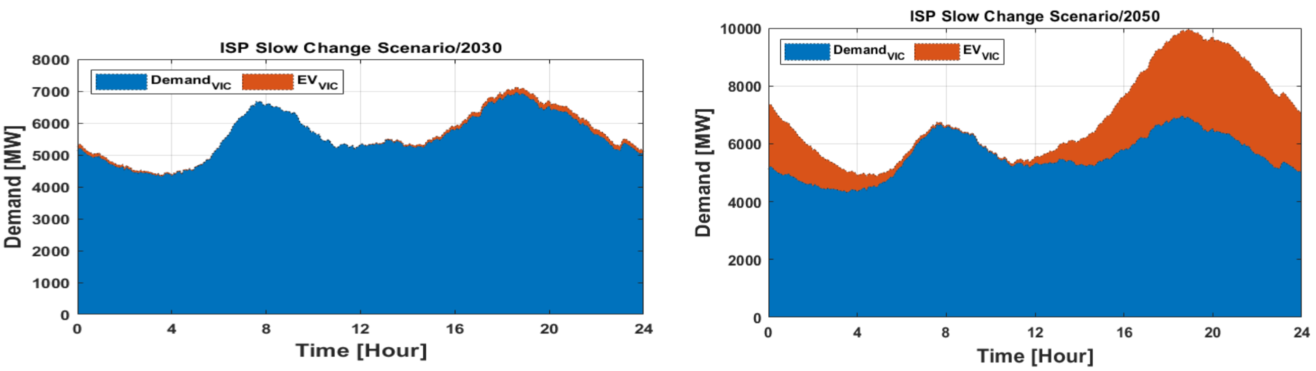

(a) *(b)*

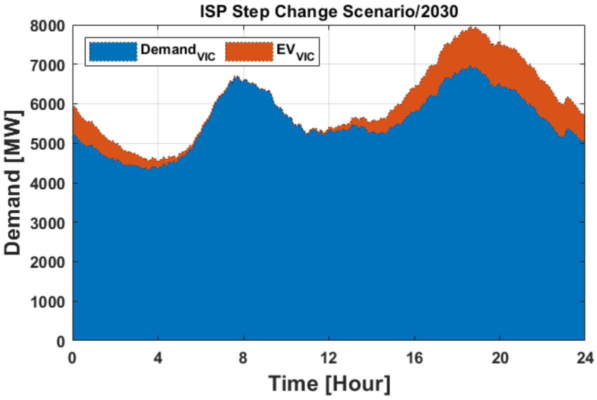

(c)

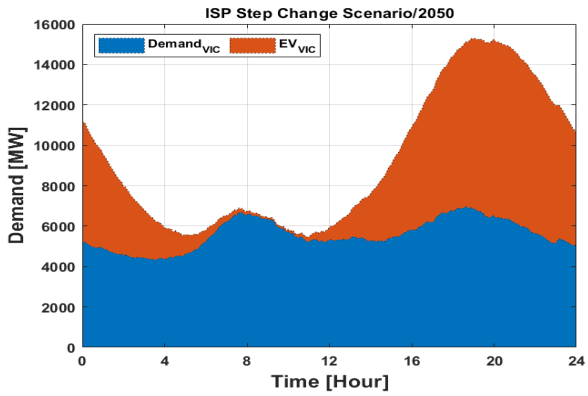

(d)

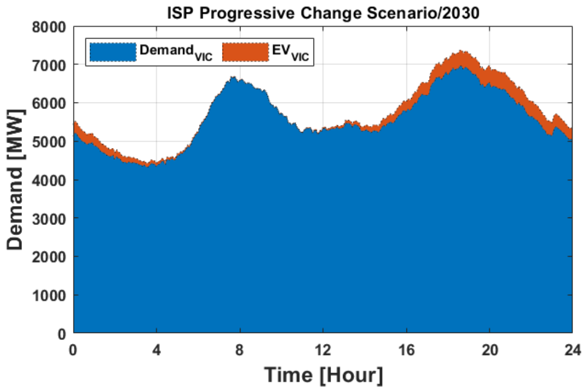

(e)

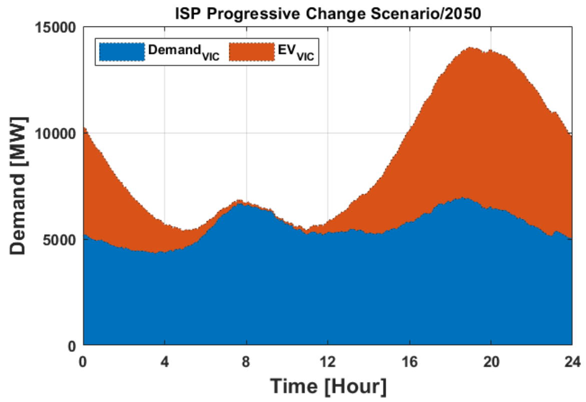

(f)

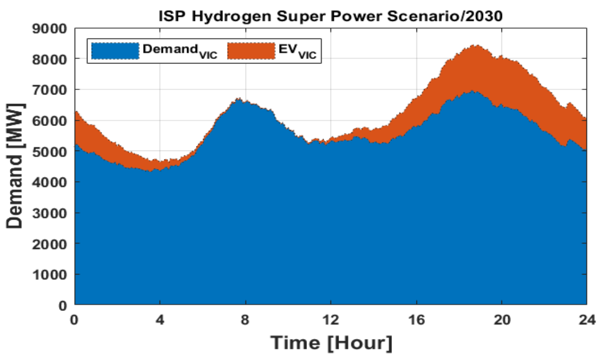

(g)

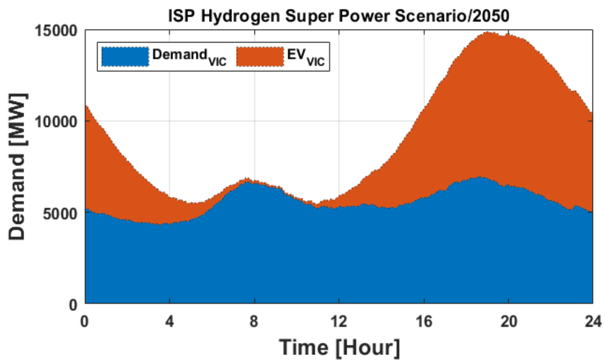

(h)

Figure 4.2. The EV demand estimation for 2030 and 2050 in Victorian Power region in case of the worst-case scenario (The Dump Charging Mode); a) slow change scenario 2030, b) slow-change scenario 2050, c) step-change scenario 2030, d) step-change scenario 2050, e) progress change scenario 2030, f) progress change scenario 2050, g) super hydrogen power scenario 2030, and h) super hydrogen power scenario 2050.

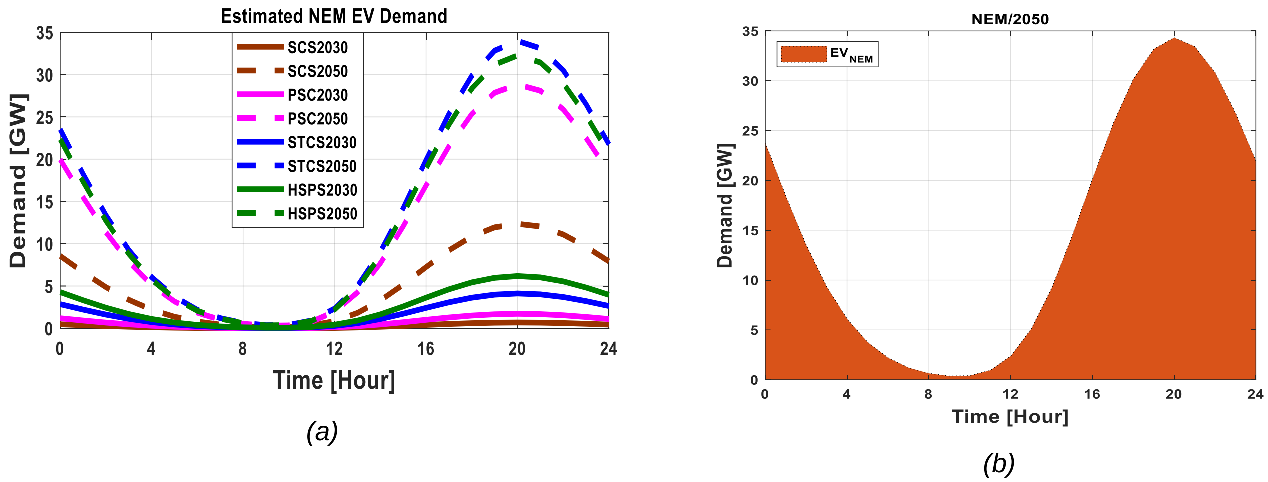

Figure 4.3. The EV demand estimation for 2030 and 2050 cross NEM system for worst-case scenario (The dump charging mode); a) the estimation for different scenarios for typical working day, and b) the estimation based on STCS 2050 scenario.

4.3. A new system frequency response model and aggregation method of EV to support frequency

B.1 An overview, Concise Literature Review, and Novelty

Due to the global warming concerns and energy resources security risks, many countries around the world have taken specific actions to de-carbonize their transport sectors and electrical power system by deploying electric vehicles (EVs) and supporting renewable energy generation [1]. Hence, a large number of renewable energy resources (RER) such as wind turbines and solar panels are integrated into power systems, which provide new challenges and opportunities to power system operators. RER technologies have the potential to bring substantial technical and economic benefits, however-a high penetration of RERs would endanger the stable and secure operation of power grids. A high penetration level of RERs in power grids would also cause some problems such as frequency fluctuation and active power imbalance due to the variations in power generated by RERs [2].

The imbalance between active power generation and demand causes a frequency deviation. From power system security point of view, the power system operator requires to maintain frequency within an acceptable range near the nominal value. This aim would be achieved by keeping the balance between the active power generation and demand by means of frequency control [3]. Due to activation time of the active power reserve, the frequency control is divided into three control level [4]:1) Primary frequency control reacts very quickly within the first a few seconds after the disturbance. 2) Secondary reserve must be fully activated after primary reserve within 30 s after the incident and be in service for 30 min. 3) Tertiary reserve is activated by re-dispatching generating units considering the economic concerns.

In contrary to conventional power systems, power systems with high penetration of RER suffer from lack of sufficient active power reserve. Battery energy storage systems (BESS) can be used as a solution to this problem. However, this solution is not economically efficient. Another solution to this problem is to provide reserve from demand response (DR) that means the participation of loads in frequency control process. Appliances such as air conditioners, refrigerators, water heaters, and freezers are suitable for this purpose.

Due to environmental concerns, there is an increasing interest in employing EVs in transportation systems. Considering the fact that EVs are equipped with a battery, they would be a good choice for providing ancillary services by controlling their charging power [5]. By using EV fleets for provision of primary and secondary active power reserve, even in conventional power systems, the most expensive primary reserve from conventional power plants can be reduced. EVs can contribute to primary and secondary reserve by controlling their charging power [6]. It has been shown in [7] that EVs can effectively improve frequency security in isolated power systems. In [8], a new estimation tool for EV demand in Great Britain power system has been provided. The simplest control approach for involving EVs in frequency control is to suddenly disconnect them from the power system following a large disturbance in the system [8]. However, if the reserve available from EVs is higher than required, this approach would result in over-frequency. Another method for employing EVs as a DR provider is to adjust EV's droop coefficient according to EV energy to achieve the best control [9]. An aggregated model of plug-in EVs for primary frequency control studies in power system has been proposed in [10]. However, these models do not consider the nonlinearities, ramp up/down rates, parameters determination, and implementation limitations.

B.2 EV dynamic frequency response model

In the following, a new dynamic EV aggregated model for the frequency studies considering the ramp up/down of EVs battery is proposed. The parameters of this model are calculated based on the proposed grouping method of EVs in section III. To this end, the EV battery and charger model is presented at subsection i. Then, method of determining the parameters of the proposed model is introduced in subsection ii.

To obtain EV frequency response model, the EV battery charger model is needed. In brief, the EV battery charger consists of an inverter to transform AC power into DC power and a buck converter to step down the voltage and increase current to an acceptable range for charging EV battery [20]. Practically, the inverter is connected to the power system through a small inductor L and a resistorR_{inv}. Power loss in the inverter is modeled by a resistorR_{loss}. Then, the final model for EV battery charger is shown in Figure 4.4.

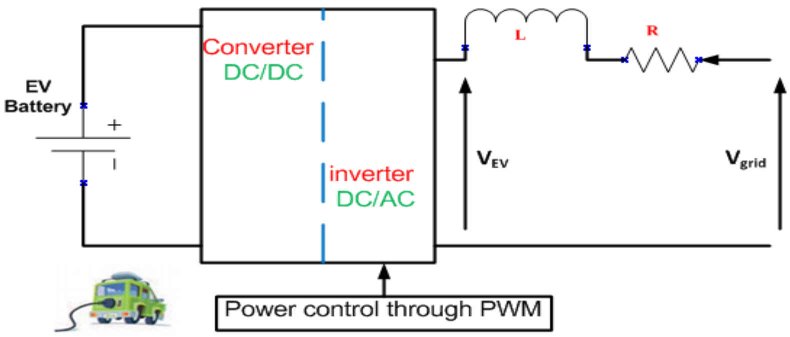

Figure 4.4. Electric model of individual EV's battery and charger [23]

The AC current between the inverter and the grid which determines the dynamic response of the inverter, is as follows,

$$\frac{di(t)}{dt} = \frac{R}{L} i(t) - \frac{1}{L}\left(V_{grid} - V_{EV}\right) \qquad (11)$$

where,

$$R = R_{loss} + R_{inv}$$

In this model, the inverter is controlled by pulse-width modulation (PWM) switching technique [21-22]. Therefore, the voltage of the inverter is determined as follows,

$$V_{EV} = \alpha M V_{DC} \sin(\omega t + \delta) \qquad (12)$$

where α, M, V_{DC}, and δare a constant (0 or 1) which depends on the inverter topology, the PWM modulation index, the voltage of the DC link, and the angle between V_{EV} and V_{grid} in degree, respectively.

It has been demonstrated in [10], [23] that in power system frequency studies, EV current response as shown in (10), thus the EV power, can be modeled by a first order transfer function as

$$G(s) = \frac{1}{1+s.T_{ev}} \qquad (13)$$

The EV time constant, T_{ev}, is equal to

$$T_{ev} = \frac{L}{R} \tag{14}$$

The EV time constant might vary between 35ms and 100ms [10], [23].

Aggregated model: The aggregated frequency response model of EVs proposed in this paper is shown in Figure 4.5. This model contains battery and charger model discussed in previous section. The dead-band block is included in the model to ignore very small frequency deviations. The droop coefficient of each EV, determined by power system operator, is sent to the EVs by the aggregator. R_{ev} is the equivalent droop coefficient of all EVs in each area of the power system. $P_{EV}^{set.point}$ stands for the sum of the demand of EVs which can participate in frequency control.

The reserve limiter block models the upper and lower limits of primary reserve provided by EVs. P_{agg}^{max} and P_{agg}^{min} are upper and lower bounds of primary reserve limiter, respectively. However, EVs have a very fast response in comparison to conventional generating units. But, to have realistic model of EVs, it is important to consider their ramp up/down rate in the EVs aggregated model. EV ramp rate block models the maximum rate of increase/decrease in the output power of EVs. The parameters of this model can be calculated based on charging demand and total available primary reserve of EVs obtained by model of section III as follows.

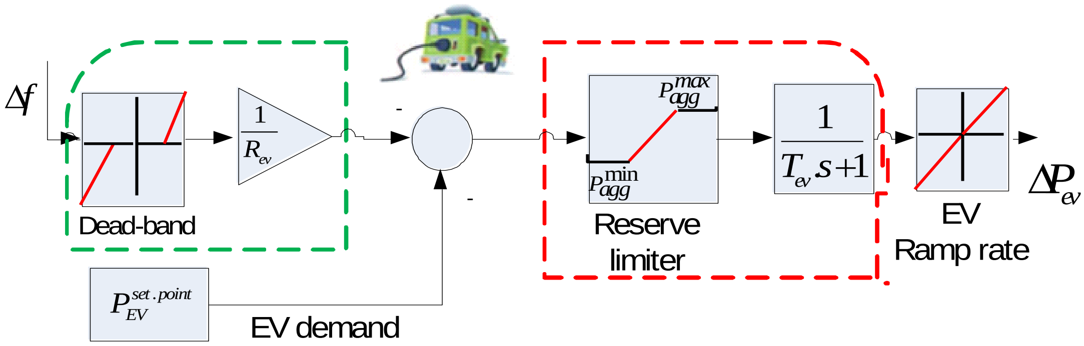

Figure 4.5. Dynamic model of EVs for primary frequency control

$$P_{EV}^{set.point} = \frac{P_{EV}^{demand}}{S_{base}} \tag{15}$$

$$P_{agg}^{max} = \frac{P_{EV}^{1r}}{S_{base}} \tag{16}$$

$$P_{agg}^{min} = \frac{P_{EV}^{demand}}{S_{base}} \tag{17}$$

B.2 Evaluation of the frequency response in case of EV support based on ISP scenarios

In addition to the above presented scenarios, the estimated amount of reserve from EVs in 2030 and 2050 is utilized to study the ability of EVs for supporting the frequency in the future system of NEM. In this study for NEM system, generic model and typical values are used. However, the operating snapshot of NEM for one day in August is used to run the simulation. Figure 4.6 shows the typical demand during 24 hours with 5-minute resolution in NEM system that is used for analyzing the ability of EVs for improving the frequency response in future system of NEM.

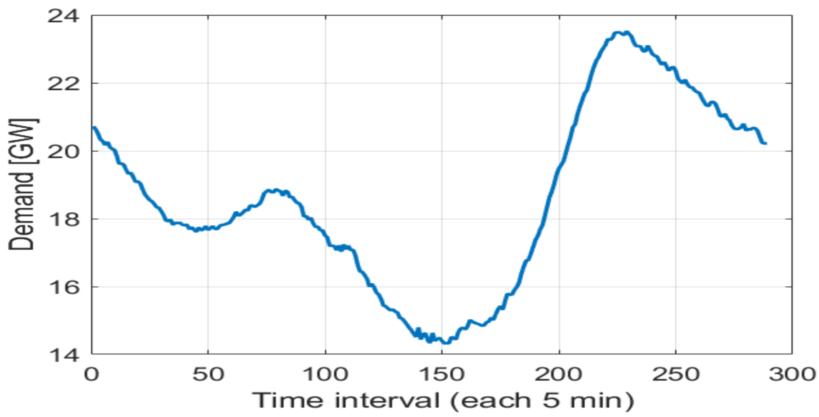

Figure 4.6. The typical demand of NEM used in the simulation

To analysis the ability of EVs for supporting the frequency in future system of NEM, especially in 2030 and 2050 under the different scenarios of AEMO's ISP. We used the estimated load and reserve of EVs in 2030 and 2050 based on the developed estimation tool in the previous sections. The AEMO's ISP scenarios have considered as input to the estimation tool. Likewise, we considered that the maximum large disturbance would ne be changed in the future power system. We are interested in the frequency nadir only in this part of the study to evaluate the ability of EVs for preventing large frequency decline in future. The typical demand of NEM is considered as input to the simulation as well, see Figure 4.6. We assess the frequency nadir during different times of the day because the operating point is changing and the demand of EVs and their active power reserve is changing from one operating point to another. Therefore, we run the simulation for 300 scenarios, where a disturbance occurs in different time in each scenario. This means we obtain the frequency nadir if a disturbance occurred every 5 minutes during the typical demand of a day in NEM system.

Figure 4.7 shows that the EVs' ability to support the frequency in NEM system in 2030 depends on the scenario. For Hydrogen super power scenario, the frequency nadir will be maintained above 49.8 Hz for whole the day except for the time duration between 6AM-2Pm. The different scenarios and the results are clearly depicted in Figure 4.7, confirming the ability of EVs for the provision of good amount of primary reserve to prevent large frequency decline. However, if the slow-change scenario based on ISP would be implemented, the EVs would not be able to provide sufficient services by 2030 to NEM system.

On the other hand, most of the ISP scenarios of deployment of EVs by 2050 confirms the ability of EVs to provide significant amount of reserve to support frequency in NEM system. The results based on 2050 scenarios of EV deployment in Australia based on ISP and their ability to support the frequency are depicted in Figure 4.8. The results show that a great opportunity is exist and therefore it is time to start invest in infrastructure to make it ready by 2030 for enabling the frequency support from EVs, and therefore offering services from reliable and affordable sources at the demand-side.

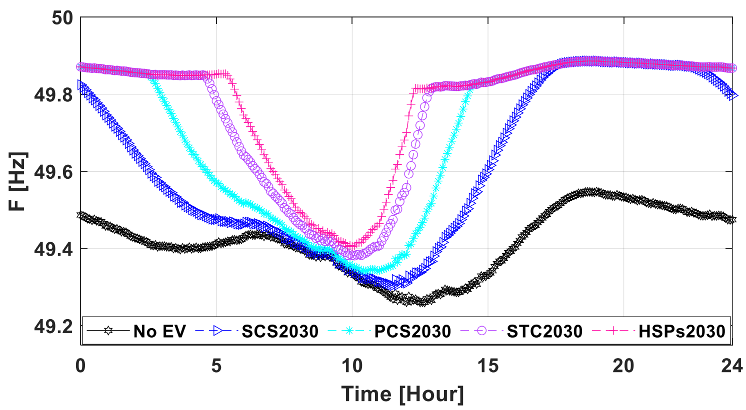

Figure 4.7. The frequency nadir in NEM system for a typical day under different scenarios of EV for 2030 based on ISP scenarios

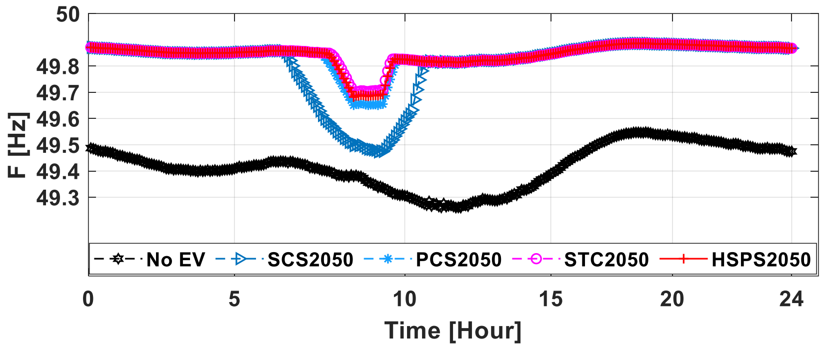

Figure 4.8. The frequency nadir in NEM system for a typical day under different scenarios of EV for 2030 based on ISP scenarios

B.7 Conclusion and used data for the simulation

In the above work, an EV aggregation method scheme for participation of EVs in primary frequency control has been proposed. The proposed aggregation method consists of four EV groups including idle EVs and charging EVs. For the proper operation of the proposed scheme, some information, such as the initial SOC and departure time are required. Also, an EV aggregate model of EVs for frequency studies has been suggested. The parameters of this model are obtained based on the data sent to the aggregator by EVs. In the model, ramp up/down rate of EVs has been considered. Simulation results showed that not considering the ramp rates in the aggregated model of the EVs leads to misleading results. Based on the simulation studies carried out on a single area and three area power systems, it was found that implementing EVs frequency response of both systems highly improves in case of disturbances. That is, not only the maximum frequency deviation decreases but also a reduction in frequency oscillations is observed. On the other hand, contribution of EVs to frequency control reduces the maximum deviation and oscillations of the output power of conventional generating units. This; in turn, increases the life time of governors of conventional generating units. Also, implementing EVs in the multi-area power system has decreased the deviations and oscillations of tie lines power.

B.8 References

[1] J. Li, C. Li, Y. Xu, Z. Y. Dong, K. P. Wong and T. Huang, "Noncooperative Game-Based Distributed Charging Control for Plug-In Electric Vehicles in Distribution Networks," in IEEE Transactions on Industrial Informatics, vol. 14, no. 1, pp. 301-310, Jan. 2018.

[2] M. H. Rehmani, M. Reisslein, A. Rachedi, M. Erol-Kantarci and M. Radenkovic, "Integrating Renewable Energy Resources Into the Smart Grid: Recent Developments in Information and Communication Technologies," in IEEE Transactions on Industrial Informatics, vol. 14, no. 7, pp. 2814-2825, July 2018.

[3] P. Kundur, N. J. Balu, and M. G. Lauby, Power System Stability and Control. New York, NY, USA: McGraw-Hill, 1994.

[4] X. Lu, X. Yu, J. Lai, J. M. Guerrero and H. Zhou, "Distributed Secondary Voltage and Frequency Control for Islanded Microgrids With Uncertain Communication Links," in IEEE Transactions on Industrial Informatics, vol. 13, no. 2, pp. 448-460, April 2017.

[5] T. Zhang, X. Chen, Z. Yu, X. Zhu and D. Shi, "A Monte Carlo Simulation Approach to Evaluate Service Capacities of EV Charging and Battery Swapping Stations," in IEEE Transactions on Industrial Informatics, vol. 14, no. 9, pp. 3914-3923, Sept. 2018.

[6] Q. Zhang, W. Deng and G. Li, "Stochastic Control of Predictive Power Management for Battery/Supercapacitor Hybrid Energy Storage Systems of Electric Vehicles," in IEEE Transactions on Industrial Informatics, vol. 14, no. 7, pp. 3023-3030, July 2018.

[7] H. R. Baghaee, M. Mirsalim, G. B. Gharehpetian and H. A. Talebi, "A Decentralized Power Management and Sliding Mode Control Strategy for Hybrid AC/DC Microgrids including Renewable Energy Resources," in IEEE Transactions on Industrial Informatics, Early Access.

[8] Y. Mu, J. Wu, J. Ekanayake, N. Jenkins, and H. Jia, “Primary frequency response from electric vehicles in the Great Britain power system,” IEEE Trans. Smart Grid, vol. 4, no. 2, pp. 1142–1150, Jun. 2013.

[9] H. Liu, Z. Hu, Y. Song, and J. Lin, “Decentralized vehicle-to-grid control for primary frequency regulation considering charging demands,” IEEE Trans. Power Syst., vol. 28, no. 3, pp. 3480–3489, Aug. 2013.

[10] S. Izadkhast, P. Garcia-Gonzalez, and P. Frias, "An Aggregate Model of Plug-In Electric Vehicles for Primary Frequency Control,", IEEE Trans. Power Syst., vol. 30, pp. 1475-1482, Aug. 2015.

[11] US Department of Transportation (2001). [Online]. Available: Highlights of the 2001 national household travel survey. http://www.bts.gov/publications/highlights_of_the_2001_national_household_travel_survey/pdf/entire.pdf.

[12] M. S. Ahmad and S. Sivasubramani, "Optimal Number of EVs for Existing Networks Considering Economic and Emission Dispatch," in IEEE Transactions on Industrial Informatics, Early Access.

[13] Guille and G. Gross, “A conceptual framework for the vehicleto-grid (V2G) implementation,” Energy Policy, vol. 37, no. 11,
pp. 4379–4390, Nov. 2009.

[14] J. Riesz, J. Gilmore, and I. MacGill. "Frequency Control Ancillary Service Market Design: Insights from the Australian National Electricity Market." The Electricity Journal vol. 28, no. 3, pp. 86-99, Apr. 2015.

[15] E. Ela et al. "Market designs for the primary frequency response ancillary service—Part I: Motivation and design." IEEE Trans. Power Syst., vol. 29, on 1, pp.421-431., Jan. 2014.

[16] N. Rahbari-Asr, M. Chow, J. Chen and R. Deng, "Distributed Real-Time Pricing Control for Large-Scale Unidirectional V2G With Multiple Energy Suppliers," in IEEE Transactions on Industrial Informatics, vol. 12, no. 5, pp. 1953-1962, Oct. 2016.

[17] T. Masuta, and A. Yokoyama. "Supplementary load frequency control by use of a number of both electric vehicles and heat pump water heaters." IEEE Trans. Smart Grid, vol. 3, on. 3, pp. 1253-1262, Sept. 2012.

[18] S. B. Peterson, J. Apt, and J. F. Whitacre, “Lithium-ion battery cell degradation resulting from realistic vehicle and vehicle-to-Grid utilization,” J. Power Sources, vol. 195, no. 8, pp. 2385–2392, Apr. 2011.

[19] R. Ball, N. Keers, M. Alexander, and E. Bower, Modeling electric storage devices for electric vehicle MERGE deliverable 2.1 of the EU project, 2011. https://paginas.fe.up.pt/~ee07155/wp_content/uploads/2012/03/Projeto-MERGE-Electric-Penetration-Scenarios-in-Germany-UK-Spain-Portugal-and-Greece.pdf

[20] L. De Sousa, B. Silvestre, and B. Bouchez, “A combined multiphase electric drive and fast battery charger for electric vehicles,” in Proc. IEEE Veh. Power Propulsion Conf., 2010, pp. 1–6.

[21] Y. Zheng, Y. Song, D. Hill and K. Meng, "Online Distributed MPC-based Optimal Scheduling for EV Charging Stations in Distribution Systems," in IEEE Transactions on Industrial Informatics, Early Access.

[22] M. Yin, G. Li, G. Li, H. Liang, and M. Zhou, “Modeling of VSCHVDC and its active power control scheme,” in Proc. Int. Conf. Power Syst. Technol., 2004, vol. 2, pp. 1351–1355.

[23] S. Jaganathan and W. Cao, “Battery charging power electronics converter and control for plug-in hybrid electric vehicles,” in Proc. IEEE Conf. Veh. Power Propulsion, Sep. 2009, pp. 440–447.

[24] R.K. Sahu, S. Panda, and S. Padhan, “A Novel Hybrid Gravitational Search and Pattern Search Algorithm for Load Frequency Control of Nonlinear Power System”, Applied Soft Computing, vol. 29, no. C, pp 310-327, Apr. 2015.

[25] REE red electrica de espana [Online]. Available: https://demanda.ree.es/movil/peninsula/demanda/total/2013-11-03

[26] Black, Veatch, 2018. Cost and Performance Data for Power Generation Technologies. Prepared for the National Renewable Energy Laboratory.

[27] H. H. Alhelou and M. E. H. Golshan, "Hierarchical plug-in EV control based on primary frequency response in interconnected smart grid," 2016 24th Iranian Conference on Electrical Engineering (ICEE), Shiraz, Iran, 2016, pp. 561-566, doi: 10.1109/IranianCEE.2016.7585585.

[28] H. Haes Alhelou, M. E. H. Golshan and M. H. Fini, "Multi agent electric vehicle control based primary frequency support for future smart micro-grid," 2015 Smart Grid Conference (SGC), Tehran, Iran, 2015, pp. 22-27, doi: 10.1109/SGC.2015.7857385.

4.4. Estimation of Available Active Power Reserve from Ambient Temperature-Dependent Loads

One of the main objectives in this project is to seek alternative solutions for the provision of frequency control ancillary services from unique reliable sources. Therefore, the focus is given to the demand-side since it is a promising source for the provision of variety of services including frequency support and flexibility services due to its flexibility, affordability, and reliability. In the previous section, the ability eMobility and electric vehicles to provide services for frequency in future power systems to enable energy transition has been investigated, where an advanced aggregation of EVs and frequency response model of the aggregator have been proposed. Additionally, an estimation tool for estimating the EV reserve at the system and power region levels has been suggested. In addition to the potentials that emobility provide for supporting the frequency in power systems, there is need to look for other alternatives that exist in today's power systems. Motivated by the need for affordable and reliable services for today's power systems, this research project's team has carefully looked at the demand-side and identified that the temperature-dependent loads as potential sources for the provision of frequency services, especially during abnormal operation period of the grid, where a significant amount of fast speed response reserve is required. Ambient temperature-dependent loads, so called thermostatically-controlled loads are unique solution for the provision of frequency support services, especially the primary frequency response services after a large disturbance. Such loads are favorited for the provision of services because they do not directly affect the costumers' convenience. For instance, stopping the air conditioning load in the grid for few seconds to few minutes during contingency would not make much difference in the room temperature, therefore, the consumers' convivence would not be affected. In fact, such action that does not impact directly the customers, would rescue the grid during contingency and give the operator the enough time to start other actions bringing the grid back to its stable operation and avoid unwanted consequences such as cascading events that might lead to blackout, leaving the customers without electricity for minutes to hours. To investigate the feasibility of implementation and availability of reserve from demand-side's thermostatically controlled loads, we assess the availability of reserve to support frequency from ambient temperature dependent loads in what follows, and develop a model for their primary frequency response in the next section.

A1. Available Reserve to Support Frequency at NEM Region and System Levels: The Data Source

It is important to estimate the available amount of reserve with high resolution, on order of minutes or an hour, to assess to what extend the ambient temperature-dependent loads can provide services to secure and stabilize the grid frequency in case of any credible event. In fact, estimating the available reserve is not an easy task which require collecting data for years and building an estimation model, followed by arduous work. Such work is usually done based on national projects. For fortune, a great effort has been attempted by The Commonwealth Scientific and Industrial Research Organisation (CSIRO) to estimate the load demand with 30-minute resolution for Australian power systems, which facilitates the completion of this project.

Thanks to the Australia's National Energy Analytics Research Program (The NEAR Program), we are able to understand the available reserve to support the frequency at NEM level from the data that estimated and published by SCIRO's NEAR project. Mahdavi and Braslavsky et al, have developed models to estimate the demand from air-conditioner loads and NEAR publishes the estimated and validate demand data for different states in Australia for several years [0000]. To understand the available reserve to support the frequency, we utilize the aforementioned data generated by SCRIO's useful projects. To this end, a mathematical formula to determine the available active power reserve from thermostatically controlled loads has been suggested. It is worth mentioning that the suggested formula calculates the active power reserve at power region and whole system levels.

A2. Determining the Available Reserve at Power Region and whole system Levels

In this subsection, we briefly introduce the suggested calculation of the available reserve at power region level of NEM based on CSIRO's NEAR project. The National Electricity Market system is divided into five power regions, i.e. VIC, NSW, SA, QLD, and TAS. NEAR project has developed a methodology to estimate the power consumption share in the total demand at substation levels. It is worth mentioning that NEAR project does not cover all substations at NEM geographical area. However, this does not impact the aim of this research, since the goal is to get understand of the reserve availability and the ability of thermostatically controlled loads for the provision of reserve to support the frequency of power systems during power system transformation and beyond.

Since the NEAR project has developed an estimation tool for estimating the demand of thermostatically controlled loads at substation levels, we need to aggregated the estimation to be at power region level. We have five power regions; therefore, we need to calculate the estimated demand of thermostatically controlled loads for different power regions. In Australia, many distribution network service providers (DNSPs) are available that provide services to customers. In some power regions, more than one DNSP is active, therefore, it is important to aggregated at the DNSP before aggregating the thermostatically controlled loads at the power region level. For instance, we have five different DNSPs at VIC power region, i.e. AusNET, CitiPower, Jemena, PowerCor, and United Energy. Each of the DNSPs covers several substations. Therefore, the estimated demand of thermostatically controlled loads for all the substations under a specific DNSP is first calculated as follows,

$$P_{DNSP,i}(t) = \sum_{i=1}^{N_{substation}} P_i^{sub}(t) \quad (1)$$

where $\mathrm{N_{substation}}$ is the number of substations under the ith DNSP, $\mathrm{P_{DNSP,i}}$ is the ith DNSP, and $\mathrm{P_i^{sub}(t)}$ is the estimated demand from thermostatically controlled load at the ith substation.

After calculating the estimated demand for thermostatically controlled loads at the DNSP level, the total estimated demand of thermostatically controlled loads at the power region level can be determined as follows,

$$P_{region,i}(t) = \sum_{i=1}^{N_{DNSP}} P_{DNSP,i}(t) \quad (2)$$

where $\mathrm{N_{DNSP}}$ is the number of DNSPs that are active in the ith power region, and $\mathrm{P_{region,i}(t)}$ is the demand of thermostatically controlled loads at the ith power region.

Equation (2) calculates the available active power reserve that can be used for supporting the frequency during abnormal operation at power region level. For NEM system, this equation can utilize NEAR project's data to calculate the estimated demand of thermostatically controlled loads for different power regions, which enough time resolution. The time resolution is 30-minute resolution which based on the data resolution provided by SCIRO's developed estimation model.

At the final state, the estimated demand of thermostatically controlled loads for different power regions can be aggregated to calculated the estimated total demand of thermostatically controlled loads at the whole system level, i.e. NEM level, which can be determined using the following equation.

$$P_{SYS}(t) = \sum_{i=1}^{N_{region}} P_{region,i}(t) \quad (3)$$

where $\mathrm{P_{SYS}(t)}$ is the aggregated power of thermostatically controlled loads at the system level which is NEM system in this research, and $\mathrm{N_{region}}$ is the number of power regions in the power system of interest.

Table 4.1. The number of substations considered for estimation by NEAR project under each DNSP in VIC power region; i.e. the $N_{substation}$ used for (1) when it is solved for VIC power region

VIC DNSPs	*AusNET*	*CitiPower*	*Jemena*	*PowerCor*	*United Energy*
$N_{substation}$	*51*	*25*	*24*	*60*	*46*

The above methodology based on the available data from CSIRO's NEAR project is applied to different power regions in NEM power system. It is worth mentioning again that not all sub-power regions are covered by NEAR project; likewise, the TAS power region has not been covered in the estimation. However, this does not impact the goal of this research. To introduce some preliminary results before moving to the next sections, let's have a look at the scale of estimation that has been done by NEAR project. Table 4.1 gives the number of substations that have been considered for the estimation under different DNSPs in VIC only. This confirms the value of the data provide by CSIRO that can pushes research on understanding the ability of the provision of services to grid not only on Australia level but also gives insights on the international systems levels. More discussion and analysis will be provided in the final report of this project.

The aggregation of the estimated demand of thermostatically controlled loads has been done based on (1-3). The inputs of (1) is the data available from CSIRO's NEAR project. For instance, Table 4.1 gives the number of substations under each DNSP in Victorian power region of NEM. Figure 4.9 illustrates the aggregation of the estimation at the DNSPs level and at the power region level of VIC power region, based on data available for 2014. It is worth mentioning that the available data of different years is evaluated and it has been found the same trend is exist confirming the availability of active power demand that can be considered for supporting the frequency in case of any credible events. However, the estimation can be done at 30-miute resolution giving the operator enough time to consider such demand side appliances in the energy and reserve dispatch market for supporting the frequency.

Figure 4.10 illustrates the active power demand at the power regions and the whole NEM system in 2013, while Figure 4.11 shows the results based on NEAR data of 2014. The obtained results show that the required reserve to secure the frequency due to the largest contingency in NEM (almost 600 MW) can be covered by demand-side in most times during the year. However, there is certain times that a combination with other sources is needed to compensate in shortfall in reserve from thermostatically controlled loads. The rational practice in reality is to mix sources of services in order to increase security and reliability. However, the demand-side is much better from this perspective compared to other sources since the thermostatically controlled loads geographically separated over all the geographical area of the system making the preventing its contribution due to different reasons such as cyberattacks impossible.

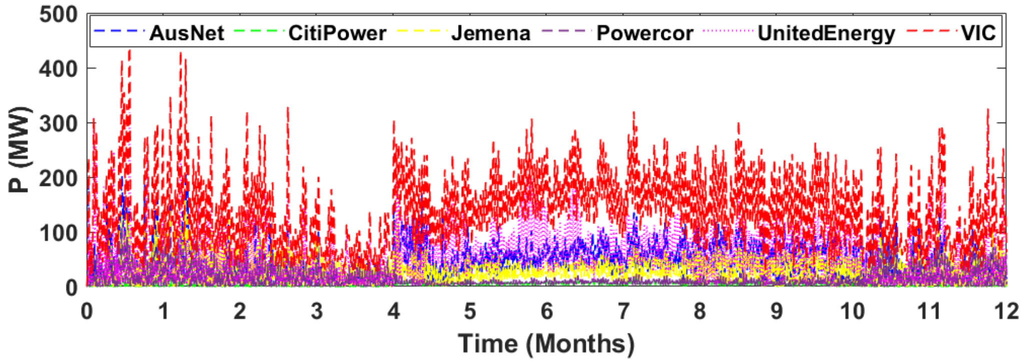

Figure 4.9. the aggregation of the estimated demand of thermostatically controlled loads at the DNSP and power region levels in VIC power region

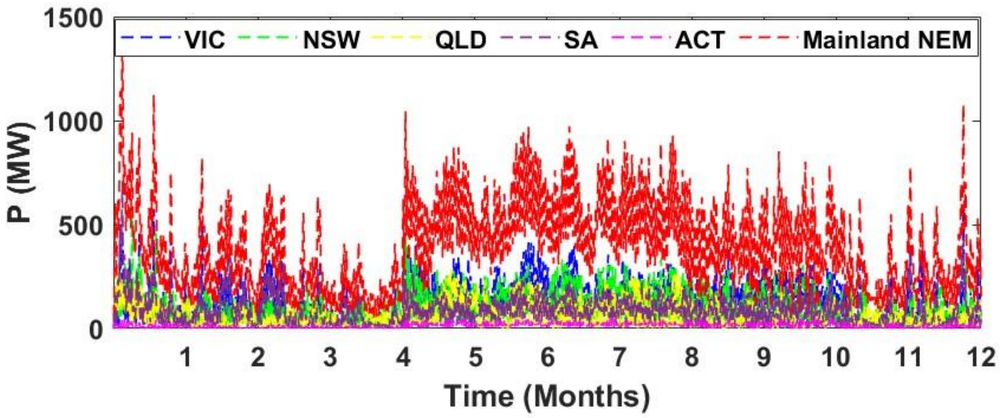

Figure 4.10. The estimated demand of thermostatically controlled loads at the power regions and system levels of NEM

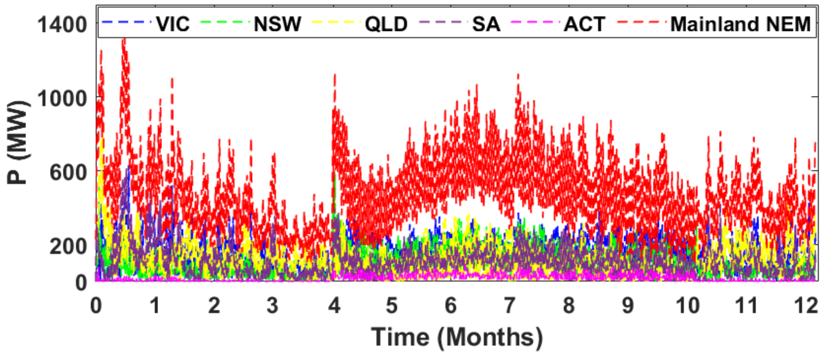

Figure 4.11. The estimated demand of thermostatically controlled loads at the power regions and system levels of NEM

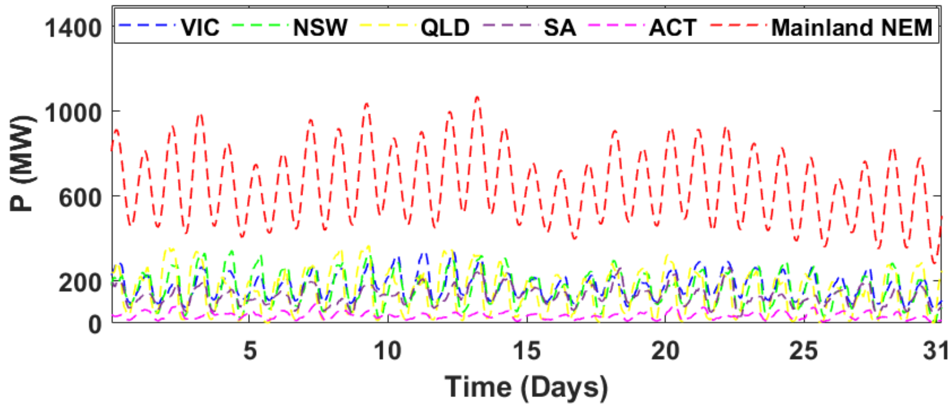

Figure 4.12. The estimated demand of thermostatically controlled loads at the power regions and system levels of NEM for one month-July 2014.

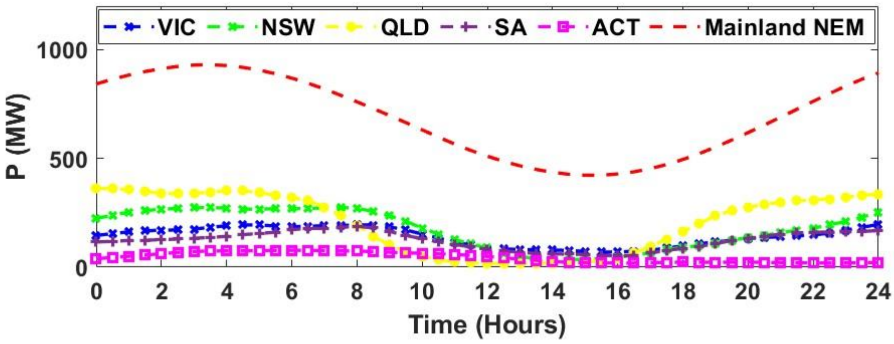

Figure 4.13. The estimated demand of thermostatically controlled loads at the power regions and system levels of NEM for one day-20 July 2013

For illustrative purposes, the estimated demand and reserve of thermostatically controlled loads that can contribute to supporting frequency at power regions and whole system levels are zoomed in to show the results for one month (July 2014) in Figure 4.12, and it is also zoomed in further to present the estimated demand for one day, i.e. 20 July 2014, in Figure 4.13. From these figures, one can observe that the thermostatically controlled loads can provide the required reserve to support frequency and secure it after a large disturbance in NEM system most of hours during a day. It is worth mentioning that the above results do not include all substations in the mainland. Further the results do not involve TAS power region. Therefore, one can conclude that the available frequency control ancillary services from thermostatically controlled load would be higher if TAS and all substations in mainland system would be considered, confirming the capability of demand-side for providing a source of services to support frequency in NEM and similar power systems at the international level. Now, it is crucial to develop a dynamic frequency response model based on the aggregation of the available reserve from thermostatically controlled loads. In what follows, we develop a novel dynamic model and use it for assessing the capability of demand-side thermostatically controlled loads for securing and stabling the frequency during large disturbances.

A.3 References:

[1] N. Mahdavi, J. H. Braslavsky and C. Perfumo, "Mapping the Effect of Ambient Temperature on the Power Demand of Populations of Air Conditioners," in IEEE Transactions on Smart Grid, vol. 9, no. 3, pp. 1540-1550, May 2018, doi: 10.1109/TSG.2016.2592522.

[2] N. Mahdavi, J. H. Braslavsky, M. M. Seron and S. R. West, "Model Predictive Control of Distributed Air-Conditioning Loads to Compensate Fluctuations in Solar Power," in IEEE Transactions on Smart Grid, vol. 8, no. 6, pp. 3055-3065, Nov. 2017, doi: 10.1109/TSG.2017.2717447.

[3] N. Mahdavi and J. H. Braslavsky, "Modelling and Control of Ensembles of Variable-Speed Air Conditioning Loads for Demand Response," in IEEE Transactions on Smart Grid, vol. 11, no. 5, pp. 4249-4260, Sept. 2020, doi: 10.1109/TSG.2020.2991835.

[4] CSIRO NEAR Project Link: ***https://near.csiro.au/***

4.5. A Novel Dynamic Model to Assess Frequency Response from Thermostatically-Controlled Loads

In this part of the research, a new simplified frequency response model of thermostatically controlled loads is proposed. The model is built to be useful for frequency studies and frequency response analysis from thermostatically controlled loads. The aim is to develop a model capable for investigating frequency response from air condition appliances to support frequency in power systems after a large disturbance. Thus, the model is applicable for primary frequency response studies in modern and future power systems.

It is important to understand the thermal model of a room. The model given in (1-2) has been thoroughly validated in literature which can be considered as a sufficient model for this research [1].

$$c_A \rho_A V \, \Delta T_A = \int (\Delta Q_{gain} - \Delta Q_{AC}) dt \quad (1)$$

$$\Delta Q_{gain} = (U_{O-A} A_S + c_A \rho_A V \xi)(\Delta T_O - \Delta T_A) + \Delta Q_{dis} \quad (2)$$

where Q_{gain}, Q_{dis}, and Q_{AC} are the total heat gains of the room, the heat power from people, lights, appliances, and other disturbances, and the refrigerating capacity of the inverter, respectively. AC. c_A, ρ_A, V, and ΔT_A are the heat capacity of the air, the density of the air, the volume of the room, and the indoor temperature, respectively. A_S is the surface area of the room. U_O, ξ, T_O, and T_A are the heat transfer coefficient and air exchange times between the room and the ambience, the ambient temperature, and the indoor temperature, respectively.

In the frequency domain by implementing the Laplace operator, i.e. s, the model can be rewritten as follows,

$$c_A \rho_A V \xi \, \Delta T_{A(s)} s = Q_{gain}(s) - Q_{AC}(s) \quad (3)$$

From the thermal model and the electrical power consumption model of the air conditioners, a thermal and electrical model of the inverter AC can be driven as depicted in Figure 4.14. We omit the mathematical background in this report and the complete mathematical background will be presented at the final report, where more details on this model can be found in []. However, the block diagram in Figure 4.14 should provide enough details of model of air conditioners that might be implemented for supporting the frequency response in power systems.

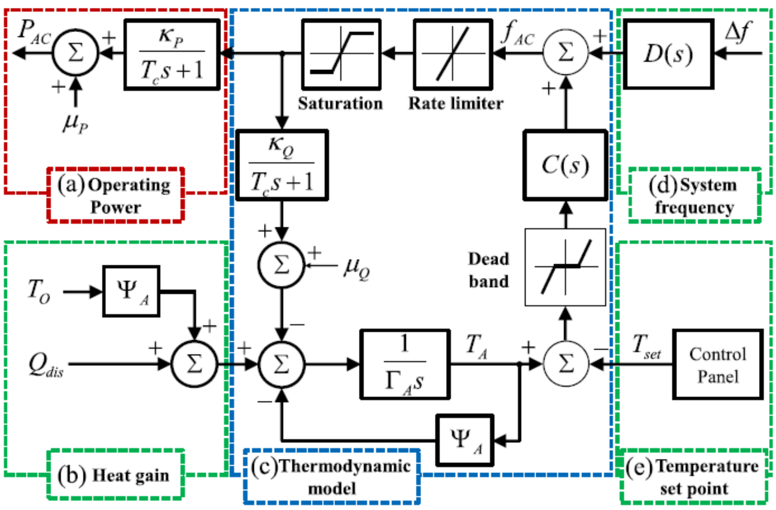

Figure 4.14. Thermal and electrical model of the thermostatically controlled loads [1].

The main parameters shown in the model that is depicted in Figure 1 are briefly described as follows. P_{AC} and Q_{AC} are the operating power and refrigerating capacity of the AC. f_{AC} is the operating frequency of the inverter AC; κ_P and κ_Q are the constant coefficients of the inverter AC; and Tc is the time constant of the compressor. μ_P and μ_Q are the constant coefficients of the inverter AC. C(s) is the temperature controller of the inverter AC and T_{dev} is the deviation between the indoor temperature T_A and the set temperature T_{set}. θ and η are the constant coefficients of the controller. Δf is the frequency deviation of the power system and D(s) is the controller of the inverter AC.

The model shown in Figure 1, can be summarised mathematically in frequency domain as follows,

$$\Delta P_{AC}(s) = \frac{k_p(\Gamma_A s+\Psi_A)(D(s)\Delta f(s)+C(s)\Delta T_{set})}{(T_C s+1)(\Gamma_A s+\Psi_A)+k_Q C(s)} + \frac{k_p C(s)(\Psi_A \Delta T_o(s)+\Delta Q_{dis}(s))}{(T_C s+1)(\Gamma_A s+\Psi_A)+k_Q C(s)} \quad (4)$$

Considering the fact that the aim of the model that is being developed here is to analysis the frequency response from thermostatically controlled loads after a large disturbance. The primary frequency response should start immediately after the start of the frequency decline, meaning that the frequency response service should be provided as primary frequency response and full utilised within 30 sec. It means that the process of primary frequency response is short time-scale process. Therefore, the ambient temperature and the radiated heat can be assumed as invariable. Based on the fact that the time-scale of the primary frequency response is very short compared to thermal process, the three deviations ΔT_{set}, ΔT_O, and ΔQ_{dis} can be considered zero during the process of primary frequency response, thus they can be omitted. Therefore, the model can be expressed as follows,

$$\Delta P_{AC}(s) = \frac{k_p D(s)(\mathrm{T}_A s+1)}{(T_C s+1)(\mathrm{T}_A s+1)+\Phi_{AC} C(s)} \Delta f(s) \quad (5)$$

In literature, some works suggested AC for providing the secondary frequency control, where $\mathrm{D}(s)$ needs to be an integrator controller to remove errors, e.g. $\mathrm{D}(s) = \delta + \gamma s$. However, it is not realistic to consider thermostatically controlled loads such as AC for the provision of secondary reserve, because of several reasons, including the direct impact on the customers' convenience, the infeasibility of implementation due to the huge cost needed to invest in infrastructure, the complexity of implementation due to the need for transferring data of all ACs to control center and receiving dispatching signal from operator putting whole process under danger of losing data or control signals due to attacks or failures which might lead to blackouts, and the secondary frequency control time scale is high and needs continuous source of reserve which is not easy to achieve from ACs. In addition to the aforementioned reasons, a real-time aggregation is required which express high complexity for implementation in near future.

We propose implementing thermostatically controlled loads, such as AC for supporting the frequency during large disturbances and contingencies. This means we propose the implementation of AC for compensating the contingency reserve, for NEM system it is to compensate contingency FCAS by demand side. The main reason the activation of contingency FCAS is enabled during large credible events, which are rarely occurred compared to the continuous fluctuation in frequency due to fluctuation in demand and uncertainty of RESs in generation side. To implement the proposed new control technique locally, the following steps are proposed:

i) Sensing the frequency locally by thermostatically controlled loads, e.g. ACs.

ii) If the frequency deviation exceeds a specific threshold, the control plan will be activated to realise the primary frequency response from ACs to stop frequency decline, thus the frequency would be stabilised by bringing it back to a stable limit. The power system operator can set the threshold based on its preference and based on the frequency control policy and arrangements adopted by a specific system.

iii) Activating the primary frequency control mode by implementing droop characteristic technique for all ACs that participate in primary frequency plan. The droop can be set by the power system operator; however, we suggest setting a droop equal to those used for power plants to maintain coordinated response between demand and generation sides.

iv) We do not recommend implementing secondary frequency control on ACs because the implementation of integrator will delay the response from ACs and it is not feasible in the near future to implement ACs for the provision of secondary reserve due to the above-mentioned reasons.

In addition to the proposed control strategy to implement ACs for primary frequency response, we also propose a low order primary frequency response model of thermostatically controlled loads, i.e. ACs. To avoid repeating the methodology given in Chapter 2, the subspace system identification (N4SD) technique, the readers can refer to chapter 2 for more information about the mathematical background. Based on the proposed identification technique of the low-order system models, the model in (7) is driven from the AC primary frequency response model in (6). It is worth mentioning that $\mathrm{D(s)} = \frac{-1}{\mathrm{R_{AC}}} = -\mathrm{K_{AC}}$ presenting the droop characteristic used for implementing primary frequency response.

$$\Delta P_{AC}(s) = \frac{-k_p K_{AC}(\mathrm{T}_A s+1)}{(T_c s+1)(\mathrm{T}_A s+1)+\Phi_{AC}C(s)}\,\Delta f(s) \qquad (6)$$

$$\Delta P_{AC}(s) = \frac{-1}{R_{AC}}\frac{1}{(T_c s+1)}\,\Delta f(s) \qquad (7)$$

The developed primary frequency response model of ACs is implemented in a generic system frequency response model with typical values for governor-turbine system, while the inertia and demand are set based on a specific operating snapshot of NEM system in Australia. It is worth mentioning that the droop gain has been set as -11 for both conventional power plants and ACs model.

Figure 4.15 shows the frequency response in the power system if a disturbance equal to 600 MW occurs in the system, under the consideration where a sufficient reserve is available from conventional power plants. The aim of the results is to confirm the ability of ACs in improving the frequency response and frequency stability if ACs are considered as a source of primary frequency response in future NEM system. Figure 4.15 clearly confirms that if there is no response from ACs to a frequency decline, the frequency will reach 49.47 Hz within 4 seconds putting the system under stress during the frequency decline. Thanks to the available reserve from AC, the frequency decline could be limited to 49.87 Hz if suitable arrangements are considered for implementing AC for supporting the frequency in power systems. In case of worst implementation of ACs, meaning that a high time constant or delay for the response is considered, the frequency will not exceed 49.8 Hz. It is clear that even if the worst case of implementation is adopted, the ACs can highly improve frequency response if they are considered for primary frequency response.

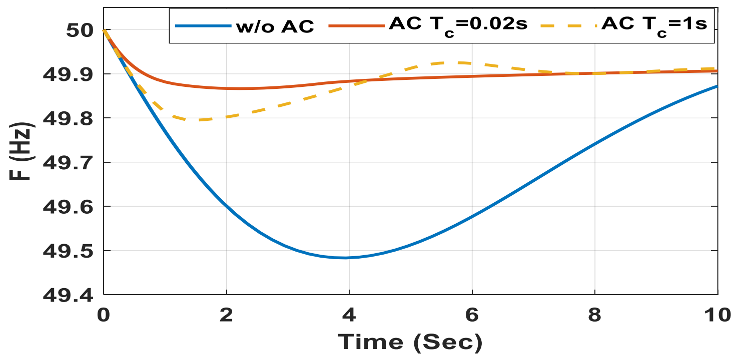

Figure 4.15. The frequency response after a large disturbance; w/o without AC participation, AC Tc=0.02 s means the time constant of AC is set to 0.02 seconds

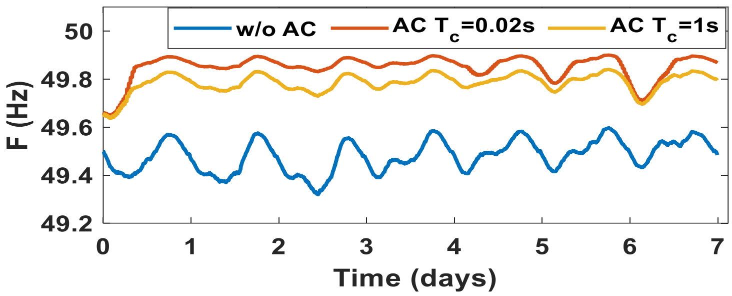

Figure 4.16. The frequency nadir if a disturbance occurred at different times in the first week of September 2022 under different scenarios of AC participation

Figure 4.16 shows the same scenario considered in Figure 4.15, however in Figure 4.16 we are interested only in the maximum frequency nadir if a disturbance occurred in different times during the first week of September 2022 in NEM system. The aim is to show that might differ due to the change in operating point and due to the difference in the available reserve amount from ACs to support the frequency after a large disturbance. However, it is clear that the ACs can maintain the frequency within a stable range in all times of the week under consideration.

Figure 4.17 depicts the dynamic response from power plant in order to stop the frequency decline under different scenarios of AC participation in frequency support. The main observation that the maximum required active power response from power plant would be highly reduced in case if ACs are considered for supporting the frequency. Another fact is that the participation of ACs in frequency support can reduce the pursuer on power plants by reducing the requirements of ramp-rate response. The required maximum active power response from power plants for different times in the first week of September 2022 under the aforementioned scenario is depicted in Figure 4.18.

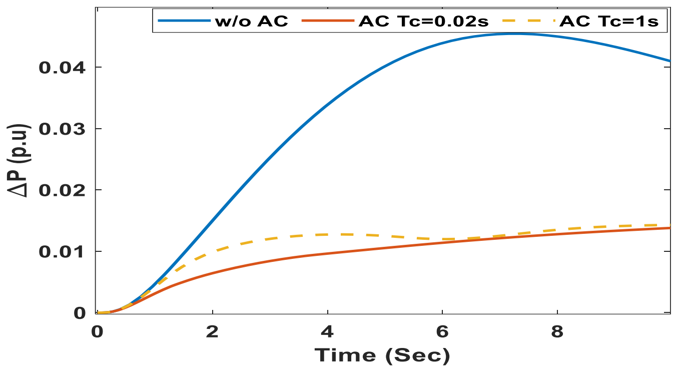

Figure 4.17. The active power response from power plants if a disturbance occurred under different scenarios of AC participation

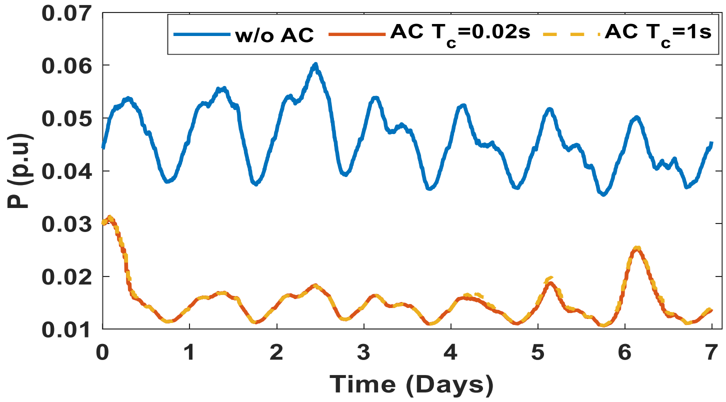

Figure 4.18. The required maximum active power from power plants if a disturbance occurred at different times in the first week of September 2022 under different scenarios of AC participation

The same analysis is implemented for analysing the active power response from ACs in case there is a large disturbance occurred in the system. Figure 4.19 depicts the dynamic response from ACs in order to stop the frequency decline under different scenarios of AC participation in frequency support. The main observation that the maximum required active power response from AC would be provided in enough speed due to the fact that the dynamic response from ACs is much better than those in power plants. The required maximum active power response from ACs for different times in the first week of September 2022 under the aforementioned scenario is depicted in Figure 4.20.

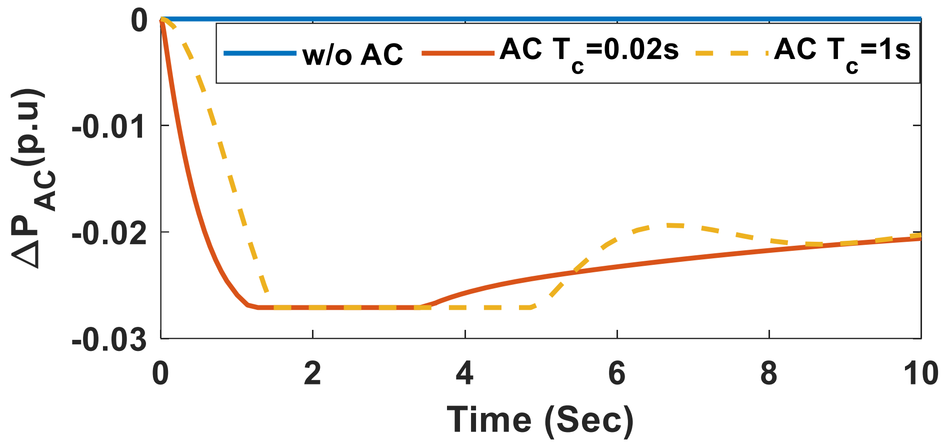

Figure 4.19. The active power response from ACs if a disturbance occurred under different scenarios of AC participation

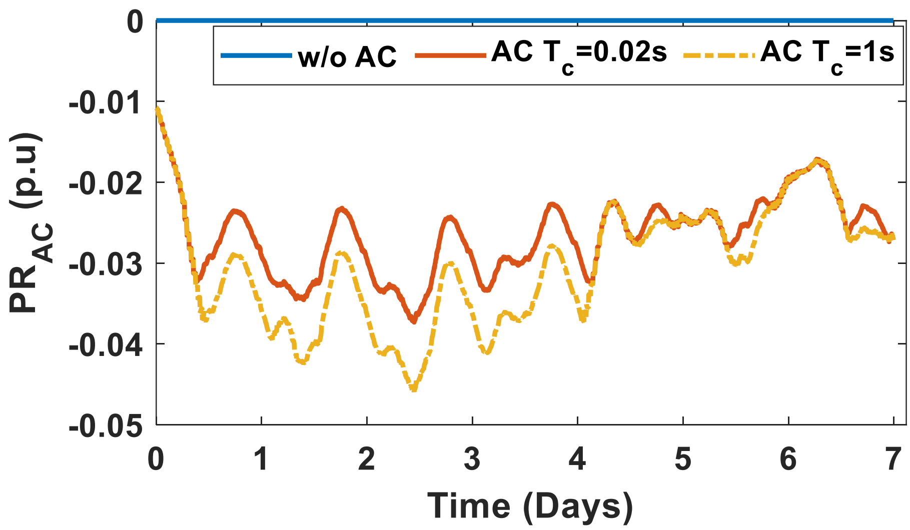

Figure 4.20. The maximum active power response from ACs if a disturbance occurred in different times during the first week of Sep 2022 under different scenarios of AC participation

In the final scenario presented in this report, the impact of thermostatically controlled loads on both rate of change of frequency (RoCoF) and the time of operating the system under dynamic pursuer due to frequency decline is analysed. Figure 4.21 depicts the results related to RoCoF. One can observe that there is a minor improvement in RoCoF by implementing fast frequency response from ACs. However, the aim of the implementation is to improve primary frequency response, not the inertial frequency response. The main reason of the fact that there is no significant improvement is that it is not easy to implement virtual inertia based on such appliances and the other fact that the delay due to measurement and control activation leads to delays preventing the ability to get the same performance compared to synchronous inertia.

One of the important and significant advantages is the reduction of time operating the system under dynamic stress. Figure 4.22 shows that the operation time of the system under frequency decline is around 4 seconds when there is no participation from ACs. If ACs are considered for supporting the frequency, the duration of time where the system encounters disturbance is highly reduced from 4 seconds to around 1.5 seconds in most times, if the disturbance occurred in the first week of September in NEM system. The results confirm the capability and superiority of ACs and thermostatically controlled loads for the provision of primary frequency response to future power systems, which helps accelerate the power system transformation worldwide.

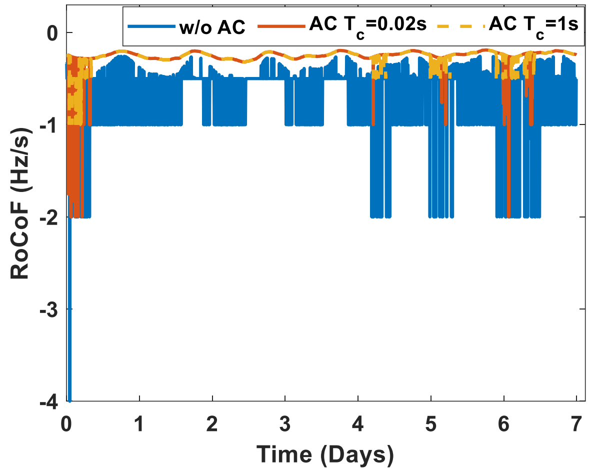

Figure 4.21. The maximum RoCoF if a disturbance occurred in different times during the first week of Sep 2022 under different scenarios of AC participation

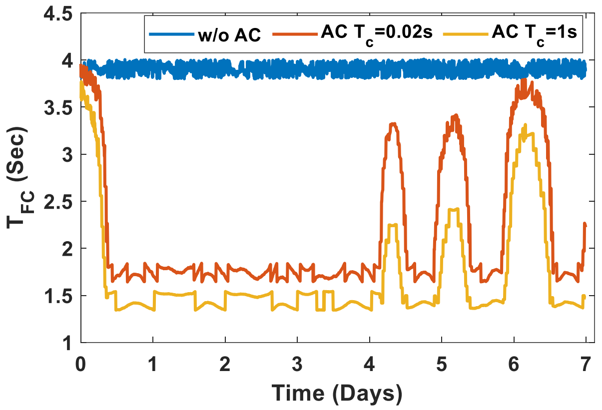

Figure 4.22. The maximum time of operating under frequency declining if a disturbance occurred in different times during the first week of Sep 2022 under different scenarios of AC participation

References:

[1] Ding, Yi, et al. Integration of air conditioning and heating into modern power systems. Springer, 2019.

Chapter 5: The requirements of Inertia and FFR for Modern Power Systems

Note: *The work in this chapter is under preparation for a scientific paper.*

5.1. An Overview

Modern power systems compared to conventional ones have shortfall in inertia and spinning reserve due to the fact that the synchronous generators are being (will be) replaced with inverter-based resources. In synchronous generating units dominated power systems, the synchronous inertia was freely and generously made available because of the direct coupling between electrical part and mechanical part of the systems through synchronous generators. The kinetic energy stored in several rotating parts of power plant based on synchronous generation can be represented a synchronous inertia. The most important feature is that the inertia responsive is instantly after a disturbance. This is because there is no need for control loops to activate the inertia responsive compared to other type of responses to frequency deviation. To conclude, the synchronous inertia will resist the change in the speed of synchronous generating units after a disturbance and therefore it will resist the change in the frequency. Therefore, the inertia is the first and only defense line to resist the change in the rate of change of frequency (RoCoF) at the moment of disturbance. To keep the frequency and especially the RoCoF within an acceptable operation limits, a specific amount of inertia should be always made available. It is crucial to understand the required minimum inertia level in the whole power system and in each power region to keep the system operated securely under reasonable assumptions of potential contingencies. It is worth mentioning that virtual inertia is different from synchronous inertia. While the synchronous inertia comes directly from the machinal part of power systems especially from turbines synchronized with the grid through synchronous generating units, the virtual inertia is a dynamic response that tries to mimic the actual response of synchronous generating unit during the inertia responsiveness. However, there are major differences where the most important one is the virtual inertia is produced using a control loop applied through power electronic interfaces to mimic the swing equation. Therefore, the major difference is that the virtual inertia would always have a delayed response compared to the synchronous one. The term “virtual inertia” needs more investigation to confirm whether it can be considered as an inertia or as a very fast frequency response. This is one of the aspects that would be discussed in the prat of research which is an additional deliverable of the project. Therefore, this part of research will focus on understanding the requirement of synchronous inertia in each power region. Furthermore, this research will also discuss the ability of fast frequency response (FFR) and virtual inertia in compensating the shortfall of synchronous inertia. Moreover, an optimization methodology will be developed to determine the required inertia and fast frequency response in interconnected power systems.

5.2. Current and Future Inertia for the NEM

AEMO regular reviews and evaluates the situation of power system inertia in the NEM due to its importance to the system stability and security. AEMO also publishes the evaluation and assessment results in useful reports that predicts the future situation of the system inertia. Readers are referred to [1-2] for more information about the current and predicted future situation of the inertia in the NEM. For instance, Figure 5.1 shows the existing the future expected inertia shortfall across NEM power regions based on the 2022 inertia assessment by the system operator. It is clear that SA and TAS have an existing inertia shortfall, while QLD and VIC will have inertia shortfall starting from 2026.

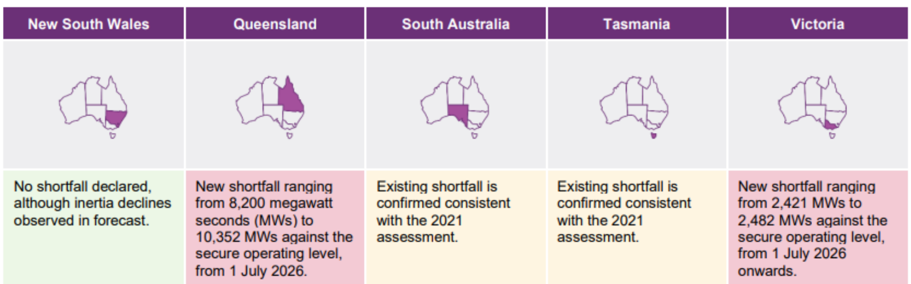

Figure 5.1. 2022 inertia review outcomes for the NEM, for the five-year period to December 2027 [1]

Table 5.1. Current inertia requirements in MWs in the NEM [3]

	Type	NSW	VIC	QLD	SA	TAS
Inertia Requirements (MWs)	Secure	12500	13900	14800	6000	3800
	Minimum	10000	9500	11900	4400	3200

Table 5.1 presents the currently required inertia in different power regions to securely operate the system, where the values are obtained based on a specific inertia requirement methodology adopted by AEMC and ESB in Australia [3]. Currently, the SA power region encounters severe inertia shortfall, and this will last until 2023, while the TAS region faces a potential inertia shortfall. Based on AEMO's estimation, the QLD power regions could face a potential inertia shortfall in 2025, while the TAS power region would encounter a severe inertia shortfall after 2024 [3]. It is worth mentioning that a number of power regions in Australia meet current inertia requirements by compensating for physical rotating inertia by fast frequency reserve due to the shortage in physical inertia in the renewable-dominated power system in NEM [3].

Recently in March 2023, AEMO has published a fact sheet in [4] to clarify and distinguish key terms related to inertia including synchronous inertia and synthesis inertia (the virtual inertia). Reference [4] explores inertia from the perspective of a transitioning power system represents AEMO's technical view on inertia in the NEM. Based on [3-4], The most important terminologies and inertia classification as accepted the system operator are as follows:

- ✓ **Power System Inertia:** An inertial response is the immediate, inherent, electrical power exchange from a device on the power system in response to a frequency disturbance. Power system inertia is the aggregate equivalent inertia of all devices on the power system capable of providing an inertial response.
- ✓ **Synchronous Inertial Response:** A synchronous inertial response is the electromechanical inertial response from stored kinetic energy in the rotating mass of a machine that is electro-magnetically coupled to the power system's voltage waveform at 50 hertz (Hz).
- ✓ **Synthetic Inertial Response:** A synthetic inertial response is the emulated inertial response from an inverter-based resource that is inherently initiated in response to a power system disturbance, and sufficiently fast and large enough to help manage RoCoF.

It is clear that currently the interconnected power systems including NEM are still being operated with support from synchronous inertia comes from synchronous generating units to meet the required level of inertia across the whole system and the requirements for each power regions. It is no clear yet for system operators across the world, how the synthesis inertia could replace the synchronous inertia since there is a lack on the studies related to quantities metrics to provide clear understanding and roadmap for the adoption of virtual inertia.

There are several features for the synchronous inertia that were not important in traditional power systems due to availability of inertia at a level that does not make concerns to the operators. Nowadays due to the shortfall of synchronous inertia in modern power systems, the separation of inertia across the system becomes a critical factor. In fact, the inertia is most important for the RoCoF limitation at the moment of the disturbance/event. It has been confirmed that the inertia has local impact on RoCoF and it is difficult to support the inertia shortfall by neighbouring power regions. The reason is that the transferring of inertia response would be delayed resulting in higher RoCoF at the power region under disturbance.

It is vital to have a vision on the future power system inertia. The Australian operator of WEM and NEM expects that the future control of RoCoF especially in NEM will be met by a combination between the synchronous inertia and synthesis inertia especially during the near future during the energy transition. Each type of inertial response will coincide with other characteristics of the devices delivering the response. This will in turn have implications for other power system phenomena that need to be understood as new sources of both synchronous and synthetic inertial response are introduced into the system [3-4]. At the moment, AEMO believes it would be prudent to maintain (where efficient) substantial levels of synchronous inertia for general power system resilience, such that this approach would not be necessary [4].

The current synthesis inertia techniques to achieve virtual inertia response are mainly applied to inverter-based resources through control loops by mimicking the swing equation. However, Inverters used in IBRs are normally current limited at significantly lower overcurrent levels than synchronous machines are capable of. This can limit an inverter's synthetic inertial response, especially when the inverter is operating near its rated capacity, resulting in different levels of inertial contribution capability at different operating points. Another challenge is that the virtual inertia is implemented through control loops and therefore it is not easy to get the same instant response of the synchronous inertia. In fact, this is the main challenge that we highlight. Therefore, there is a need to quantify the virtual inertia response and to understand how virtual inertia can compensate part of the synchronous inertia shortfall if the RoCoF needs to be kept within a specific limit. This wide question needs an in-depth analysis that would results in a standard for the implementation of virtual inertia in interconnected power systems. Likewise, there is a need to discuss the differences between very fast frequency response and virtual inertia response. At the moment, a number of power systems including the NEM are using the very fast frequency response to compensate the inertia shortfall. The additional research has been done on this identified by our team that the virtual inertia and FFR can help compensating the inertia shortfall, provided that a sufficient RoCoF ride through capability would be guaranteed.

5.3. Simultaneous Estimation of Inertia Constant and Damping Coefficient

The estimation of the available inertia and load frequency relief is crucial towards safe and secure operation of power systems. The accurate estimate can help allocate sufficient inertia and reserve during different operational time intervals. To address this issue, an approach is developed to estimate the inertia constant and damping coefficient in each power region and across the system. The developed approach requires less information of the system, where only some synchronised measurements are required. To this end, the generated and consumed power and the frequency are required for the developed approach. If the regional or zonal inertia is required, then the above-mentioned information is required for region in addition to measurements of the exchanged active power between the power region of interest with its neighbouring power regions.

The estimation approach is developed based on the subspace state estimation theory, where detailed information and its mathematical background is presented in Chapter 2. The main steps and equations are as follows:

i. *Formulating the problem*

In this step, the type of the required inertia should be specified whether it is a zonal inertia or the total inertia across the system.

ii. *Specify the required measurements*

If the total inertia across whole the system is required, then the frequency and the active power deficit measurements are required. If the zonal inertia is required, the measurements of transferred active power are required in addition to the measurements of the frequency and active power deficit. The active power deficit is given below,

$$\Delta P = P_G - P_D \qquad (1)$$

where $P_G \ and \ P_D$ are the total power generation and the total power demand in MW.

iii. *Pre-processing of data and measurements*

In this step, the measurements should be arranged to form the input and output data in the Hankel Signal Matrices forms. We need to form Up, Uf, Yp, Yf and their respective +/- modifications.

iv. *Calculate the projection*

In this stage, we determine the Oblique Projections to determine O_h.

v. *Main mathematical calculations*

In this step, we compute Singular Value Decomposition (SVD) of the weighted oblique projection.

vi. *Obtaining the system order and dynamic states*

Determine the system order by inspecting the singular values of S and partition the SVD accordingly to obtain U1 and S1. Then, we determine the state sequences.

vii. *Estimation process*

In this stage, we estimate the parameters A, B, C and D, and predict the stochastic parameters Re and K from the covariance estimate of the residuals. This stage will result in the estimation of the total or zonal inertia as required as well as the load damping coefficient.

It is worth mentioning the results of this section, the estimation of the inertia and its accuracy is given in Chapter 2.

5.4. Inertia Requirements in Power systems

Inertia and system strength are among the most important factors that impact the operation stability and security in modern power systems. These factors, in fact, have direct influence on power system transformation. The increase of the penetration of renewable energy resources and retirement of synchronous generating units or replacing it by inverter-based resources have attracted high attention to the shortfall of synchronous inertia and system strength in modern and future power systems.

The sources of inertia in power systems is the synchronous generating units-based power plants. Therefore, such inertia is called as synchronous inertia. It is a mechanical rotating inertia electro-magmatically coupled with the electrical system. The most important feature of synchronous inertia is that there is no external control applied to it and it is available all time. It can be activated instantly at the moment of disturbance/event by sensing the change in the rotating speed of the turbine, and therefore by sensing the change in the frequency of the voltage waveform.

The most important question is that why synchronous inertia is needed in power systems. In fact, the synchronous inertia is needed due to:

i. <u>*Limiting the RoCoF at the moment of a disturbance*</u>

It is vital to keep the RoCoF less than a specific limit at the moment of a disturbance. This is due to the fact that if the RoCoF is higher than a specific value, then the protection system will trip the synchronous generating units due to safety requirements. This concept can be more tolerant in modern systems by implementing RoCoF ride through capabilities.

ii. <u>*Reducing the maximum frequency deviation*</u>

The higher inertia constant is available at the system, the less frequency deviation will be encounter due to the same disturbance magnitude. This is due to the fact that the higher inertia will give the system enough time to release more spinning reserve to intercept the frequency decline.

It can be seen that the main factor that determine the required rotating synchronous inertia in power systems is the maximum RoCoF allowed in the system after a disturbance.

5.5. Minimum Synchronous Inertia Requirements in a Bulk Power System

As discussed above, the allowed maximum RoCoF is the main factor to determine the required inertia in a power system. In this section, we discuss the minim required synchronous inertia in a power system, under the following assumptions:

1. The required inertia is the whole system, meaning that the system is modelled and operated as bulk power system.
2. The system is a synchronous generation-dominated power grid, meaning that only synchronous inertia is considered for limiting the RoCoF in the system.
3. There is no sufficient RoCoF ride through capabilities.

Under the above assumptions, the maximum RoCoF at the moment of the disturbance is determined by the conventional swing equation as follows,

$$\dot{\omega}_i(t) = \frac{\omega_{si}}{2H_i}\left(\begin{array}{l} P_{mi}(t) - (\mathrm{x}''_{qi} - \mathrm{x}''_{di})\mathrm{i}_{di}(\mathrm{t})\mathrm{i}_{qi}(\mathrm{t}) - \mathrm{D}_i\ \omega_i(t) + \mathrm{D}_i\ \omega_{si}(t) - \dfrac{\mathrm{x}''_{di} - \mathrm{x}_{si}}{\mathrm{x}'_{di} - \mathrm{x}_{si}} E'_{qi}(t) i_{qi}(t) \\ - \dfrac{\mathrm{x}'_{di} - \mathrm{x}''_{di}}{\mathrm{x}'_{di} - \mathrm{x}_{si}} \psi_{1di}(t) i_{qi}(t) - \dfrac{\mathrm{x}''_{qi} - \mathrm{x}_{si}}{\mathrm{x}'_{qi} - \mathrm{x}_{si}} E'_{di}(t) i_{di}(t) - \dfrac{\mathrm{x}'_{qi} - \mathrm{x}''_{qi}}{\mathrm{x}'_{qi} - \mathrm{x}_{si}} \psi_{2qi}(t) i_{di}(t) \end{array}\right) \quad (2)$$

where $\omega = f$ in per unit system. The different variables in (2) are well-described in [5].

This equation (2) can be simplified to the well-known swing equation that describes the relationship between the RoCoF and the active power deficit, as given below,

$$2H\frac{d\omega}{dt}|_{t=0^+} = 2H\frac{df}{dt}|_{t=0^+} = P_t^m - P_t^e = \Delta P \tag{3}$$

Where P_t^m is the mechanical power (represent the generated active power) at time t, P_t^e represents the active power demand at time t.

To determine the minimum required synchronous inertia in a power system, the following information and data is needed:

- The maximum allowed rate of change of frequency, $RoCoF_t^{allowed}$, at the moment of the disturbance in the system from security view of point. This value needs to be determined by the system operator based on knowledge of type of different elements connected to the grid and their ability to handle a RoCoF less than the determined allowed RoCoF.
- The maximum disturbance in the system, ΔP_t^{max}, at operational interval t. This value can be determined by the operator as well. However, it is worth mentioning that the maximum event could change from one day to other and even from one time to other during the day. This depends on the maximum source of the power connected to the grid at time of interest for calculating the required minimum inertia. However, if the operator would like to consider a disturbance other than single event/disturbance like multiple simultaneous disturbances or disconnection of a major interconnector, the maximum disturbance is still calculatable by the operator. However, the general practice is to protect the system in case of tripping the largest power plant connected to the grid at the time of interest for understanding the minimum required inertia in power systems operated as bulk power systems, i.e. $\Delta P_t^{max} = P_t^{G,max}$.
- The operation time interval (OTI). For example, the system is dispatched for 5 minutes in the NEM. Therefore, the minimum inertia could be calculated for each 5 minutes, though there would not be much change if the largest power plant would not be connected or disconnected.

Once the above-mentioned data is made available, the minimum required synchronous inertia, $H_t^{S,req}$, would be calculated using for each time interval shown in Figure 5.2 using the formula given in (4).

$$H_t^{S,req} \geq \frac{f_n}{2\times RoCoF_t^{allowed}} \times \left|max\{P_t^{G,i,max}\}\right| \tag{4}$$

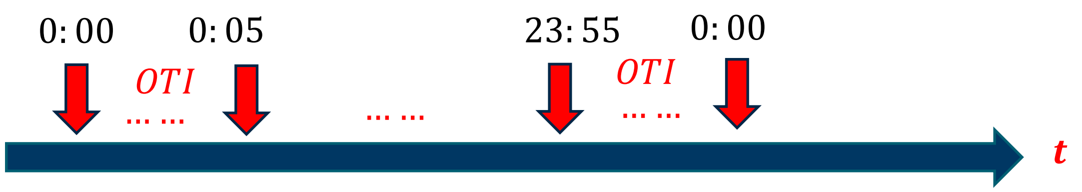

Figure 5.2. The calculation of the minimum synchronous inertia for each operational time interval during a one day.

5.6. Minimum Synchronous Inertia Requirements in a Multi-Area Power System Under Regionalisation Concept

In modern power systems, the security of operation becomes of the main challenges. In modern power systems security, it is crucial to maintain minimum requirements of inertia and spinning reserve and services in each power region. In fact, it is rationale to have minimum inertia requirements in each power region instead of having the inertia for whole power system with no matter from which region it would be supplied. The main reasons are:

i. Modern power systems consist of multi power regions connected through controlled tie-lines like HVDC links. Due to many limitations, HVDC can not transfer the inertial response from one power region to support other power region under operation stress from RoCoF point of view.

ii. RoCoF is a local/regional metric which means only the area/power region where the disturbance occurs will suffer from high RoCoF. In fact, the RoCoF is a local variable, while the frequency is a global variable (however, the frequency is going to be quasi-global in modern power systems with possibility to become local variable in future power systems beyond energy transition subjected to the philosophy how power systems would be operated in the future). Form this feature, one can understand that the inertia in one power region can help supporting frequency stability in other power regions from maximum frequency deviation view of point, but the inertia in one power region can not help the RoCoF limitation in other power regions especially if power regions connected with HVDC links or linked through AC links with high synchronisation coefficients.

Therefore, it is logical to consider having minimum synchronous inertia in each power region. To determine the required minimum synchronous inertia, let us consider a power system consists of N power region connected through different types of interconnectors. Figure 5.3 shows the general topology of an interconnected power regions forming a mesh interconnected power system and also depicts the topology of the NEM which forms a radial interconnected power system.

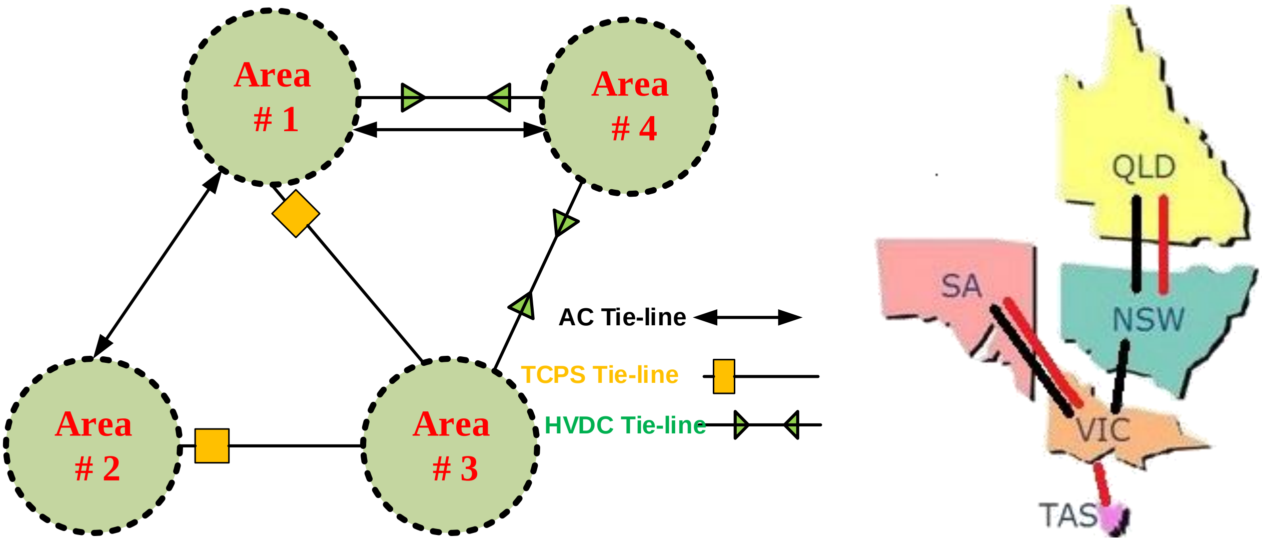

Figure 5.3. A general topology of N power regions (N=4) interconnected through different types of interconnectors and the topology of the NEM where red interconnectors represents HVDC links.

To determine the minimum regional synchronous inertia, more information is required compared to the minimum synchronous inertia for whole system presented in the previous section. The main difference is that in an interconnected power system, there is a need to determine the maximum single disturbance for each power region i.e. $\forall i \in N$. To determine the maximum disturbance, there is need of the following information for each interval or for each period of time for which the minimum regional synchronous inertia is needed to be calculated:

1. The maximum single power source in the power region,
2. The maximum single load in the power region. This is important in case there is a single load which is higher than a single power source in a specific power region.
3. The maximum exchanged power with neighbouring power regions. There is a need to understand the maximum power to be sent or/and imported through different interconnectors connected to the power region of interest.
4. The allowed maximum RoCoF in a specific power region. Usually, the power system shares the same standard through different power regions, but in case there is a different RoCoF limitation in each power region, it is vital to consider the local standard, specially in this case in order to meet the operation requirements.

The aforementioned data and information are important to facilitate the calculation of the minimum synchronous inertia for the ith power region based on

$$\forall i \in N\{1,2,\ldots,n\} \tag{5}$$

$$H_t^{S,region,i} \geq \frac{f_n}{2\times RoCoF_t^{allowed,i}} \times \left|max\{P_t^{G,i,max}, P_t^{T,i,max}\}\right| \tag{6}$$

Where $H_t^{S,region,i}$ is the minimum synchronous inertia required in the ith power region considering that other power regions can not provide inertia support to the ith power region, $P_t^{G,i,max}$ is the maximum power source or connected load to the ith power region of interest, $P_t^{T,i,max}$ is the maximum transferred power between the ith power region and other neighbouring power regions, $RoCoF_t^{allowed,i}$ is the allowed maximum RoCoF in the ith power region based on the operation standard or based on the operator's preference.

The adoption of inertia regionalisation concept will increase the total required inertia across the system (as a sum up of the individual regional inertia constants of all power regions) if compared to the traditional concept in the previous section once the grid is operated as a bulk power system. Nevertheless, the regionalisation is an important concept that might be considered as an urgent need for modern power systems going through energy transition in order to make the power system transformation more secure and safe by improving the overall security of multi-area power systems on regional bases.

5.7. Inertia Sources for Modern Interconnected Power Systems: Synchronous and Synthesis Inertia

In the previous sections, approaches for determining the minimum required inertia for the whole system and the different power regions are introduced. The main assumption in the previous sections is that the main source of inertia is the synchronous generating units, therefore the focus was on the synchronous inertia. In what follows, the previous approaches are developed to adapt with other sources of inertia services such as virtual inertia from battery energy storage systems and other inverter-based resources.

Equations (4) and (5) remains valid for determining the required minimum inertia regardless the source of the inertia and its type due to the fact that the total inertia amount is determined by the allowed RoCoF and the disturbance, not by the inertia type. There are several sources could provide inertia services, including synchronous generators, synchronous condensers, flywheel energy storage systems, Superconducting Magnetic Energy Storage (SMES) such as supercapacitor, battery energy storage systems, wind turbine through inertia emulation techniques, etc. We divide the inertia sources for modern power systems into three main categorises as follows,

i. *Synchronous inertia:* it mainly comes from synchronous generating units, synchronous condensers, and flywheel energy storage systems.

ii. *Virtual inertia:* it can be provided from IBRs including ESS and battery energy storage systems, and modern wind turbines.

iii. *SMES-based inertia:* it can be essentially provided from supercapacitors and other SMES devices.

The total synchronous inertia, $H_t^{S,region,i}$, provided to each power region at time interval, t, can be calculated as follows,

$$H_t^{S,region,i} = \sum_{j\in\varphi^{SG}} H_j^t x_j^t + \sum_{k\in\varphi^{SC}} H_k^t y_k^t + \sum_{r\in\varphi^{FES}} H_r^t z_r^t \tag{7}$$

where SG refers to synchronous inertia from synchronous generating units, SC refers to synchronous inertia from synchronous condensers, and FES refers to synchronous inertia from flywheel energy storage systems. x, y, and z are used to determine if the ith source of the inertia is dispatched at the time interval of interest, t, or not, therefore their values is 1 if connected and 0 is not dispatched for providing inertia services at t.

The total virtual inertia, $H_t^{S,region,i}$, provided to each power region at time interval, t, can be calculated as follows,

$$H_t^{IBR,region,i} = \sum_{j\in\varphi^{IBR}} H_j^t x_j^t \tag{8}$$

The total SMES inertia, $H_t^{SMES,region,i}$, provided to each power region at time interval, t, can be calculated as follows,

$$H_t^{SMES,region,i} = \sum_{j\in\varphi^{SMES}} H_j^t x_j^t \tag{9}$$

In addition to the inertia sources located within the power region, the operator can consider supporting the power region with inertia provided from other power regions under specific assumptions. Therefore, the transferred inertia services through AC links can be modelled as follows,

$$H_t^{T,region,i} = \sum_{j\in\varphi^T} H_j^t x_j^t \tag{10}$$

where φ^T is the set of the interconnectors (AC, TCPS, HVDC) connected to the ith power region and under some assumptions by operator are considered to transfer inertia.

The total available inertia for the ith power region can be calculated as follows,

$$H_t^{region,i} = H_t^{S,region,i} + H_t^{IBR,region,i} + H_t^{SMES,region,i} + H_t^{T,region,i} \tag{11}$$

In (11), if the IBR, SMES, and T inertia providers are neglected, then we can get only the synchronous inertia which its required minimum value is calculated based on (6). From, theoretical perspective, IBR, T, and SMES can compensate the synchronous inertia shortfall if they have the same behaviour. However, the current technology still encounters some problems in mimicking the exact behaviour of synchronous inertia by IBR and SEMS, because there is a need for control loop to active and mimic synchronous inertia, thus there is a delay in the response, preventing the achievement of the instant response of synchronous inertia.

5.8. Remarks and Discussion on Synthesis Inertia and Synchronous Inertia

In this section, several simulation scenarios are carried out to investigate the capability of synthesis inertia under the current technology in compensating the shortfall of synchronous inertia. To generalise the results, let's consider a generic system frequency response model of a power system which can result in outcomes could be generalised for modern and future power systems. We assume a power system was being operated under base case scenario with H=3.62 Sec. If a disturbance of a 0.1 p.u applied at time t=1 Sec to the system under normal operating conditions, then the frequency will start declining until reaching maximum deviation of 0.65 Hz at t=3 Sec as shown in Figure 5.4.a.

To assess the capability of virtual inertia in compensating the synchronous inertia shortfall, let us consider the result shown in Figure 5.4.a as a base scenario. We consider two different scenarios for compensating the synchronous inertia shortfall as follows,

i. Compensating the inertia shortfall using the virtual inertia concept where the model of virtual inertia is given in Chapter 2 of this report.

ii. Compensating the synchronous inertia shortfall using the fast frequency response.

To evaluate the ability of compensating the inertia shortfall by FFR and virtual inertia concept, the synchronous inertia amount in the base scenario is reduced to 1.62 Sec from 3.62 Sec. This means that the system is encountering a synchronous inertia shortfall of 2 Sec. Under this scenario of inertia shortfall, the maximum frequency deviation would be increased from 0.65 Hz to 1.17 Hz as shown in Figure 5.4.b under the "*w/o virtual H*" scenario. It is clear by comparing Figure 5.4.a to Figure 5.4.b, especially to the scenario of "*w/o virtual H*", one can found that the inertia shortfall impacts the frequency stability leading to larger frequency deviation and higher rate of change in the frequency. The other important factor is that the inertia shortfall leads to more stress of the system operation from time perspective. For instance, in case of the inertia shortfall the frequency nadir will be reached at 1.7 Sec while in case of base scenario without inertia reduction, the frequency will reach the nadir value at t=3 Sec. This time difference is important for the operator to make actions and activate several control and protection schemes to maintain the stable and secure operation of the system.

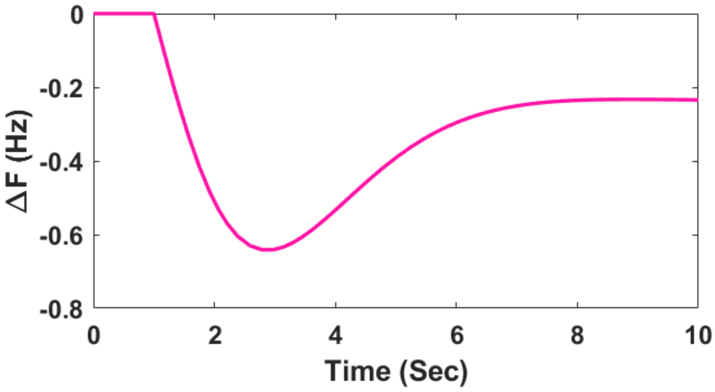

(a)

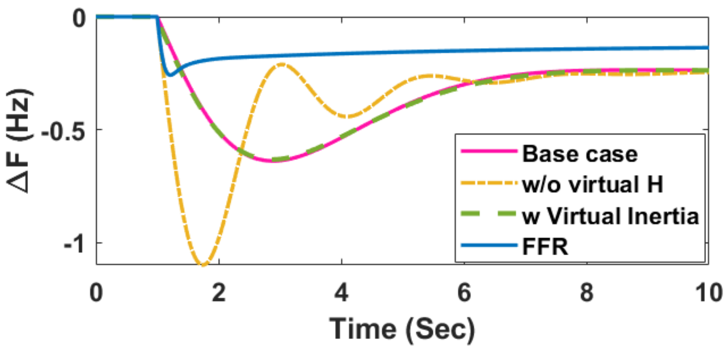

(b)

Figure 5.4. The frequency deviation due to 0.1 p.u. disturbance at t=1 Sec: a) under system operation with synchronous inertia of 3.62 Sec; b) under different scenarios of compensating synchronous inertia shortfall by virtual inertia and FFR.

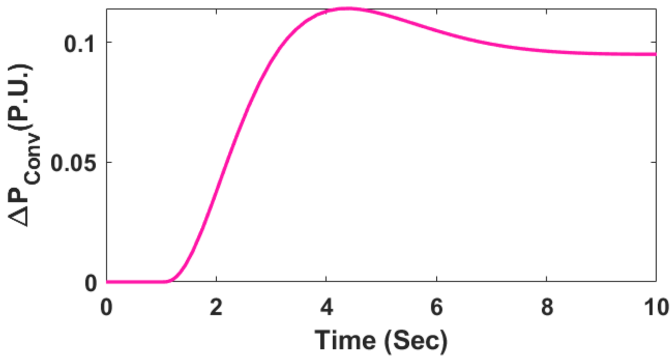

(a)

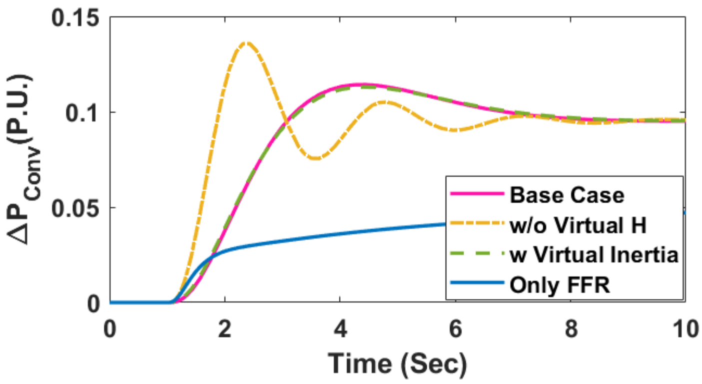

Figure 5.5. The deviation of the generated active power as a response to 0.1 p.u. disturbance at t=1 Sec: a) under system operation with synchronous inertia of 3.62 Sec; b) under different scenarios of compensating synchronous inertia shortfall.

The first scenario of compensating the inertia shortfall is to provide the same amount of inertia deficit though virtual inertia concept. It is assumed that such virtual inertia services would be provided either through IBR-based BESSs or through supercapacitor technology. This means that under the “w Virtual Inertia” Scenario, the virtual inertia amount is 2 Sec and the synchronous inertia is 1.62 Sec to meet the total inertia in the system of 3.62 Sec just similar to the base scenario before the inertia reduction. In Figure 5.4.b, it can be seen that this scenario, i.e. “w virtual Inertia”, we can get the same frequency response before the inertia reduction. This means that the virtual inertia can completely compensate the synchronous inertia shortfall from frequency stability view of point. It is to emphasis that it can compensate from frequency perspective only, where the ability of virtual inertia to compensate from RoCoF perspective will be assessed later. It worth mentioning that this excellent performance from the only frequency view of point is not sufficient to confirm the ability of virtual inertia to replace the synchronous inertia. It can be seen from the same figure that the FFR can highly improve the frequency stability (without focus on the RoCoF). From frequency view of point, the compensation of synchronous inertia shortfall by FFR could be beneficial if the impact of RoCoF on the system is neglected. Furthermore, the impact on the response of power plants due to a disturbance is also assessed. The same lessons can be mapped to the impact of virtual inertia and FFR in compensating the synchronous inertia shortfall on the active power response as shown in Figure 5.5. To evaluate the ability of virtual inertia and FFR in compensating the shortfall in the synchronous inertia, it is vital to check their impacts on the RoCoF. In fact, the main concern for the inertia shortfall is high RoCoF that could lead to stability and security issues. While both FFR and virtual inertia can compensate for inertia shortfall from frequency perspective, there is a need to understand the situation of the RoCoF under different scenarios of inertia shortfall compensation.

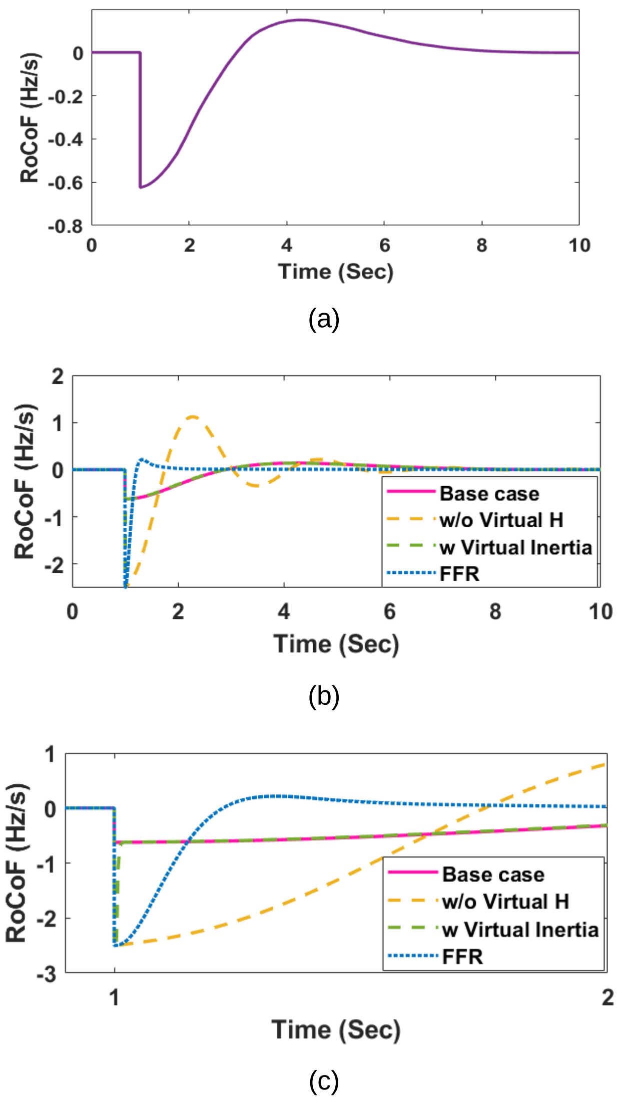

Figure 5.6. The RoCoF as a response to 0.1 p.u. disturbance at t=1 Sec: a) under system operation with synchronous inertia of 3.62 Sec; b) under different scenarios of compensating synchronous inertia shortfall; c) zoom in around t=1 Sec

Under the same disturbance scenario, the maximum RoCoF is 0.65 Hz/Sec in the base case scenario as shown in Figure 5.6.a. If the same inertia shortfall with the previous study is applied, i.e. (reducing the total inertia from 3.62 Sec to 1.62 Sec and then compensating the shortfall through FFR and virtual inertia), the results are depicted in Figure 6.b. It can be seen from Figure 5.6.b that the shortfall in the inertia has led to an increase of the RoCoF from 0.65 Hz/Sec to 2.5 Hz/Sec, in case there is no compensation as shown in the “w/o Virtual H” scenario. Similar to the previous study on the frequency response, the different scenarios for compensating the inertia shortfall are considered, i.e. the FFR and virtual inertia scenarios. Figure 5.6.b shows that both virtual inertia and fast frequency response under the current technology can not perfectly compensate the synchronous inertia shortfall from RoCoF view of point. Figure 6.c shows that although both virtual inertia and FFR can not reduce the maximum RoCoF (the RoCoF spike i.e. 2.5 Hz/Sec), the RoCoF dynamic response is different for both of them. If a new metric would be defined as the width of interest of the RoCoF response, then we can develop an approach to make the response of virtual inertia acceptable for the operation of modern power systems from RoCoF perspective. This width can be renamed as the RoCoF ride through to enable the compensation through virtual inertia. For instance, if the system would be made a resilient for a RoCoF spike that lasts less than 0.1 sec, then some of technologies like supercapacitor and advanced virtual inertia based on BESS could be used to compensate the synchronous inertia from RoCoF perspective. Therefore, we introduce this metric and modify it to become based on the direct measurement of the frequency derivative, i.e. $RoCoF^{meas} = \frac{df}{dt}|_{t\sim10-500ms}$. This means that if the system can be tolerant for few milli seconds at the moment of disturbance, let us say 10-50 mSec, then the virtual inertia can completely compensate the synchronous inertia. However, the tolerance/resilient time should be determined based on the technology used to provide the virtual inertia. For instance, the time of virtual inertia provided from grid following inverter is higher that the time of response needed for the grid forming inverters because of the way how they implement the control and how they mimic swing equation. To summarise, the time in the above introduced metric should be determined from the control loop time constant that used for implementing the swing equation in addition to the time delay due to the measurements and measurement and data processing stages. While with the introduced metric, the virtual inertia could compensate the synchronous inertia shortfall from both frequency and RoCoF perspectives, the FFR would be able to compensate the virtual inertia from RoCoF perspective. Although FFR can not compensate the synchronous inertia from RoCoF view of point, it can provide better performance for enhancing the frequency and active power performance as shown in Figures 5.4 and 5.5. Therefore, there is a need to determine the optimal combination of them to reach optimal operation from financial and economic perspectives to maximize the benefits and reduce the costs in addition to the above study focused on the technical perspectives, which is one of the goals in the G-PST stage 3 project. More time-domain simulations based on 300 different scenarios are carried out to validate the outcomes described above. Few simulation scenarios are depicted in Figures 5.7 and 5.8 in case scenario there is a disturbance occurs in SA power region with different magnitude considering different levels of virtual inertia. The results confirm the obtained outcomes mentioned above and verify capabilities of virtual inertia subjected to the conditions as discussed above.

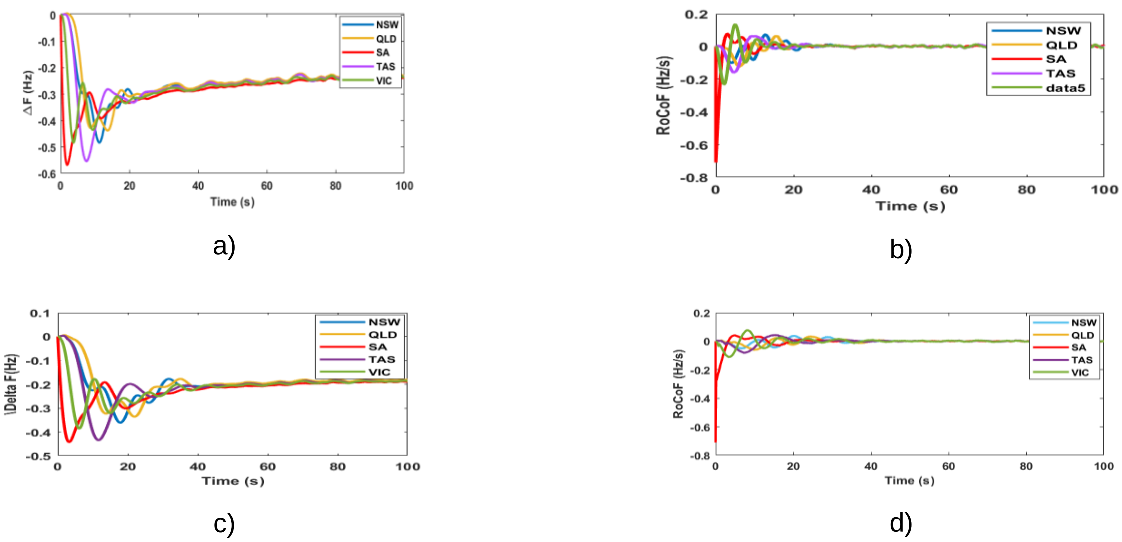

Figure 5.7. The frequency and RoCoF in different power regions due to a 0.1 p.u. disturbance in SA: a-b) no virtual inertia, c-d) an additional H_v=5 sec as virtual inertia in SA

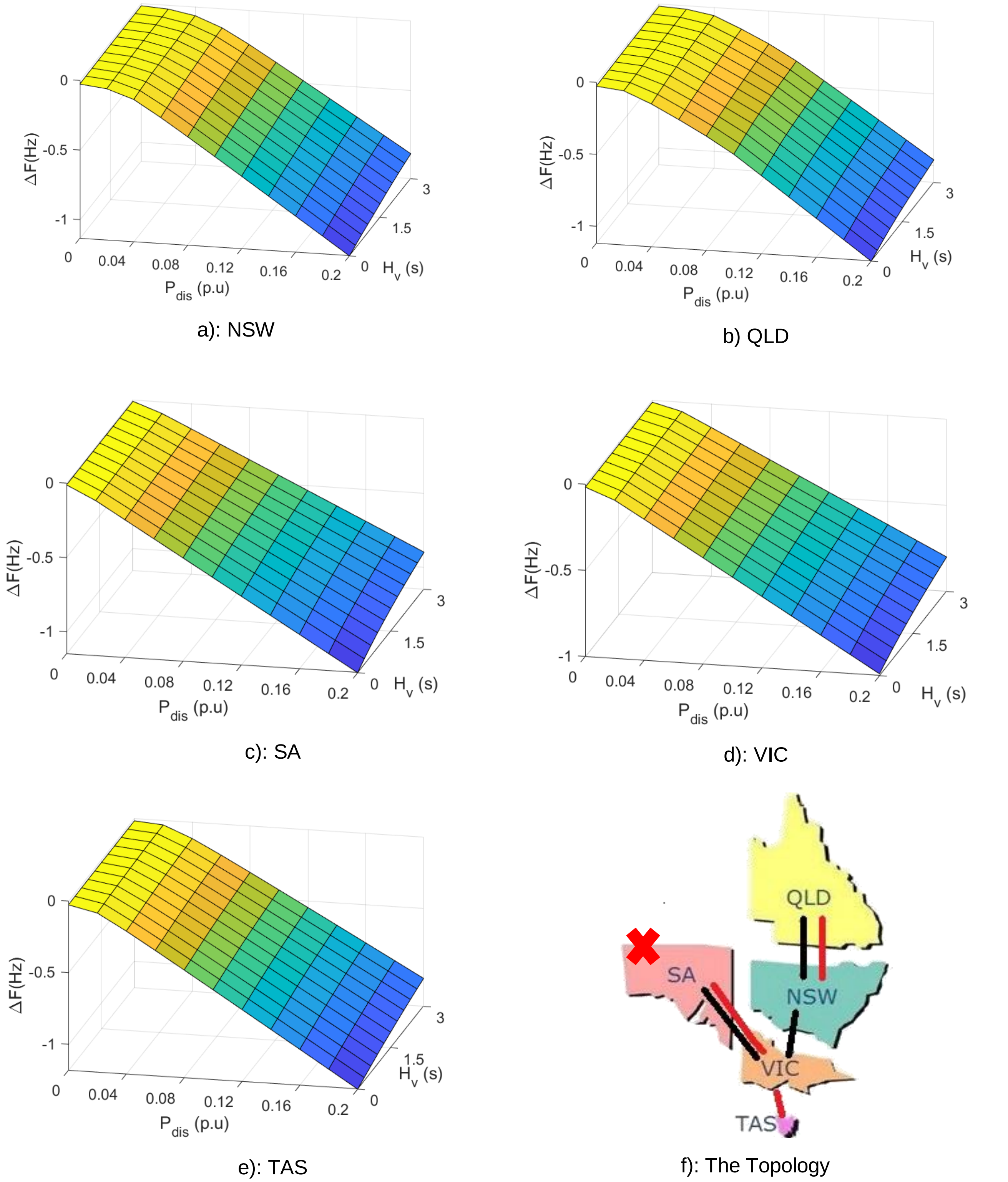

Figure 5.8. The frequency deviation in different power regions due to different step active power disturbances occur in SA as shown in the topology (f) considering different virtual inertia levels.

References

[1] AEMO, “2022 Inertia Report: A report for the National Electricity Market” by AEMO, December 2022. Link: https://aemo.com.au/-/media/files/electricity/nem/planning_and_forecasting/operability/2022/2022-inertia-report.pdf?la=en

[2] AEMC and AEMO, “Essential system services and inertia in the NEM” in AEMO Website, Jun 2022. Link: https://www.aemc.gov.au/sites/default/files/2022-06/Essential%20system%20services%20and%20inertia%20in%20the%20NEM.pdf

[3] H.H. Alhelou, B. Bahrani, J. Ma, D. Hill, “Australia’s Power System Frequency: Current Situation, Industrial Challenges, Efforts, and Future Research Directions”, In IEEE TechRxiv, 2023.

[4] AEMO, “Inertia in the NEM explained”, in AEMO website, March 2023. Link: https://aemo.com.au/-/media/files/initiatives/engineering-framework/2023/inertia-in-the-nem-explained.pdf?la=en

[5] H. Haes Alhelou, M. E. H. Golshan and N. D. Hatziargyriou, "A Decentralized Functional Observer Based Optimal LFC Considering Unknown Inputs, Uncertainties, and Cyber-Attacks," in IEEE Transactions on Power Systems, vol. 34, no. 6, pp. 4408-4417, Nov. 2019, doi: 10.1109/TPWRS.2019.2916558.

[6] H. Gu, et al, "Zonal Inertia Constrained Generator Dispatch Considering Load Frequency Relief," in IEEE Transactions on Power Systems, vol. 35, no. 4, pp. 3065-3077, July 2020, doi: 10.1109/TPWRS.2020.2963914.

Chapter 6: Remarks, Research Gaps, and Future Research Directions

Note: *Part of the work in this chapter has been published in the following preprint: H.H. Alhelou, B. Bahrani, J. Ma, D. Hill, "Australia's Power System Frequency: Current Situation, Industrial Challenges, Efforts, and Future Research Directions", In IEEE TechRxiv, 2023.*

The research outcomes have been discussed in each chapter separately. This research has resulted in new methods, approaches and tools to enable power system transformation from frequency services perspectives. The research has concluded that the power system transformation in Australia is urgent especially for the NEM to prepare the system to the upcoming changes before reaching 100% renewable energy sources dominated power systems. There is a need for several actions to prepare for the integration between the power grid and the future electric transportation sector and other energy sectors. In fact, Australian power grids especially the NEM have great potential for going safely through energy transition towards green and clean power systems. The research on services has highlighted great potential for demand-side to become more active in supporting the grid resilience, security, and stability. The demand side including future electric vehicles, virtual power plants and advanced demand response program can play a vital role for offering affordable services for the grid. For instance, the research completed through this project highlighted the capability of thermostatically controlled load for providing affordable and sufficient contingency reserve for the grid in the near future. It is to highlight that the ICT infrastructure needs more investigation to understand the complexity and security level of implementing advanced approaches for supporting the frequency in modern power systems, like the NEM.

In what follows, we briefly discuss the technical challenges and industry-oriented research gaps of NEM's frequency and generalise the discussion for power systems under transformation in the aim of bringing attention to important issues that need to be adequately addressed. The discussion is followed by highlighting future industry-oriented research directions on each topic. It is to acknowledge that there is a lot of moving parts in the frequency space within industry, especially by AEMO and AEMC, such that some of these might stop being research gaps very soon.

The discussion on FCAS services in previous sections, that have been adopted in Australia's power systems, highlights an important point that each power system is uniquely designed and operated based on several factors, including the geographical location, community behaviour and its response to energy usage, economic growth, availability of energy and reserve sources, and interaction between policy and technical/market bodies. Therefore, a focus on real-case power systems would increase the impact of solved issues, especially in FCAS studies. The industry-oriented research gaps in NEM are summarized in the following points.

6.1. Inertia Response Services:

Due to their importance, the required inertia and system strength should be determined on the basis of both stability and security analysis. For the NEM system, there is a need to thoroughly review and revise the inertia requirements to consider regional inertia and possible future virtual inertia to avoid any cascading events in case of separation of one or more power regions, which is one of the highest risks in NEM based on the events that occurred in the past. It is worth mentioning that AEMO already does this as part of the inertia shortfall framework, however, it would be useful to combine elements can provide services during energy transition such as virtual inertia etc in the assessment. It is also mandatory to specify the required inertia for different time-horizons of operation due to the fact that the required inertia in the day-demand differ from those in night-demand, and the same is true for different operational seasons. Similarly, the minimum need for physical inertia should be determined and which inertia mix is required to be provided from different sources such as inertia emulation from wind farms and virtual inertia from ESSs. Furthermore, the impact of different inertia levels in different power regions on power flow through tie-lines and stability in other connected regions needs to be investigated. Moreover, the compensation of part of the required inertia by fast frequency response should be studied to quantify its impact on the operation stability and security of the power system. The resilience of virtual inertia, the real-time estimation of available inertia and its type, and the design of the inertia market are future industry-oriented research directions on this important topic.

6.2. Primary Frequency Control Services:

There are several practices for the implementation of PFC in different power systems around the world. It is suggested to work on one norm for implementing PFC internationally and the most important is to uniform the way of implementing PFC in one system. NEM might need to specify the deadband for governors in conventional power plants and for control actions from other participants, such as ESSs. The industry-research gap here is to optimally specify the needed deadband and droop for a specific system and operation time interval based on the operation social welfare. Furthermore, it is an industry-oriented research issue to evaluate the impact of adopting different deadbands and droops for different PFC providers in the same power region and in different power regions, and these interactions should be thoroughly studied to assess the impact on both frequency stability and security. The industry-oriented research gap is how to allocate the FCAS and PFR reserve in different power regions to improve operation stability and security and reduce operational and reserve procurement costs. It is worth mentioning that, NEM is moving to enduring mandatory PFR and distribution of PFR will be widespread. As another research gap, the impact of adopting a central FCAS market on operation security needs to be discussed as well as what arrangements should be adopted to convert the system to be based on a fully decentralized FCAS market and operation. The important research-oriented direction is to investigate how to use different tie-lines to enhance primary frequency response, especially in power systems that have different types of tie-lines, e.g., AC tie-lines and HVDC links, like Australia's power system.

6.3. Secondary Frequency Control Services:

The implementation of AGC in the Australian NEM system is completely different from international practices. NEM does not consider tie-line power flow deviations in online calculation of the area control error, and consequently, it would not be involved in the AGC system. The main concern in NEM is the high-power flow fluctuations through tie-lines between different power regions during normal operational periods because of the ignoring of tieline control. In fact, NEM operates the whole power system as one power region even though the system is divided into several power regions due to the geographical locations and the long distances between the different power regions. This industryoriented challenge affects the security of the power system and could lead to cascading events after one tie-line separation; the QLD power region separation in 2018 is a clear example of such issues. Furthermore, optimal allocation of secondary reserves in different power regions can help involve tie-line power flow deviation in AGC without more procurement of FCAS reserves, which is one of the future industry-oriented research directions. Moreover, the security and cybersecurity of AGC implementation is an industry-oriented research gap and future research direction for Australia's power system due to the fact that NEM still implements a centralized AGC system. The arrangements for converting the current AGC system to be quasi- or fully decentralized one is another important industry issue and research gap for NEM. Finally, the measurement sampling rate used for both primary and secondary control systems needs to be revised to be more accurately based on higher rates, especially for the AGC system, where the system infrastructure may convert to be based on wide-area monitoring (WAM) and PMU measurements instead of old SCADA systems.

6.4. Current FCAS Market Issue:

NEM encounters technical and policy issues that affect the allocation of FCAS services in different regions. The main challenge is related to the regulation of FCAS services, where most of the amount offered for the operation of the power system comes from the VIC region. This might put the overall security of the system in danger because these services, i.e., regulation raise and regulation lower services, are crucial for solving imbalance issues in normal operational periods. The security issues raised from the fact that there are BESSs registered for providing the regulation FCAS, which are highly competitive to other sources, and since this regulation services will be provided by one or limited number of sources, this put the system under security issues. The other issues are the potential power flow fluctuation in interconnectors, and some time they can not be used to deliver the regulation services to other regions due to technical issues, e.g. BassLink, which also challenge the system stability and security. However, HVDC links other than Basslink do not provide frequency response services in NEM which might require review and upgrade. To avoid stability and security issues, AEMO has enforced FCAS allocations, under the Regionalization of Regulation FCAS Concept as an interim solution. The solution places constraints on the spot market that at least 25% of the total required regulation FCAS in NEM, i.e. 220 MW raise regulation FCAS and 210 MW lower-regulation FCAS, should be delivered from outside of the VIC region, i.e. QLD + NSW + SA > 25% of the regulation FCAS requirement. However, this is an important technical and market issue that needs to be properly solved to maintain the transparency of the market, and operation stability and security of the system.

6.5. Current Technical Issues in NEM's FCAS:

One of the important technical parameters in determining the required contingency FCAS is the load damping factor, known as the load frequency relief in NEM, because the procured contingency FCAS amount is equal to the largest credible contingency minus the assumed load relief. Since 2001, the load relief has been selected as 1.5% and 1% for the Mainland and TAS, respectively. Analysis of events that occurred in 2020 confirmed the inaccuracy of the aforementioned values; therefore, AEMO reduced the Mainland load relief to 0.5% and the TAS load relief to 0-0.1%. However, this is one of the great challenges in today's power systems, especially for NEM, since the modern rotating loads are being connected to the grid through power electronic devices; therefore, there is a research gap and industry challenges for mid-term and short-term estimation/measurement of load relief, since it highly impacts the amount of the procured contingency FCAS, and thus the operational cost of the system.

6.6. Emerging Issues:

The time response requirements from different FCAS markets need to be evaluated for the systems going through power system transformation since the dynamic behaviour and the source of services would be changed, and more adaptive time scales are needed to adapt to the new characteristic of the system to enable and smooth the energy transition. Two of the challenges in Australia's power system that would be great challenges in the future operation of the international systems as well are the uncertainties and variability. The industry- 10 oriented research gap is how to quantify power variations and uncertainties in different power regions and how to assess and value their impacts on other power regions from the perspective of frequency stability and security issues, and from other perspectives as well. In Australia, the SA power region reached the high-power share from renewable energy sources in October 2021 while other power regions connected to SA still operated with different levels of power generation mix. In such a case, a new market needs to be defined to address such issues, such as the causer of variability and the need for FCAS services, and consequently the reserve should be allocated based on one short-term estimation of uncertainties in each area to avoid excessive tie-line power flow fluctuation and high difference between local frequencies. Furthermore, the local frequency is a real threat to the operation stability and security in a system such as NEM. The local frequencies should be qualified/quantified online in monitoring centers and controlled to keep the system in a good situation of connectivity between different power regions. Finally, Australian power systems including NEM and other international systems with high penetrations of RESs and IBRs are in urgent need of new metrics that can be evaluated online and in real-time, including assessing frequency and local frequencies and their stability and security. In fact, most of the existing metrics are designed for systems with low variability and are calculated based on the SCADA rate; therefore, developing advanced metrics for frequency in modern power systems would help enable the global power system transformation.

For further reading on remarks, research gaps, future research directions, the readers are referred to our publications from this project [1-4]. The references [1-4] are open access publications in IEEE TechRxiv, IEEE and IET, therefore, they are considered as appendices to this report where readers can access them easily.

References:

[1] *H.H. Alhelou, B. Bahrani, J. Ma, D. Hill, "Australia's Power System Frequency: Current Situation, Industrial Challenges, Efforts, and Future Research Directions", In IEEE TechRxiv, 2023.*

[2] *Haes Alhelou, Hassan; Bahrani, Behrooz; Ma, Jin, "An Affordable Sophisticated Frequency Control for Australian National Electricity Market System Considering Industry and Infrastructure Challenges", TechRxiv. Preprint 2023. https://doi.org/10.36227/techrxiv.22709575.v1*

[3] *AX Irudayaraj, V. Veerasamy, M. Premkumar, M. Radzi, NB. Sulaiman, and H. Haes Alhelou, "Decentralized frequency control of restructured energy system using hybrid intelligent algorithm and non-linear fractional order proportional integral derivative controller", IET Renewable Power Generation, Jun 2023.*

[4] *H. H. Alhelou, N. Nagpal, N. Kassarwani and P. Siano, "Decentralized Optimized Integral Sliding Mode-Based Load Frequency Control for Interconnected Multi-Area Power Systems," in IEEE Access, vol. 11, pp. 32296-32307, Jun 2023, doi: 10.1109/ACCESS.2023.3262790.*